

| | |
|--|---|
| NASA CR-151955 | |
| 4. TITLE (and Subtitle) | 5. TYPE OF REPORT & PERIOD COVERED |
| A TECHNIQUE FOR MEASURING ROTORCRAFT DYNAMIC STABILITY IN THE 40- BY 80-FOOT WIND TUNNEL | Interim Report 16 Jan 1976 - 15 Jan 1977 |
| 7. AUTHOR(s) | 6. PERFORMING ORG. REPORT NUMBER |
| Narendra K. Gupta and Jeff G. Bohn | |
| 9. PERFORMING ORGANIZATION NAME AND ADDRESS | 8. CONTRACT OR GRANT NUMBER(s) |
| SYSTEMS CONTROL, INC. (vt) 1801 Page Mill Road Palo Alto, CA 94304 | NAS2-8799 |
| 11. CONTROLLING OFFICE NAME AND ADDRESS | 10. PROGRAM ELEMENT, PROJECT, TASK AREA & WORK UNIT NUMBERS |
| | |
| 14. MONITORING AGENCY NAME & ADDRESS (if different from Controlling Office) | 12. REPORT DATE |
| National Aeronautics & Space Administration Ames Research Center Moffett Field, CA. | February 1977 |
| Technical Monitor: Dr. W. Johnson | 13. NUMBER OF PAGES |
| | |
| 16. DISTRIBUTION STATEMENT (of this Report) | 15. SECURITY CLASS. (of this report) |
| | UNCLASSIFIED |
| | 15a. DECLASSIFICATION/DOWNGRADING SCHEDULE |
| | |
| 17. DISTRIBUTION STATEMENT (of the abstract entered in Block 20, if different from Report) | |
| | |
| 18. SUPPLEMENTARY NOTES | |
| | |
| 19. KEY WORDS (Continue on reverse side if necessary and identify by block number) | |
| Wind Tunnel Testing Flutter Testing XV-15 Dynamic Stability Measurement | |
| 20. ABSTRACT (Continue on reverse side if necessary and identify by block number) | |
| This report describes an on-line technique for the measurement of tilt rotor aircraft dynamic stability in the Ames 40- by 80-Foot Wind Tunnel. The technique is based on advanced system identification methodology and uses the instrumental variables approach. It is particularly applicable to real time estimation problems with limited amounts of noise-contaminated data. | |

DD FORM 1 JAN 73 1473 EDITION OF 1 NOV 68 IS OBSOLETE

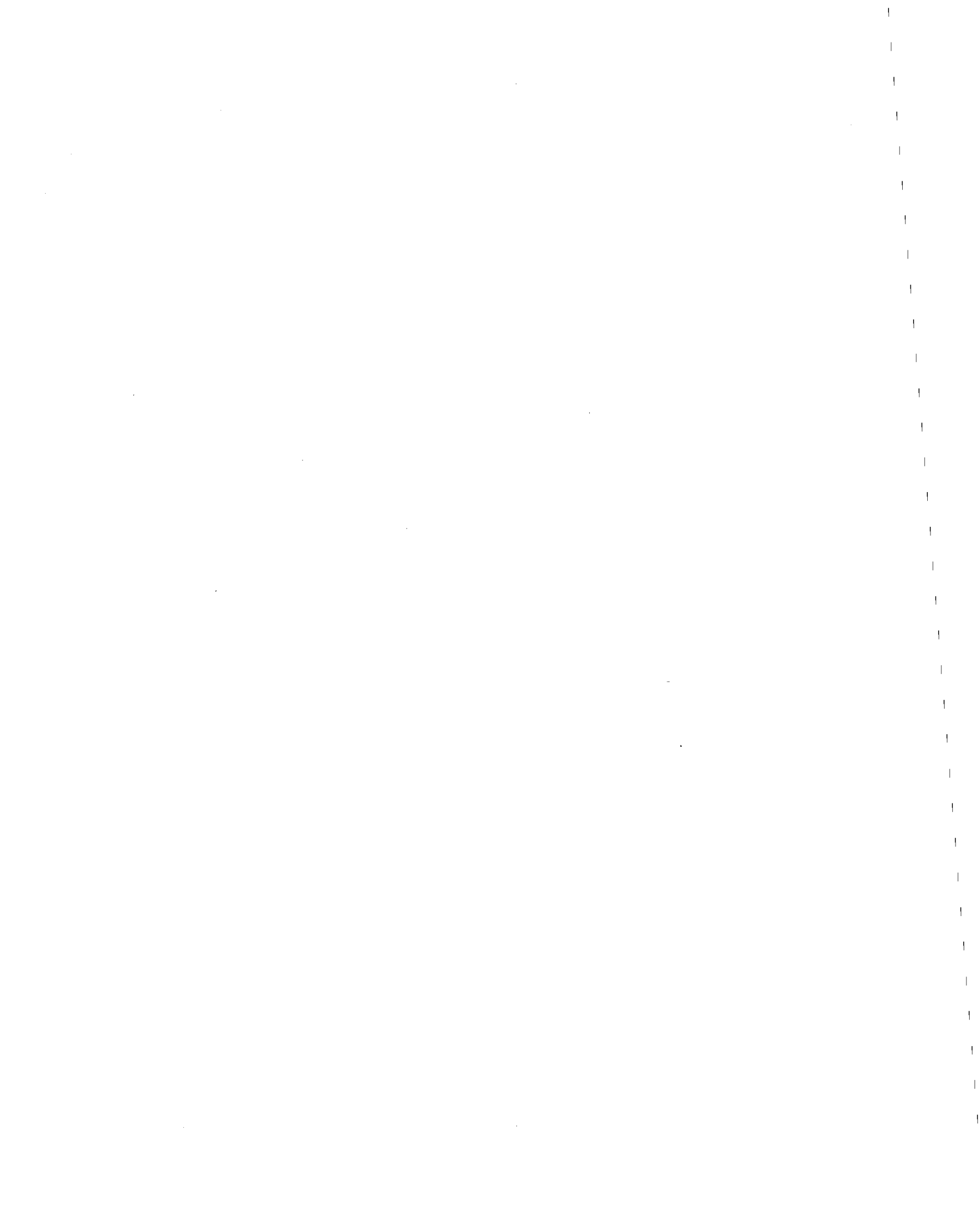
SECURITY CLASSIFICATION OF THIS PAGE (When Data Entered)

ABSTRACT (Continued)

Several simulations are used to evaluate the algorithm. Estimated natural frequencies and damping ratios are compared with simulation values. The algorithm is also applied to wind tunnel data in an off-line mode. The results are used to develop preliminary guidelines for effective use of the algorithm.

FOREWORD

This report was prepared for the National Aeronautics and Space Administration, Ames Research Center, Moffett Field, California under Contract NAS2-8799. This work was performed between 16 January 1976 and 15 January 1977. The technical monitor at NASA was Dr. Wayne Johnson. At SCI (Vt), the project was directed by W.E. Hall, Jr. N.K. Gupta was the principal investigator and N.K. Gupta and J.G. Bohn were the project engineers. K.S. Nakano was the analyst/programmer. Report preparation was done by D. Buenz.



CONTENTS

| | PAGE |
|--|------|
| FOREWORD | ii |
| ABSTRACT | iii |
| NOMENCLATURE | vi |
| I. INTRODUCTION AND SUMMARY | 1 |
| 1.1 Introduction | 1 |
| 1.2 Background | 2 |
| 1.3 Method of Approach | 3 |
| 1.4 Principal Contributions | 4 |
| 1.5 Summary | 5 |
| II. APPROACHES TO DYNAMIC STABILITY MEASUREMENT | 7 |
| 2.1 Introduction | 7 |
| 2.2 Previous Approaches | 7 |
| 2.3 Advanced System Identification Techniques | 11 |
| 2.4 Summary | 14 |
| III. A NEW REAL TIME TECHNIQUE FOR MODEL IDENTIFICATION | 15 |
| 3.1 Introduction | 15 |
| 3.2 Problem Discussion and Model Representation | 15 |
| 3.3 Parameter Estimation | 17 |
| 3.4 Model Order Determination | 20 |
| 3.5 Application of the Modal Estimation Algorithm to Ground Resonance Simulation Data | 21 |
| 3.6 Application of the Modal Estimation Algorithm to Simulation Data of a Cantilever Wing With Rotors at Each Wing Tip | 30 |
| 3.7 Conclusions | 33 |
| IV. APPLICATION TO XV-15 SIMULATION MODEL | 35 |
| 4.1 Introduction | 35 |
| 4.2 XV-15 Analytic Model | 35 |
| 4.3 Application to XV-15 Simulation Model: Sym- metric Modes | 38 |
| 4.4 XV-15 Model Identification: Antisymmetric Modes | 68 |
| 4.5 Summary | 68 |
| V. APPLICATION TO CANTILEVER WING WIND TUNNEL DATA | 81 |
| 5.1 Introduction | 81 |
| 5.2 Single Input, Single Output | 81 |
| 5.3 Single Output, Multi-Input | 87 |
| 5.4 Multi-Input, Multi-Output | 89 |
| 5.5 Summary | 90 |
| VI. CONCLUSIONS | 91 |
| 6.1 Algorithm Development | 91 |
| 6.2 XV-15 Mode Identification | 92 |
| 6.3 Application to Wind Tunnel Data | 93 |
| 6.4 Recommendations | 94 |

CONTENTS (Concluded)

| | PAGE |
|--|------|
| APPENDICES | |
| A STATE, GENERALIZED STATE, AND ARMA MODELS . . . | 95 |
| B ON-LINE PARAMETER ESTIMATION USING THE INSTRU- MENTAL VARIABLES APPROACH | 98 |
| C XV-15 MODEL AND DYNAMIC CHARACTERISTICS | 107 |
| REFERENCES | 123 |

NOMENCLATURE

| | |
|-----------------|--|
| a, A_{ij} | arrays of coefficients ($i, j=1, 2$) |
| A_0, A_1, A_2 | dynamical equation spring, damper, and mass coefficient matrices, respectively |
| b | vector array of instrumental variable elements |
| B | dynamical equation control input matrix |
| C | system random disturbance coefficient matrix |
| C_y | rotor support damping |
| C_ζ | rotor lag damping |
| E | expected value operator |
| F | (1) system state matrix, (2) shaker input forcing function |
| g | gust input vector |
| G | system control matrix |
| H | system observation matrix |
| I | inertia |
| j | $\sqrt{-1}$ |
| M_y | rotor support mass |
| n | model order or time derivative of degree n |
| p | (1) wing torsion mode and degree of freedom; (2) transfer function pole (complex) |
| P | matrix array of instrumental variables coefficients |
| q_1 | wing vertical heading mode and degree of freedom |
| q_2 | wing chordwise bending mode and degree of freedom |
| Q | matrix array of system inputs and measurements |
| R | autocorrelation function |
| s | Laplace transform variable |

NOMENCLATURE (Continued)

| | |
|--------------|---|
| S | (1) inertia; (2) power spectrum |
| Δt | length of sampling interval |
| t | time |
| T | (1) total length of data sample, (2) measured transfer function |
| u | system input vector |
| U | array of time derivatives of input vectors |
| V | airspeed, knots, true airspeed at sea level |
| x | vector of generalized variables of dynamical equation |
| x_{TIP} | wingtip longitudinal displacement, positive aft |
| y | (1) measurement vector; (2) rotor lateral hub motion |
| z | transfer function zero (complex) |
| z_{TIP} | wingtip vertical displacement, positive up |
| Z | instrumental variables matrix uncorrelated with noise |
| ∇ | gradient operator |
| GREEK | |
| α_p | rotor pylon angle, 0° = cruise, 90° = hover |
| β | rotor blade flapping degree of freedom |
| β_{1c} | rotor longitudinal flapping degree of freedom |
| β_{1s} | rotor lateral flapping degree of freedom |

NOMENCLATURE (Continued)

| | |
|------------------------|--|
| β_0 | collective flapping mode |
| β_{+1} | high frequency rotor flapping mode |
| β_{-1} | low frequency rotor flapping mode |
| Γ | system disturbance matrix |
| δ_F | flaperon deflection |
| Δ | system characteristic polynomial ($\Delta(s)$) |
| ε | zero-mean white noise function |
| ζ | (1) damping ratio; (2) rotor blade inplane degree of freedom |
| ζ_0 | collective inplane mode |
| ζ_{+1} | high frequency inplane mode |
| ζ_{-1} | low frequency inplane mode |
| ζ_{1c} | rotor cyclic inplane degree of freedom |
| ζ_{1s} | rotor cyclic inplane degree of freedom |
| θ_0 | rotor collective pitch |
| θ_{1c} | collective pitch cosine harmonic coefficient |
| θ_{1s} | collective pitch sine harmonic coefficient |
| v | system random disturbance vector |
| v_ζ | rotor blade inplane natural frequency |
| ξ_{x_i}, ξ_{z_i} | wingtip longitudinal and vertical deflection constants |
| Π | product operator |
| τ | time delay parameter |
| ψ_s | rotor RPM mode and degree of freedom |
| ω | frequency, per rev. |

NOMENCLATURE (Continued)

| | |
|------------|---------------------------------|
| ω_n | natural frequency of mode |
| ω_y | rotor support natural frequency |
| Ω | rotor rotational speed |

ABBREVIATIONS

| | |
|--------------------|---|
| ARMA | Auto-Regressive Moving Average |
| LS | Least Squares |
| IV | Instrumental Variable |
| DOF | Degree of Freedom |
| RMS | Root Mean Square |
| FFT | Fast Fourier Transform |
| $\text{Im}(\cdot)$ | imaginary part of (\cdot) |
| BV | Balance Vertical mode and degree of freedom |
| BL | Balance Longitudinal mode and degree of freedom |
| BY | Balance Yaw mode and degree of freedom |
| BS | Balance Side mode and degree of freedom |
| SL | Strut Longitudinal mode and degree of freedom |
| SS | Strut Side mode and degree of freedom |
| PY | Pylon Yaw mode and degree of freedom |

NOMENCLATURE (Continued)

SUBSCRIPTS

- i index of time derivatives and their coefficients,
or of transfer function singularities
- o denotes zeroth-order time derivative
- p (1) denotes transfer function resonant peak;
(2) denotes dimension of array
- n denotes natural frequency
- (•) denotes (•) vector formed from generalized dy-
namical equation

SUPERSCRIPTS

- (n) denotes time derivative of degree n
- T denotes transpose of vector or matrix
- j exponent of Laplace transform variable(s)
- denotes time derivative
- 1 denotes matrix inverse
- ^ denotes estimated quantity
- * denotes complex conjugate



CHAPTER I INTRODUCTION AND SUMMARY

1.1 INTRODUCTION

The XV-15 is an advanced tilt rotor research aircraft (Figure 1.1) currently under development by the National Aeronautics and Space Administration and the U.S. Army Air Mobility R&D Laboratory. An important element of the aircraft development is an extensive full-scale wind tunnel test to be conducted in the Ames Research Center 40- by 80-foot wind tunnel. Since wind tunnel scale model and full-scale tests of the tilt rotor concept have been effective in previous years, it is desired to conduct the forthcoming XV-15 tests in a comprehensive manner and to continue to minimize uncertainties in system characteristics. A previous study evaluated specific test requirements which impact the conduct of these tests [1].

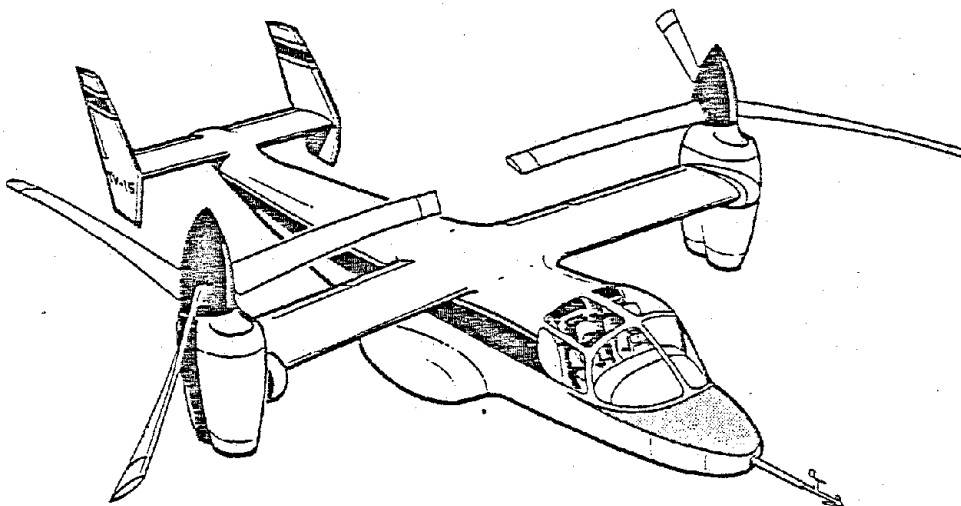


Figure 1.1 The NASA/Army XV-15

The present study describes a parameter identification method by which the dynamic stability characteristics of the XV-15 may be calculated on-line, during a wind tunnel test run. This is accomplished through the use of an advanced parameter identification algorithm, developed specifically for this application. The development of this algorithm and its application to several simulations and cantilever wing wind tunnel test data are the subjects of this report.

1.2 BACKGROUND

It is now recognized that the use of comprehensive software for aircraft wind tunnel and flight test data reduction can significantly enhance vehicle usefulness by producing the following results:

- (1) improvement in knowledge of vehicle static and dynamic characteristics: comprehensive software, accounting for typical disturbances in the data, can provide more accurate definition of the desired test objective parameters (e.g. stability);
- (2) reduction of test costs: more engineering results can be obtained with less test and analysis time and specialized personnel; and
- (3) enhancement of test safety: for real time software, rapid determination of test system status allows faster response to problems.

The testing of advanced rotorcraft, such as the XV-15, is a current requirement for such software. This vehicle sets a particularly stringent data reduction requirement for many reasons including the following:

- (1) Previous tunnel experience of a similar configuration, the XV-3, demonstrated fundamental phenomena whose subsequent successful analysis has led to the current XV-15 design [2-8]. This experience indicates the importance of the analysis of the tunnel test data analysis.

- (2) Extensive tunnel testing of the XV-15 is planned to thoroughly investigate regimes of the subsequent flight tests, and also provide a basis for evaluation of the flight test data reduction system. This requires a data reduction capability which is not only comprehensive (e.g. applicable to many flight phenomena), but may be applicable to flight data as well.
- (3) The advanced configuration of the XV-15 requires an advanced multivariable data reduction technique for on-line estimation of modal frequency and damping. This is a requirement for a new technique, compatible with existing Ames 40- by 80-foot wind tunnel computers.

Several previous analytical developments have been made to aid the wind tunnel tests. Some of the important developments are:

- (1) a comprehensive XV-15 analysis has been developed and used for study of partial and full-scale models [5-8], simulation of transient responses [1], and linear stability analysis [1,5-8];
- (2) investigations of input and instrumentation requirements for the XV-15 tunnel test, based on the model of (I) [1]; and
- (3) study of various off-line data reduction techniques for determining stability estimates from tunnel test data, including: (a) time series analysis techniques, and (b) maximum likelihood identification techniques [1].

To complete the XV-15 tunnel test requirement, it was considered necessary to develop a new algorithm to extract the most information from the wind tunnel test data.

1.3 METHOD OF APPROACH

The requirements of the previous section demand a data processing algorithm with many special features. The algorithm should produce accurate estimates of damping ratios and frequencies of various lightly damped modes, should require small

computation time and storage, should account for measurement and process noise, and should require minimum a priori information.

To meet these requirements, the dynamic model of the XV-15 tilt rotor is written in a continuous time, autoregressive moving-average (ARMA) form. The ARMA representation is equivalent to a state variable form or a generalized state form (see Appendix A).

The estimates of the ARMA model parameters are obtained using a time domain instrumental variable technique. The instrumental variables technique minimizes the effects of process and measurement noise and provides a computationally efficient technique which does not require any a priori estimates. This time domain formulation is converted into a frequency domain formulation for ease of implementation.

1.4 PRINCIPAL CONTRIBUTIONS

The contributions of this work include basic theoretical developments and applications study. The theoretical developments lead to a modal estimation algorithm and the application results develop procedures for using the algorithm effectively.

New theoretical contributions include the following:

- (1) A special autoregressive moving average (ARMA) form is developed for dynamic systems, with general model structure, for the purpose of measuring dynamic stability. The coefficients of the system are directly obtained from the autoregressive part of the model.
- (2) An instrumental variables algorithm is developed for estimating the parameters of the ARMA model. The identification procedure gives the transfer function numerator and denominator polynomials directly. The algorithm can use a multi-input, multi-output data efficiently and minimizes the

effects of measurement and process noise. The frequency range over which the model is required may be specified.

- (3) A heuristic approach for model order determination is developed based on approximate cancellation of identified poles and zeros.

The application study has lead to the following major contributions:

- (1) Tentative procedures have been developed for setting various algorithm parameters for the most effective use of the algorithm.
- (2) Procedures for obtaining good numerical conditioning in the application of the algorithm, particularly with many degrees-of-freedom.

These contributions have established the superiority of this system identification-based algorithm over classical approaches. Further work is required, however, in maximizing its effectiveness in on-line application to measure stability in the Ames 40- by 80-foot Wind Tunnel.

1.5 SUMMARY

Subsequent chapters of this report are organized as follows. Chapter II describes qualitatively approaches to estimating stability parameters of aeroelastic modes. Chapter III discusses the problem, the choice of models, and the methodology used in the development of the parameter estimation algorithm. The algorithm is applied to ground resonance and cantilever wing simulations. The algorithm is further studied using XV-15 simulations in Chapter IV. Chapter V describes the application of the algorithm to a scaled-model wind tunnel test. The conclusions are given in Chapter VI.

Appendix A describes the relationship between various forms of dynamic models. A detailed derivation of the algorithm is given in Appendix B. Appendix C shows the salient features of the XV-15 simulation used in Chapter IV.

CHAPTER II APPROACHES TO DYNAMIC STABILITY MEASUREMENT

2.1 INTRODUCTION

Interest in damping ratios and natural frequencies of modes is as old as linear dynamic models. Damping ratios determine the extent of stability and the natural frequencies determine the "speed" of a system. Early work in the determination of dynamic stability parameters from test data was performed to evaluate handling qualities of airplanes. This work can be traced back to Milliken [32], who made important observations not only from the viewpoint of data processing but test design as well. Prony's response function methods, and analog matching techniques, were used extensively with limited success. The development of high speed digital computers in the early 1960's considerably advanced the computational capabilities without a parallel development in estimation techniques. Only in the last five years has sufficient work been done to enable accurate estimation of dynamic stability parameters from limited noisy test data. A qualitative review of current approaches to the problem of determining stability (i.e., modal damping ratio) from experimental measurements is presented in the following, as background to the new parameter identification algorithm discussed in the remainder of this report.

2.2 PREVIOUS APPROACHES

Estimates of modal frequency and damping ratio have been obtained using well-understood methods of spectral analysis and known dynamic characteristics of second-order systems [10-13]. These methods generally give good results: (a) when

modes are not closely coupled, (b) when noise levels are low (i.e., when the second-order characteristics of a mode are discernible), and (c) with subjective interpretation of an experienced analyst. Several methods that have given acceptable results are discussed in Ref. 9 and are reviewed in the following. These methods include: (1) transient decay, (2) moving block analysis of transient decay, (3) the method of random decrement signatures; (4) spectral analysis, and (5) transfer function analysis.

Transient decay methods [13] determine damping ratio from the envelope of a decaying oscillation. If the oscillation is assumed to be second-order, damping ratio may be determined from response amplitudes at two points, one or more cycles apart. This method is susceptible to error from noise and extraneous modes which cause the appearance of the signal to deviate from that of a second-order system. In some cases, filters can be used to make the mode of interest more prominent, and careful input selection can often avoid exciting other modes.

In the method of "moving block" analysis, portions of the response signal are Fourier-analyzed at successive points in time. The damping ratio is then calculated as in the transient decay method, but using the magnitude of the spectral line at the fundamental frequency of the mode of interest rather than the measured signal amplitude. This method has the advantage of filtering out a portion of noise, if there is a reasonable frequency separation between the noise and the signal. Damping ratio calculation may be mechanized relatively easily, an advantage over the transient decay method. In practice, a fast Fourier transform (FFT) method may be used, but three or four periods should be included in each block to achieve sufficient accuracy. The method is thus

applicable only to low damped modes such as are encountered in aeroelastics.

The method of random decrement (RANDOMDEC) signatures [17,18] is a technique for determining the impulse response of a linear system from measurements of its response to random disturbances. When the system is under random excitation, as from wind tunnel turbulence or a specific random input, measurements are taken at times which have identical initial conditions on the system states. In taking repeated measurements in this manner, random effects cancel out, leaving in principle the system response to initial conditions. The method as developed by Cole [17] may be easily mechanized on a digital computer. The drawbacks of the method are:

(a) the presence of coupling modes reduces the effectiveness of the technique, (b) it is difficult to achieve the same initial condition on every state variable (not only on every output) in each run, (c) most of the data cannot be used because of the requirement of the same initial condition, therefore the test time is too high, and (d) the errors in triggering are not averaged out.

Analysis of the power spectrum of the measured signal can be used to estimate the natural frequency of a mode by the location of its resonant peak. For this purpose, the system exciting function spectrum should be relatively "flat" near the resonant frequency [14]. By relating measured spectra, which may be averaged over successive measurements, to the spectrum of a second-order system, estimates of damping ratio can be obtained. The presence of system zeros or other poles near the root of interest makes the comparison to a second-order system invalid and reduces the accuracy of the damping ratio calculation.

Closely related to this method is a method based on a measured transfer function, calculated from cross- and power-spectra of the input and the measurement [14,15]. By analogy to the transfer function of a pure second-order system near the resonant peak, the damping ratio may be expressed as [9]:

$$\zeta = \frac{1}{\pi\omega_n} \frac{\left[\int_0^{\infty} \text{Im}(T)\omega \, d\omega \right]^2}{\int_0^{\infty} |T|^2 \omega^2 \, d\omega}$$

where $T = T(j\omega)$ is the measured transfer function. In practice, the transfer function often has other zeros and poles, therefore the limits of integration have to be limited about the natural frequency. If the damping ratio is small (0.01-0.05), the resonant peak frequency may be treated as the natural frequency. The integration limits $0.8\omega_p$ to $1.2\omega_p$ are often adequate, and can be further reduced if necessary to lessen the effects of nearby roots or noise [1]; with 100 spectral lines in the range $0.8\omega_p$ to $1.2\omega_p$, good damping values can be obtained by integrating from $0.95\omega_p$ to $1.05\omega_p$. With 10-15 spectral lines between $0.8\omega_p$ to $1.2\omega_p$, the integration range $0.90\omega_p$ to $1.10\omega_p$ is adequate. Damping ratio is thus given approximately by:

$$\zeta = \frac{.32}{\omega_n} \frac{\left[\int_{.9\omega_p}^{1.1\omega_p} \text{Im}(T)\omega \, d\omega \right]^2}{\int_{.9\omega_p}^{1.1\omega_p} |T|^2 \omega^2 \, d\omega}$$

The principal effect of nearby modes is to shift the phase angle of the measured transfer function. This effect can be minimized if, before computing ζ by the above formula, the phase of the measured transfer function is changed by setting

$$T_{\text{new}} = T \cdot \left\{ -j \frac{T_p}{|T_p|} \right\}$$

where T_p is the measured transfer function at the resonant peak.

Other methods of identifying transfer functions attempt to determine numerator and denominator polynomials in $j\omega$ by matching the experimentally determined magnitude and phase data [16]. The factored denominator then shows the system modes, and the damping of the mode of interest may be calculated. These methods require specification of overall model order, however, and often fail to converge if the data contains noise.

2.3 ADVANCED SYSTEM IDENTIFICATION TECHNIQUES

System identification is a broad technology which may be used to verify system simulations or develop new mathematical models of static or dynamic systems based on experimental data. These techniques are based on sound mathematical and statistical principles such that the resulting models and the estimated model parameter possess desirable statistical characteristics. The classical techniques based on heuristic approaches are, therefore, being slowly replaced by more systematic system identification methods.

The overall system identification approach is divided into pretest evaluation and algorithm verification and post-test

data processing. The post-test data processing consists of data conditioning, model structure estimation, parameter estimation and model verification (see Figure 2.1). The data conditioning involves filtering and removing undesirable characteristics from data (e.g., spikes, outliers). The model order and the important linear and nonlinear terms are estimated in the model structure determination phase. The parameters of the selected model are identified in the next stage. The model verification stage applies several statistical techniques to validate the overall model. A detailed description of the system identification process is given in Ref. 19. Other parameter identification methods are discussed in Refs. 20-27.

Model order determination techniques select the simplest system which can explain the measured response adequately. The criteria for determining model adequacy include: (a) prediction error, (b) Akaike information criteria, (c) fit error, (d) F-ratio and several others. A detailed description is given in Refs. 30 and 31.

The parameter estimation methods may be divided into two broad classes, the off-line approaches and on-line approaches. Several methods have been developed for off-line application but the maximum likelihood method has been the most successful. The likelihood function of the output with respect to the parameters is maximized by selecting the parameter values. For numerical purposes, the negative logarithm of the likelihood function is minimized. The method optimally treats both the state disturbance noise and the measurement noise. Accurate estimates of all required parameters are obtained at the cost of high computation time and storage requirements.

One of the more successful on-line parameter identification techniques is the instrumental variables approach. It

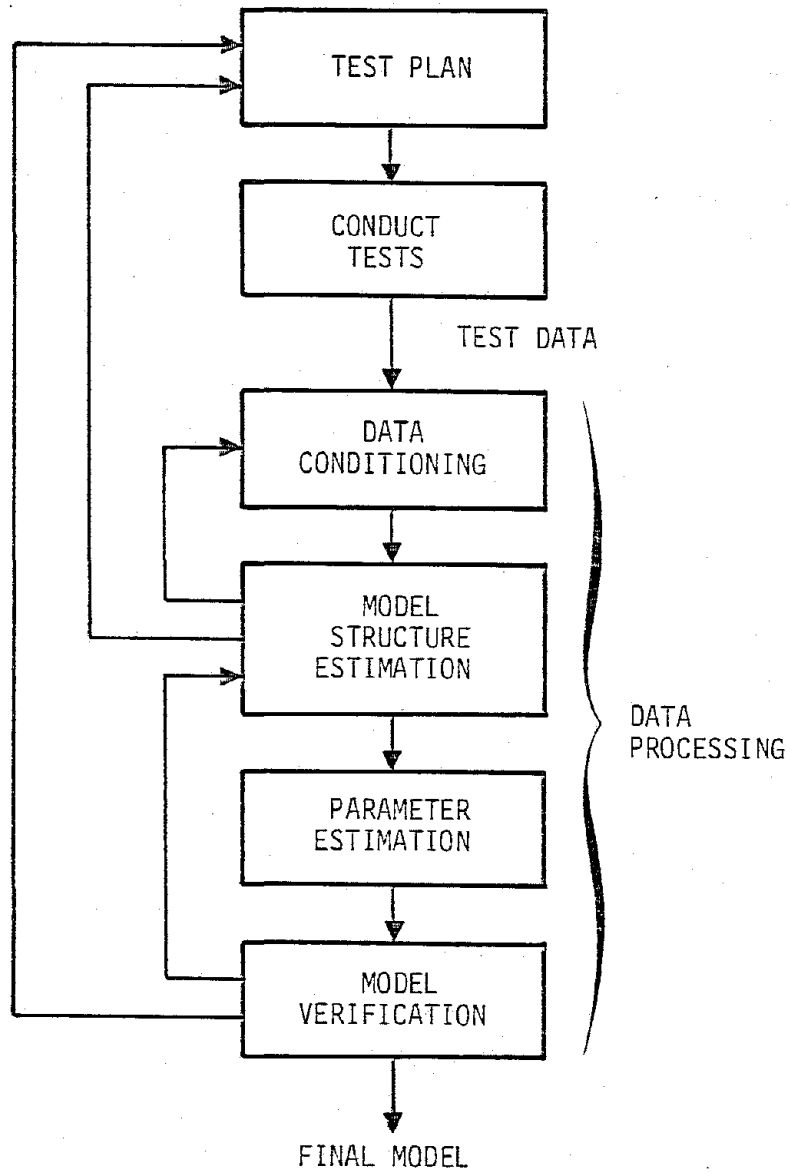


Figure 2.1 General System Identification Approach

is an extension of classical least squares techniques, but accounts for all noise sources. It is discussed in more detail in the next chapter.

System identification techniques determine all unknown parameters of the system directly and can therefore estimate frequencies and dampings of all modes. Therefore, modes that are close to each other in frequency may be isolated and the effects of noise in the process and the measurements are minimized.

2.4 SUMMARY

This chapter reviewed methods which have been used or attempted in the on-line determination of the stability of dynamic systems. Some are capable of being automated, while others require substantial subjective interpretation by the analyst. All except parameter identification methods place considerable weight on analogies to classical, well-understood, second-order dynamics, and are hampered by experimental conditions which obscure this analogy, such as noise or the presence of nearby modes. Parameter identification methods, on the other hand, can resolve these problems effectively, but they must be specialized to the problem of on-line dynamic stability measurement.

The next chapter describes a new on-line parameter identification algorithm, based on the instrumental variables method, that overcomes these problems. Its derivation and initial evaluation are discussed in the remainder of this report.

CHAPTER III A NEW REAL TIME TECHNIQUE FOR MODEL IDENTIFICATION

3.1 INTRODUCTION

From the previous discussion, it is clear that current approaches have several deficiencies. To obtain reliable estimates of frequencies and dampings of various modes from a limited wind tunnel test time, it is desirable to have an algorithm which can extract the maximum information from the data. Such an algorithm must be able to handle multi-input, multi-output responses, must correct for measurement errors (errors in instrumentation) and process noise errors (random wind tunnel turbulence), and must consider interaction between many modes. An on-line or real time technique is required and it should be able to handle modes with low damping ratios (0.01 to 0.10), characteristic of structural modes near regions of aeroelastic instability.

3.2 PROBLEM DISCUSSION AND MODEL REPRESENTATION

The dynamic relationships between the inputs and the outputs may be expressed in several forms. For the purpose of measuring dynamic stability in the 40- by 80-foot wind tunnel, a general model is most suitable since the mode shapes are not known a priori and may change with test condition. The model may be either: (a) modal state variable or autoregressive moving average (Appendix A), (b) discrete time or continuous time, and (c) in time domain or in frequency domain. The ARMA representation is better than the state variable form because approximate values of natural frequencies and dampings (required in parameter estimation in model state variable representations) of the modes are not available. The continuous

time representation is used, in spite of discrete measurements, mainly for improved numerical conditioning, when the damping ratios are small (less than 0.10). The algorithm is developed in time domain and is subsequently converted into frequency domain for convenience of implementation.

For the multi-input/multi-output systems, there are several forms of the continuous ARMA representation (see Hannan [29] for corresponding discrete ARMA representations). We use the following

$$\sum_{i=0}^n a_i I y^{(n-i)}(t) = \sum_{i=0}^{n_1} B_i u^{(n-i)}(t) + \sum_{i=0}^{n_2} C_i v^{(n-i)}(t)$$

$$0 \leq t \leq T$$

$$a_0 = 1, C_0 = I \quad (3.1)$$

where $y \in R^p$, $u \in R^q$, $v \in R^p$, $B_i \in R^{p \times q}$, $C_i \in R^{p \times p}$, $a_i \in R$ and $(\cdot)^{(i)}$ denotes the i th differential of (\cdot) . The order of the model n is twice the number of modes. n_1 is the number of zeros of the transfer function between the outputs and the inputs and n_2 is the number of zeros of the transfer function between the outputs and noise. n_1 and n_2 are usually equal to or less than n . Since a_i 's are scalars, the poles of the system are roots of the equation

$$\sum_{i=0}^n a_i s^i = 0 \quad (3.2)$$

which depends only on parameters a_i (that is why we use the form of Eq. (3.1)). Matrices B_i together with a_i determine the input/output transfer functions, i.e.

$$y(s) = \frac{1}{\Delta(s)} \sum_{i=0}^n B_i s^{n-i} u(s) \quad (3.3)$$

where

$$\Delta(s) = s^n + a_1 s^{n-1} + a_2 s^{n-2} + \dots + a_n \quad (3.4)$$

3.3 PARAMETER ESTIMATION

As mentioned in the previous section, the input/output transfer function depends only on coefficients a_i and matrices B_i . Therefore, in the measurement of dynamic stability it is of major interest to estimate these parameters accurately. Matrices C_i give the noise-output transfer function and need not be estimated. The presence of correlated noise terms, however, precludes straightforward application of the least squares method.

Instrumental variables is an ideal technique for such application. Developed initially by econometricians, it was studied in detail by Wong and Polak [23] and recently applied to vehicle estimation problems by Gupta and Hall [28]. To explain the technique, let us consider a static system, where the p outputs y are related to the $p \times m$ independent variables X and m parameters θ by the equation

$$y = X\theta + \varepsilon \quad (3.5)$$

where ε is a zero mean white noise with unit covariance. If ε and X are uncorrelated, an efficient estimate (one with the smallest mean square error) is

$$\hat{\theta}_{LS} = (X^T X)^{-1} X^T y \quad (3.6)$$

The mean and covariance of $\hat{\theta}_{LS}$ are

$$E(\hat{\theta}_{LS}) = \theta$$
$$E[E(\hat{\theta}_{LS}) - \theta][E(\hat{\theta}_{LS}) - \theta] = (X^T X)^{-1} \quad (3.7)$$

where $E(\cdot)$ is the expected value of (\cdot) . However, if ε and X are correlated, the least square estimator is biased

$$E(\hat{\theta}_{LS}) = \theta + (X^T X)^{-1} E(X^T \varepsilon) \quad (3.8)$$

An instrumental variables estimator could give unbiased estimates. In this method, we select a pxm matrix, Z , which is uncorrelated with ε . Then,

$$\hat{\theta}_{IV} = (Z^T X)^{-1} Z^T y \quad (3.9)$$

This estimator is unbiased. The accuracy of the estimate depends upon the choice of Z .

The application of the instrumental variables technique to the estimation of ARMA parameters is described in Appendix B and shown schematically in Figure 3.1. The following highlights of the algorithm are especially pertinent:

- (1) The estimation of parameters using the instrumental variables approach requires the solution of a set of linear equations. These equations have a very specific form for the multi-input, multi-output case. This specific structure must be utilized to save computation time and storage.
- (2) The elements of the matrix in the linear equations depend upon the Fourier transforms of inputs and outputs. A fast Fourier transform should be used for this purpose and, if feasible, 2^σ data points should be collected, where σ is an integer.

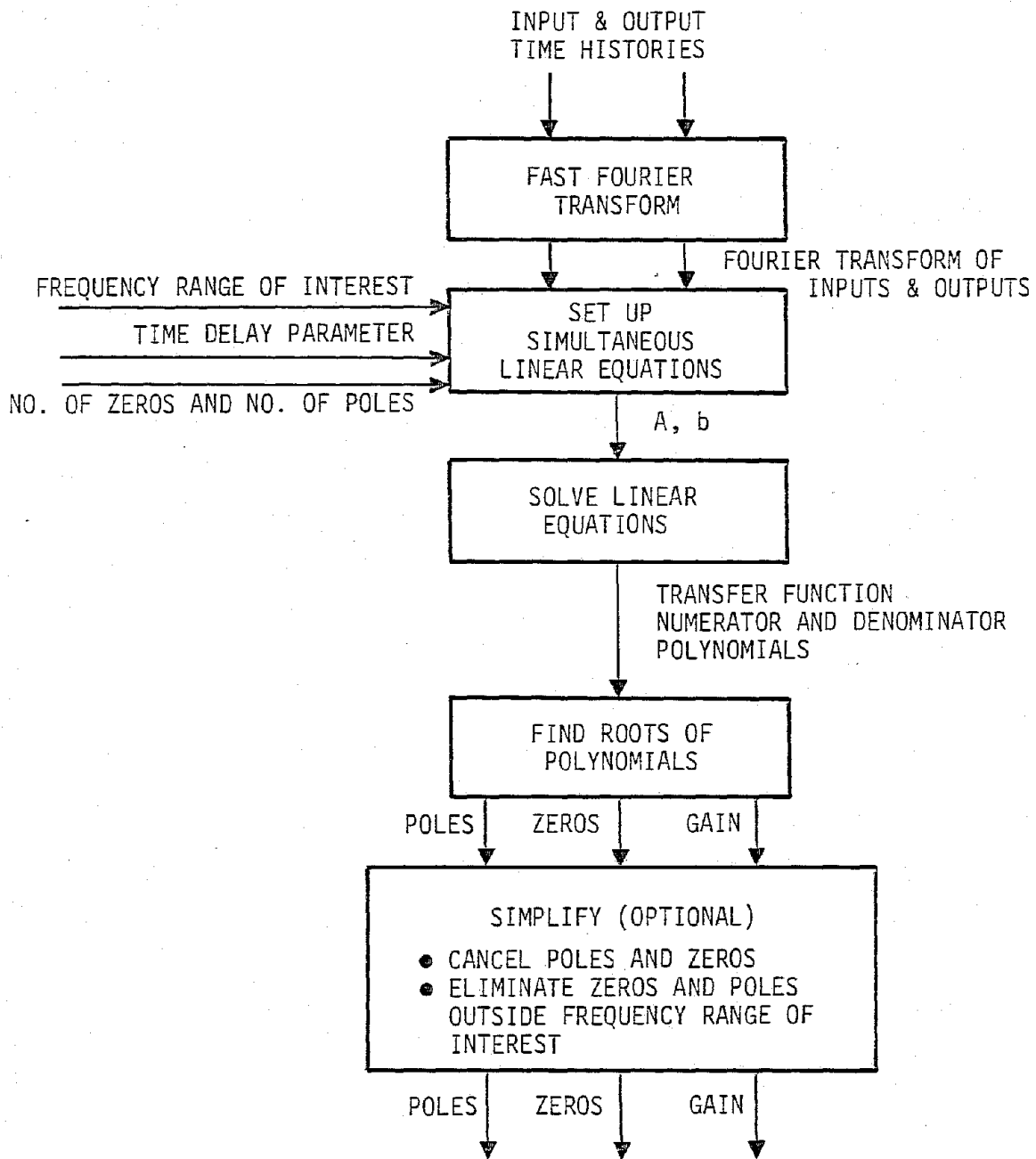


Figure 3.1 Schematic Flow Chart of the On-Line Dynamic Stability Measurement Algorithm

- (3) The algorithm is flexible in that the frequency range of interest may be selected a priori.
- (4) The inputs and outputs may be scaled for better numerical conditioning without affecting pole and zero locations.

3.4 MODEL ORDER DETERMINATION

In real time estimation of dynamic stability, the number of important modes is not known, particularly in complex aero-elastic models. Therefore, it is often necessary to estimate the number of significant modes in the output measurements. Methods to determine model order have been described by Akaike [30] and Tse and Weinert [31]. These techniques are applicable for systems driven by unknown random inputs.

We propose here a fundamentally different approach to the problem of estimating the order of the model based on input/output measurements. The basic idea is as follows. If the specified model order is lower than the true model order, the identification algorithm in this chapter will give incorrect estimates of poles and zeros. If the specified model order is the same as the true model order, correct poles and zeros will be identified. However, if the specified model order is higher than the true model order, there will be many superfluous poles and zeros in addition to the true poles and zeros. The superfluous poles must approximately cancel out the superfluous zeros. Therefore, if we specify a maximal model order in the algorithm of this chapter, the true model order could be obtained after the transfer function is simplified by cancelling the poles and zeros which are very close to each other.

The identified transfer function may be simplified as follows. First, poles and zeros which are very close to each other may be eliminated reducing the order of the transfer function.

Second, the poles and zeros outside the frequency range of interest may be removed. Let the identified transfer function be

$$TF = \frac{G \prod_{i=1}^{n_z} (s-z_i)}{\prod_{i=1}^{n_p} (s-p_i)} \quad (3.10)$$

Let the first j zeros and j' poles be at $\omega \ll \omega_{\min}$ and the last k zeros and k' poles be at $\omega \gg \omega_{\max}$. Then the above transfer function may be simplified to

$$TF \approx G s^{j-j'} \frac{\prod_{i=n_z-k+1}^{n_z} (-z_i)}{\prod_{i=n_p-k'+1}^{n_p} (-p_i)} \times \frac{\prod_{i=j+1}^{n_z-k} (s-z_i)}{\prod_{i=j'+1}^{n_p-k} (s-p_i)}$$

$$= G' s^{j-j'} \frac{\prod_{i=j+1}^{n_z-k} (s-z_i)}{\prod_{i=j'+1}^{n_p-k} (s-p_i)} \quad (3.11)$$

3.5 APPLICATION OF THE MODAL ESTIMATION ALGORITHM TO GROUND RESONANCE SIMULATION DATA

A simplified model for the ground resonance phenomenon is

$$\begin{bmatrix} I_{\zeta} & 0 & -S_{\zeta} \\ 0 & I_{\zeta} & 0 \\ -S_{\zeta} & 0 & M_y \end{bmatrix} \begin{bmatrix} \ddot{\zeta}_{1c} \\ \ddot{\zeta}_{1s} \\ \ddot{y} \end{bmatrix} + \begin{bmatrix} C_{\zeta}/\Omega & 2I_{\zeta} & 0 \\ -2I_{\zeta} & C_{\zeta}/\Omega & 0 \\ 0 & 0 & M_y 2C_y \left(\frac{\omega_x}{\Omega}\right) \end{bmatrix} \begin{bmatrix} \dot{\zeta}_{1c} \\ \dot{\zeta}_{1s} \\ \dot{y} \end{bmatrix} \\
+ \begin{bmatrix} I_{\zeta}(\nu_{\zeta}^2 - 1) & C_{\zeta}/\Omega & 0 \\ -C_{\zeta}/\Omega & I_{\zeta}(\nu_{\zeta}^2 - 1) & 0 \\ 0 & 0 & M_y \left(\frac{\omega_y}{\Omega}\right)^2 \end{bmatrix} \begin{bmatrix} \zeta_{1c} \\ \zeta_{1s} \\ y \end{bmatrix} = \begin{bmatrix} 0 \\ 0 \\ 1 \end{bmatrix} F$$

(3.12)

where

ζ_{1c} , ζ_{1s} are cyclic lag modes;

y is lateral hub motion;

F is the shaker input;

I_{ζ} , S_{ζ} , lag inertias = 1;

M_y , support mass = 30

C_y , support damping = 0.05

ω_y , support frequency = 5 Hz

ν_{ζ} , lag frequency = 0.25

C_{ζ} , lag damping; and

Ω , the rotor speed = 10 Hz.

Time has been nondimensionalized with the rotor speed. A linear simulation was conducted at 10 Hz rotor speed with the lag damping of 31.4. Using Eqs. (3.12), the poles and zeros of the transfer function between the lag modes and lateral motion vs. the shaker input are shown in Table 3.1. A sine sweep input is

Table 3.1
Poles and Zeros of the Ground Resonance Simulation

POLES

| MODE | EIGENVALUE | NATURAL FREQUENCY | DAMPING FACTOR |
|-------------|--------------------|-------------------|----------------|
| Upper-Lag | $-.287 \pm 1.164j$ | 1.20 | .239 |
| Lower-Lag | $-.224 \pm .867j$ | .896 | .250 |
| Lateral Hub | $-.0230 \pm .503j$ | .503 | .0457 |

| | OUTPUT ζ_{1c} | OUTPUT ζ_{1s} | LATERAL HUB POSITION, Y |
|--------|---------------------|---------------------|-------------------------|
| ZEROES | -1.25 | -.25 | $-.271 \pm 1.00j$ |
| | .75 | 0.0 | $-.229 \pm 1.00j$ |
| | 0.0 | 0.0 | |
| | 0.0 | | |
| GAIN | .0345 | .069 | .0345 |

applied and 512 measurements are taken at intervals of 0.5. The algorithm of Section 3.3 is applied to determine the effects of: (a) time delay parameter τ in the instrumental variables approach, (b) output noise level, (c) outputs used in estimation, (d) number of data points, and (e) discrete frequency noise, on poles and zeros estimation accuracy. In the application of the algorithm, the nondimensional frequency range of interest is limited to $0.4 < \omega < 1.2$ and the numbers of poles and zeros in each transfer function are specified to be six and five, respectively.

Effect of Time Delay Parameter τ

Table 3.2 shows the estimated poles and zeros between outputs ζ_{1c} , ζ_{1s} and y and the shaker input as a function of the time delay parameter τ when each output is contaminated by 10% random noise. Since the system is of order 6, the instrumental variables approach requires a value of τ exceeding 12 sample points or 6 seconds. The estimates of the poles are shown in Figure 3.2. Note that the estimates of the poles are most accurate at $\tau = 10$ sec. As explained before, the estimated transfer functions for $\tau = 10$ may be simplified to:

$$\begin{aligned}\frac{\zeta_{1c}(s)}{F(s)} &= \frac{.0432s^2(s - .513)}{\Delta} \\ \frac{\zeta_{1s}(s)}{F(s)} &= \frac{.0117s(s + .589)(s - .667 \pm .205j)}{\Delta} \\ \frac{y(s)}{F(s)} &= \frac{.0291(s + .245 \pm .937j)(s + .202 \pm 1.05j)}{\Delta}\end{aligned}\tag{3.13}$$

$$\Delta = (s + .0233 \pm .503j)(s + .221 \pm .854j)(s + .267 \pm 1.15j)\tag{3.14}$$

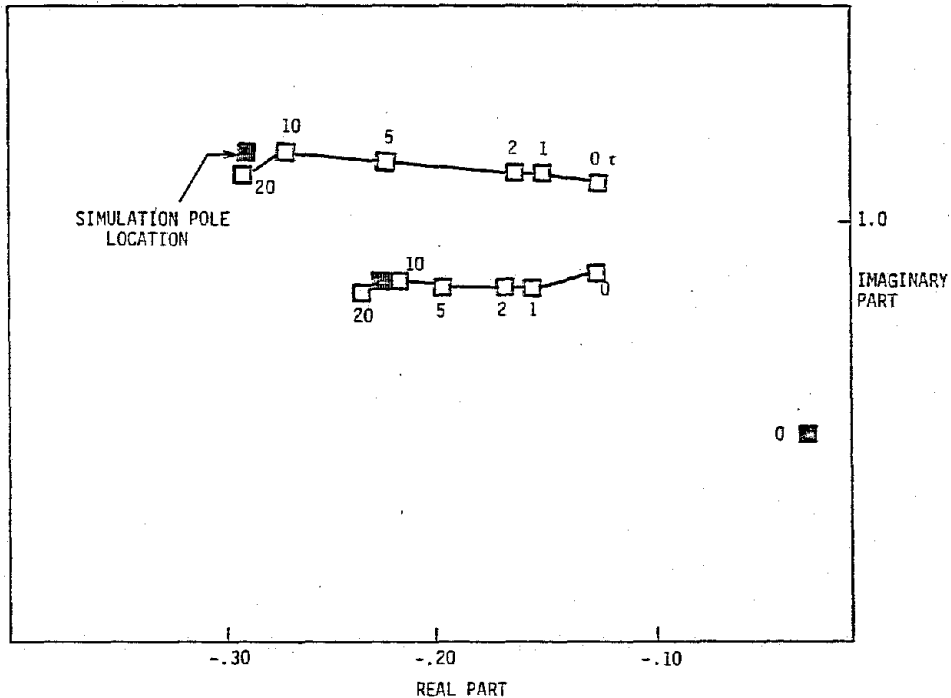
Note that the estimates of poles are more accurate than those of the zeros. This is because all three outputs contain information regarding the poles while the information about the zeros of any particular transfer function is contained only in one output.

Effect of Output Noise Level

Keeping the time delay parameter fixed at 10, the output noise level is varied. Table 3.3 shows the poles and zeros for various noise levels up to 100% (see also Figure 3.3).

Table 3.2
Effect of Time Delay Parameter τ on Estimates of Poles and Zeros

| | | SIMULATION | $\tau = 0$ | $\tau = 2$ | $\tau = 10$ | $\tau = 20$ |
|------------------------------|--------|---|---|--|--|---|
| POLES | | $-.287 \pm 1.164j$ $-.224 \pm .867j$ $-.0230 \pm .503j$ | $-.124 \pm 1.098j$ $-.122 \pm .875j$ $-.0245 \pm .504j$ | $-.149 \pm 1.13j$ $-.151 \pm .871j$ $-.0244 \pm .504j$ | $-.267 \pm 1.15j$ $-.221 \pm .864j$ $-.0233 \pm .503j$ | $-.285 \pm 1.124j$ $-.223 \pm .854j$ $-.0232 \pm .503j$ |
| $\frac{\zeta_{Ic}(s)}{F(s)}$ | ZEROES | -1.25 .75 0.0, 0.0 | $-.218 \pm 1.02j$.285 \pm .439j -.591 | $-.334 \pm 1.11j$.302 \pm .401j -.481 | $-1.64 \pm 1.44j$.513 -.0130, .114 | -.896 +.698, 175.7 -.0157 \pm .0687j |
| | GAIN | .0345 | .0359 | .0309 | .00907 | -.000191 |
| $\frac{\zeta_{Is}(s)}{F(s)}$ | ZEROES | -.25 0.0 0.0 | $-.202 \pm .988j$.109 \pm .333j 4.0 | $-.334 \pm 1.02j$.108 \pm .361j 4.56 | $.667 \pm .205j$ -.589, -.0387 7.47 | .266 -.191 \pm .280j -2.93, 2.83 |
| | GAIN | .069 | -.0113 | -.00847 | -.00156 | -.00605 |
| $\frac{y(s)}{F(s)}$ | ZEROES | $-.229 \pm 1.00j$ $-.271 \pm 1.00j$ | $-.0867 \pm 1.09j$ $-.103 \pm .882j$ 21.0 | $-.112 \pm 1.10j$ $-.132 \pm .889j$ 20.2 | $-.202 \pm 1.05j$ $-.245 \pm 937j$ 15.0 | $-.18 \pm 1.04j$ $-.287 \pm .891j$ 11.8 |
| | GAIN | .0345 | -.00141 | -.00146 | -.00194 | -.0023 |



NOTE: The scale on the x-axis is five times larger than the scale on the y-axis

Figure 3.2 Effect of τ on Estimates of Poles (Complex Conjugate Poles Not Shown)

Table 3.3

Estimates of Poles and Zeros for Various Output Noise Levels

| | | SIMULATION | 0% NOISE | 5% NOISE | 10% NOISE | 20% NOISE | 50% NOISE | 100% NOISE |
|--|-------|---|--|--|--|--|--|---|
| POLES | | $-.0230 \pm .503j$ $-.224 \pm .867j$ $-.287 \pm 1.164j$ | $-.0230 \pm .503j$ $-.226 \pm .867j$ $-.289 \pm 1.16j$ | $-.0231 \pm .503j$ $-.224 \pm .865j$ $-.282 \pm 1.16j$ | $-.0233 \pm .503j$ $-.221 \pm .864j$ $-.267 \pm 1.15j$ | $-.0237 \pm .502j$ $-.210 \pm .865j$ $-.227 \pm 1.15j$ | $-.0251 \pm .502j$ $-.190 \pm .873j$ $-.129 \pm 1.14j$ | $-.0277 \pm .500j$ $-.185 \pm .861j$ $-.0744 \pm 1.13j$ |
| $\zeta_{1c}(s)$ $\frac{F(s)}{F(s)}$ | ZEROS | -1.25 .75 0.0 0.0 | .0834 -.0815 .730 -1.22 18.24 | -.0514 .0885 .636 -1.543 -9.63 | -.0130 .114 .514 -1.64 ± 1.44j | .0338 .251 ± .145j -.604 ± 1.41j | .0620 .188 ± .322j -.169 ± 1.21j | .252 .109 ± .362j -.0769 ± 1.16j |
| | GAIN | .0345 | -.00156 | .00257 | .00907 | .0233 | .0514 | .0651 |
| $\zeta_{1s}(s)$ $\frac{F(s)}{F(s)}$ | ZEROS | -.25 0.0 0.0 | -.0937 .0889 -.245 5.745 -8.72 | .374 ± .118j -.379 -5.51 5.63 | .667 ± .205j -.599 -.0387 7.47 | .0897 ± .297j -1.39 ± .822j -28.07 | .0926 ± .384j -.283 ± 1.26j -5.35 | .0869 ± .413j -.122 ± 1.19j -3.94 |
| | GAIN | .069 | -.00109 | -.00165 | -.00156 | .000531 | .00683 | .0121 |
| $y(s)$ $\frac{F(s)}{F(s)}$ | ZEROS | $-.271 \pm 1.00j$ $-.229 \pm 1.00j$ | $-.272 \pm .975j$ $-.225 \pm 1.02j$ 12.27 | $-.283 \pm .953j$ $-.214 \pm 1.03j$ 13.1 | $-.245 \pm .937j$ $-.202 \pm 1.05j$ 15.0 | $-.204 \pm .921j$ $-.174 \pm 1.08j$ 25.98 | $-.124 \pm .904j$ $-.827 \pm 1.11j$ -18.6 | $-.0583 \pm .885j$ $-.0350 \pm 1.09j$ -6.28 |
| | GAIN | .0345 | -.00234 | -.00222 | -.00194 | -.00113 | .00166 | .00559 |

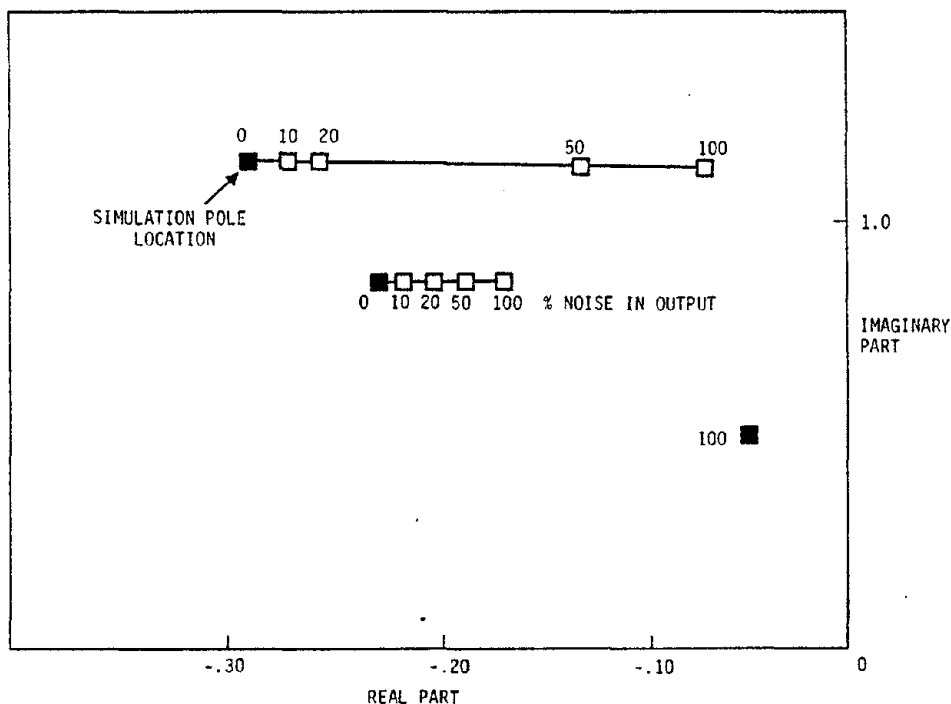


Figure 3.3 Effect of Noise Level of Estimates of Pole Locations (Complex Conjugate Poles Not Shown)

Many of the estimated transfer functions may be simplified as shown before.

Effect of Outputs Used in Estimation

For a 10% noise in outputs and $\tau = 10$, Table 3.4 shows the effect of outputs on the estimation accuracy of poles and zeros. Note that none of the outputs can individually estimate all the poles accurately. However, a combination of outputs, particularly ζ_{1c} , ζ_{1s} and y , gives excellent estimates of all poles and a reasonable estimate of the zeros.

Effect of Number of Data Points

The estimates of poles and zeros obtained using 512 points are compared with the estimates obtained using only 128 and 256 points in Table 3.5. The sampling interval is kept fixed at 0.5, the noise level is 10% and τ is 10. The estimate of the damping factor for the lateral hub mode deteriorates quite significantly when the estimate is based only on 128 points.

Effect of Discrete Frequency Noise

Table 3.6 gives the estimates of poles and zeros when the outputs have various levels of one per rev noise in addition to the 10% random noise. Again τ is set at 10 and the frequency range of interest is set at $0.4 < \omega < 1.2$. A 10% one per rev noise causes a large error in the estimates of the frequencies and dampings of the system modes.

Next, the frequency range of interest is reduced to $0.4 < \omega < 0.95$ and $1.05 < \omega < 1.20$ to reject the one per rev noise. The new estimates are shown in Table 3.7. These estimates are more accurate than the estimates of Table 3.6.

Table 3.4

Estimates of Poles and Zeroes of Transfer Functions for Varying Sets of Outputs Used in Estimation

| | SIMULATION | ζ_{1c} | ζ_{1s} | y | ζ_{1c} AND ζ_{1s} | ζ_{1s} AND y | ζ_{1c} , ζ_{1s} , AND y |
|------------------------------|--------------------|--------------------|--------------------|---------------------|-------------------------------|--------------------|-------------------------------------|
| POLES | $-.023 \pm .503j$ | $-.0220 \pm .500j$ | $-.0216 \pm .507j$ | $-.0233 \pm .503j$ | $-.0233 \pm .504j$ | $-.0228 \pm .502j$ | $-.0233 \pm .503j$ |
| | $-.224 \pm .807j$ | $-.237 \pm .910j$ | $-.240 \pm .762j$ | $-.0401 \pm .858j$ | $-.211 \pm .838j$ | $-.178 \pm .878j$ | $-.221 \pm .864j$ |
| | $-.287 \pm 1.164j$ | $-.365 \pm 1.30j$ | $-.263 \pm 1.04j$ | $-.0167 \pm 1.11j$ | $-.237 \pm 1.14j$ | $-.192 \pm 1.20j$ | $-.267 \pm 1.15j$ |
| $\frac{\zeta_{1c}(s)}{F(s)}$ | -1.25 | | | | | | |
| | .75 | $.0109 \pm .341j$ | | | $.393 \pm .221j$ | | $-.0130$ |
| | 0.0 | $1.00 \pm 1.21j$ | | | $-.612 \pm .396j$ | | $.114, .514$ |
| GAIN | 0.0 | -4.05 | | | -7.58 | | $-1.64 \pm 1.44j$ |
| $\frac{\zeta_{1s}(s)}{F(s)}$ | .0345 | $-.00914$ | | | $+ .00390$ | | $+ .00907$ |
| | -.25 | | | | 3.11 | | |
| | 0.0 | | $-.205 \pm .498j$ | | $-.0836$ | $.0929 \pm .300j$ | $.667 \pm .205j$ |
| ZEROES | 0.0 | | $-.514$ | | $.156$ | $-1.00 \pm 1.30j$ | $-.589$ |
| GAIN | 0.0 | | $.604 \pm .538j$ | | $-.529$ | -28.71 | $-.0387$ |
| $\frac{Y(s)}{F(s)}$ | .069 | | $-.0458$ | | -1.65 | | 7.47 |
| | | | | | $-.0067$ | $.000582$ | $-.00156$ |
| | $-.271 \pm 1.00j$ | | | $-.0293 \pm .864j$ | | $-.207 \pm .916j$ | $-.245 \pm .937j$ |
| ZEROES | $-.229 \pm 1.00j$ | | | $-.00250 \pm 1.10j$ | | $-.172 \pm 1.12j$ | $-.202 \pm 1.05j$ |
| GAIN | .0345 | | | 14.68 | | 7.15 | 15.0 |
| | | | | $-.00193$ | | $-.00392$ | $-.00194$ |

Table 3.5

Effect of Length of Data Estimates of Poles and Zeros of Transfer Function

| | | SIMULATION | 128 POINTS | 256 POINTS | 512 POINTS |
|------------------------------|---------|---|--|--|--|
| POLES | | $-.0230 \pm .503j$ $-.224 \pm .867j$ $-.287 \pm 1.164j$ | $-.0389 \pm .496j$ $-.223 \pm .855j$ $-.308 \pm 1.13j$ | $-.0232 \pm .503j$ $-.235 \pm .862j$ $-.307 \pm 1.13j$ | $-.0233 \pm .503j$ $-.221 \pm .864j$ $-.267 \pm 1.15j$ |
| $\frac{\zeta_{1c}(s)}{F(s)}$ | ZERONES | -1.25 | -.0445 | -.185 | -.0130 |
| | | .75 | $-.382 \pm .337j$ | .238 | .114 |
| | | 0.0 | .967 | .507 | .513 |
| | | 0.0 | 4.95 | -23.3 | $-1.64 \pm 1.44j$ |
| GAIN | | .0345 | -.0119 | .00241 | .00907 |
| $\frac{\zeta_{1s}(s)}{F(s)}$ | ZERONES | -1.25 | .314 | .264 | $.667 \pm .205j$ |
| | | 0.0 | $-.208 \pm .433j$ | $-.200 \pm .273$ | -.589 |
| | | 0.0 | 3.97 | -2.91 | -.0387 |
| | | 0.0 | 4.27 | 3.15 | 7.47 |
| GAIN | | .069 | -.00562 | -.00871 | -.00156 |
| $\frac{y(s)}{F(s)}$ | ZERONES | $-.271 \pm 1.00j$ | $-.218 \pm .819j$ | $-.297 \pm .830j$ | $-.245 \pm .937j$ |
| | | $-.229 \pm 1.00j$ | $-.118 \pm 1.08j$ | $-.135 \pm 1.05j$ | $-.202 \pm 1.05j$ |
| | | | 1.78 | 4.32 | 15.0 |
| | | | | | |
| GAIN | | .0345 | -.0308 | -.0124 | -.00194 |

Table 3.6

Effect of 1/Rev Discrete Frequency Noise on Estimates of Poles and Zeros (Random Noise 10%, $\tau = 10$, $.4 < \omega < 1.2$)

| | | SIMULATION | 50% 1/REV NOISE | 20% 1/REV NOISE | 10% 1/REV NOISE | 1% 1/REV NOISE |
|------------------------------|---------|---|---|--|--|--|
| POLES | | $-.0230 \pm .503j$ $-.224 \pm .867j$ $-.287 \pm 1.164j$ | $-.0350 \pm .497j$ $-.0621 \pm 1.00j$ -.868 1.17 | .113 $-.0286 \pm .497j$ $-.144 \pm .988j$ -.693 | $-.0232 \pm .502j$ $-.416 \pm .726j$ $-.213 \pm .993j$ | $-.0233 \pm .503j$ $-.227 \pm .864j$ $-.278 \pm 1.14j$ |
| $\frac{\zeta_{1c}(s)}{F(s)}$ | ZERONES | -1.25 | $.171 \pm .591j$ | .0748 | $-.314 \pm .324j$ | -.0120 |
| | | .75 | $-.307 \pm .954j$ | $-.846 \pm .223j$ | $.310 \pm .422j$ | .110 |
| | | 0.0 | 1.79 | $.259 \pm .593j$ | -7.91 | .520 |
| | | 0.0 | | | | $-2.16 \pm 1.06j$ |
| GAIN | | .0345 | .0817 | .0490 | .00826 | .00727 |
| $\frac{\zeta_{1s}(s)}{F(s)}$ | ZERONES | -1.25 | -.300 | $.211 \pm .492j$ | $-.176 \pm .276j$ | $.531 \pm .174j$ |
| | | 0.0 | $.204 \pm .619j$ | $-.318 \pm .417j$ | .336 | -.473 |
| | | 0.0 | $-.348 \pm .987j$ | 2.94 | -7.59 | -.354 |
| | | | | | 1.31 | 5.12 |
| GAIN | | .069 | .148 | -.0281 | -.0315 | -.00264 |
| $\frac{y(s)}{F(s)}$ | ZERONES | $-.271 \pm 1.00j$ | $.0514 \pm .918j$ | .217 | $-.550 \pm .689j$ | $-.269 \pm .963j$ |
| | | $-.229 \pm 1.00j$ | -.849 | $-.0514 \pm .942j$ | $-.101 \pm .956j$ | $-.198 \pm 1.01j$ |
| | | | $.986 \pm 1.58j$ | -.942 | -37.8 | 16.17 |
| | | | | -77.16 | | |
| GAIN | | .0345 | -.0165 | .000385 | .000733 | -.00180 |

Table 3.7

Effect of 1/Rev Discrete Frequency Noise on Estimates of Poles and Zeros (Random Noise 10%, $\tau = 10$, $.4 < \omega < .95$, $1.05 < \omega < 1.20$)

| | | SIMULATION | 50% 1/REV NOISE | 20% 1/REV NOISE | 10% 1/REV NOISE | 1% 1/REV NOISE |
|------------------------------|--------|--|---|--|--|--|
| POLES | | $-.0230 \pm .503j$ $-.224 \pm .867j$ $-.287 \pm 1.164j$ -1.25 | $-.0223 \pm .504j$ $-.182 \pm .660j$ $-.184 \pm 1.02j$ $-.130 \pm .542j$ | $-.0232 \pm .503j$ $-.240 \pm .802j$ $-.238 \pm 1.06j$ $.356 \pm .281j$ | $-.0234 \pm .503j$ $-.223 \pm .834j$ $-.247 \pm 1.10j$ $.354 \pm .179j$ | $-.0235 \pm .503j$ $-.207 \pm .850j$ $-.237 \pm 1.14j$ -1.191 |
| $\frac{\zeta_{1c}(s)}{F(s)}$ | ZEROES | .75 0.0 0.0 | $.297 \pm .506j$ -3.28 | $-.359 \pm .388j$ -6.75 | $-.351$ -8.63 -3.56 | $.344 \pm .132j$ -1.29 \pm 1.21j |
| | GAIN | .0345 | .0197 | .00654 | .00831 | .0120 |
| $\frac{\zeta_{1s}(s)}{F(s)}$ | ZEROES | -.25 0.0 0.0 | $.150 \pm .344j$ $-.167 \pm .618j$ 1.65 1.46 | $-.0516$.275 $-.444 \pm .519j$ 2.00 | $.0463$.131 $-.666 \pm .474j$ | $.0883 \pm .179j$ $-.953 \pm .495j$ 3.28 |
| | GAIN | .069 | -.0373 | -.0253 | -.0153 | -.00706 |
| $\frac{v(s)}{F(s)}$ | ZEROES | $-.271 \pm 1.00j$ $-.229 \pm 1.00j$ | $-.185 \pm .605j$ $-.0183 \pm .940j$ 5.43 | $-.358 \pm 784j$ $-.0768 \pm .967j$ 7.22 | $-.347 \pm .910j$ $-.115 \pm .973j$ 14.98 | $-.172 \pm .940j$ $-.254 \pm 1.06j$ -246.8 |
| | GAIN | .0345 | -.0800 | -.00452 | -.00193 | .000109 |

3.6 APPLICATION OF THE MODAL ESTIMATION ALGORITHM TO SIMULATION DATA OF A CANTILEVER WING WITH ROTORS AT EACH WING TIP

The symmetric motions of a cantilever wing with rotors at each wingtip are approximately described by a 9-DOF model discussed by Johnson [5]. Of the four possible inputs, we will restrict our discussion to the collective pitch input, θ_0 . Two outputs which will be considered are the vertical wing bending, q_1 , and chordwise wing bending, q_2 . The poles of the system and the zeros between the outputs q_1 and q_2 and the collective pitch input are shown in Table 3.8. Note that in the q_1/θ_0 transfer function, four complex zero pairs approximately cancel four pole pairs, while in the q_2/θ_0

Table 3.8
Symmetric Modes of a Cantilever Wing

| MODE | POLE | NATURAL FREQUENCY* | DAMPING FACTOR, ζ |
|-------------------------------------|-----------------------|--------------------|-------------------------|
| Coupling (β_0) | $-0.2095 \pm 2.5548j$ | 2.5633 | .08174 |
| Upper Inplane (ζ_{+1}) | $-.07283 \pm 2.4345j$ | 2.4355 | .0299 |
| Upper Out-of-Plane (β_{+1}) | $-.3016 \pm 1.8546j$ | 1.8789 | .1605 |
| Wing Torsion (ρ) | $-.07785 \pm 1.344j$ | 1.3462 | .0578 |
| Wing Chordwise (q_{w2}) | $-.02839 \pm .6661j$ | .6667 | .0426 |
| Wing Vertical (q_{w1}) | $-.01914 \pm .3985j$ | .399 | .04798 |
| Lower Inplane (ζ_{-1}) | $-.08848 \pm .3356j$ | .3471 | .255 |
| Lower Out-of-Plane (β_{-1}) | $-.312 \pm .1763j$ | .3584 | .871 |
| ζ_0 | -.1445 | | |
| ψ_s | -.04319 | | |

| | OUTPUT q_1 | OUTPUT q_2 |
|-------|---------------------|--------------------|
| ZEROS | $-.0758 \pm 2.435j$ | $-.329 \pm 8.73j$ |
| | $.0111 \pm 2.05j$ | $-.0673 \pm 2.43j$ |
| | $-.297 \pm 1.838j$ | $-.303 \pm 1.85j$ |
| | $-.141 \pm 1.069j$ | $-.0760 \pm 1.34j$ |
| | $.0762 \pm .621j$ | $-.311 \pm .173j$ |
| | $-.340 \pm .145j$ | $-.0196 \pm .399j$ |
| | $-.0939 \pm .323j$ | $-.0890 \pm .336j$ |
| | $-.0159$ | $-.00305$ |
| | 0.0 | 0.0 |
| GAIN | -.0121 | -.00198 |

*Per rev

transfer function, six zero pairs approximately cancel six pole pairs. In fact, in the frequency range of interest, $0.2 < \omega < 0.75$, the transfer functions q_1/θ_0 and q_2/θ_0 may be written as (see Eqs. (3.10) and (3.11))

$$\frac{q_1(s)}{\theta_0(s)} = \frac{.00498(s - .0762 + .621j)}{(s + .0284 \pm .666j)(s + .0191 \pm .3985j)}$$

$$\frac{q_2(s)}{\theta_0(s)} = \frac{.0230}{(s + .0284s \pm .666j)}$$

A simulation was conducted using a sine sweep collective pitch input. The outputs q_1 and q_2 and the input θ_0 were sampled at intervals of 0.5. 512 samples are used in the identification. The frequency range of interest is $0.2 < \omega < 0.75$ and a 5-DOF model is specified. The identified poles and zeros for two cases are given in Table 3.9. It is clear that many estimated poles are close to estimated zeros. When output

Table 3.9
Identified Poles and Zeros for Cantilever
Wing Simulation Data
5 Modes, $\tau = 10$, 512 Points, 0.5 Sec Sampling
 $0.2 < \omega < 0.75$

| | | SIMULATION | OUTPUTS USED IN ESTIMATION | |
|------------------------------|-------|--------------------|----------------------------|--------------------|
| | | | q_2 | q_1 AND q_2 |
| POLES | | $-.0284 \pm .666j$ | $-.0257 \pm .566j$ | $-.0283 \pm .661j$ |
| | | $-.0191 \pm .398j$ | $.0068 \pm .437j$ | $-.0137 \pm .395j$ |
| | | $-.0885 \pm .336j$ | | |
| | | $-.312 \pm .176j$ | $-.036 \pm .156j$ | |
| | | $-.144$ | | $-.011 \pm .129j$ |
| | | $-.0432$ | | |
| | | | $0.0 \pm .694j$ | $-.002 \pm .691j$ |
| | | | $.011 \pm .616j$ | $.015 \pm .532j$ |
| $\frac{q_2(s)}{\theta_0(s)}$ | ZEROS | $-.0196 \pm .399j$ | -2.72 | -2.81 |
| | | $-.0311 \pm .173j$ | $0.0 \pm .691j$ | $-.005 \pm .637j$ |
| | | $-.0889 \pm .336j$ | | |
| | | 0.0 | $.010 \pm .615j$ | $.0119 \pm .532j$ |
| | 0.0 | $.0028 \pm .435j$ | $-.0193 \pm .393j$ | |
| | | $0.0 \pm .155j$ | $.0318 \pm .154j$ | |
| | GAIN | | .00793 | .00799 |
| $\frac{q_1(s)}{\theta_0(s)}$ | ZEROS | $.0762 \pm .621j$ | | -2.06 |
| | | $-.340 \pm .145j$ | | $-.0037 \pm .692j$ |
| | | $-.0939 \pm .323j$ | | $.0671 \pm .623j$ |
| | | $-.0159$ | | $.0154 \pm .536j$ |
| | 0.0 | | $.0382 \pm .150j$ | |
| | GAIN | | | -.00206 |

q_2 is used in estimation, the estimated transfer function is approximately

$$\frac{q_2(s)}{\theta_0(s)} = \frac{.0216}{(s + .0257 \pm .666j)}$$

When the outputs q_1 and q_2 are used in estimation, the transfer functions may be simplified to

$$\frac{q_1(s)}{\theta_0(s)} = - \frac{.00424(s - .0671 + .623j)}{(s + .0283 \pm .661j)(s + .0137 \pm .395j)}$$

$$\frac{q_2(s)}{\theta_0(s)} = \frac{.0225}{(s + .0283 \pm .661j)}$$

This shows that when the specified model order is much higher than necessary, enough poles and zeros cancel out to give a low order transfer function. Also, the estimate of the chord-wise wing bending mode improves when both outputs q_1 and q_2 are used in estimation.

3.7 CONCLUSIONS

A new algorithm based on the instrumental variables approach is developed for dynamic stability estimation from input/output signals. A preliminary evaluation of the algorithm on simulation data of low order models demonstrates its effectiveness in estimating frequencies and damping factors of important modes.



CHAPTER IV APPLICATION TO XV-15 SIMULATION MODEL

4.1 INTRODUCTION

The on-line modal identification algorithm of Chapter III was demonstrated on low-order models. This chapter describes the application of this algorithm to high-order simulated data from an XV-15 math model and examines both algorithm characteristics per se, as applied to this model, and its ability to identify XV-15 aeroelastic modes of interest across the aircraft's flight envelope.

The following sections present a description of the XV-15 math model used in this investigation, and discuss the ability of the algorithm to identify prominent XV-15 structural modes from measurements of the model states or, alternatively, from measurements (obtained from a typical wind tunnel test) comprised of one or several model states. The math model is considered in Section 4.2. The application of the algorithm to time histories of symmetric and antisymmetric motions is described in Sections 4.3 and 4.4., respectively, and a summary of results is given in Section 4.5.

4.2 XV-15 ANALYTIC MODEL

The XV-15 model used in this study is a linear simulation of the elastic airplane mounted on the model support system of the NASA full-scale (40- x 80-ft) wind tunnel. The model, furnished by NASA and described in Ref. 5, utilizes predicted XV-15 structural characteristics and configuration parameters, and contains a total of 13 degrees-of-freedom: ten of the aircraft and three of the support system, in each of a set of symmetric equations and a set of antisymmetric equations.

~~PRECEDING PAGE BLANK NOT FILMED~~

These degrees of freedom, and their associated modes, are identified in Appendix C, Table C.1. Since each equation set contains 13 modes, it has a characteristic equation of 26th order. This model has produced, in previous investigations, results showing very good agreement with experimental data [3-5].

Typical XV-15 dynamic characteristics are shown by the symmetric roots plotted in Figure 4.1. A number of low-damped oscillatory roots are seen along the $j\omega$ -axis; these roots include the wing bending and torsion and wind tunnel balance modes. Higher-damped rotor modes are seen farther left of the $j\omega$ -axis. Typical damping ratios of the former are on the order of 1 to 2%. These roots change with airspeed and airplane configuration (pylon angle), and as illustrated by arrows in this figure, tend to move toward the $j\omega$ -axis with increasing speed.

NASA-derived dynamic model data used here consists of the coefficient matrices of the dynamical equation, in NASA formulation,

$$A_2\ddot{x} + A_1\dot{x} + A_0x = Bu \quad (4.1)$$

where x and u are described in Table C.2 (Appendix C), the A_0 , A_1 , and A_2 matrices contain system aerodynamic, structural, and inertial characteristics, and B is a control or disturbance input effectiveness matrix. The elements of these matrices vary according to flight condition.

This equation may be easily rewritten to treat the degrees of freedom as state variables:

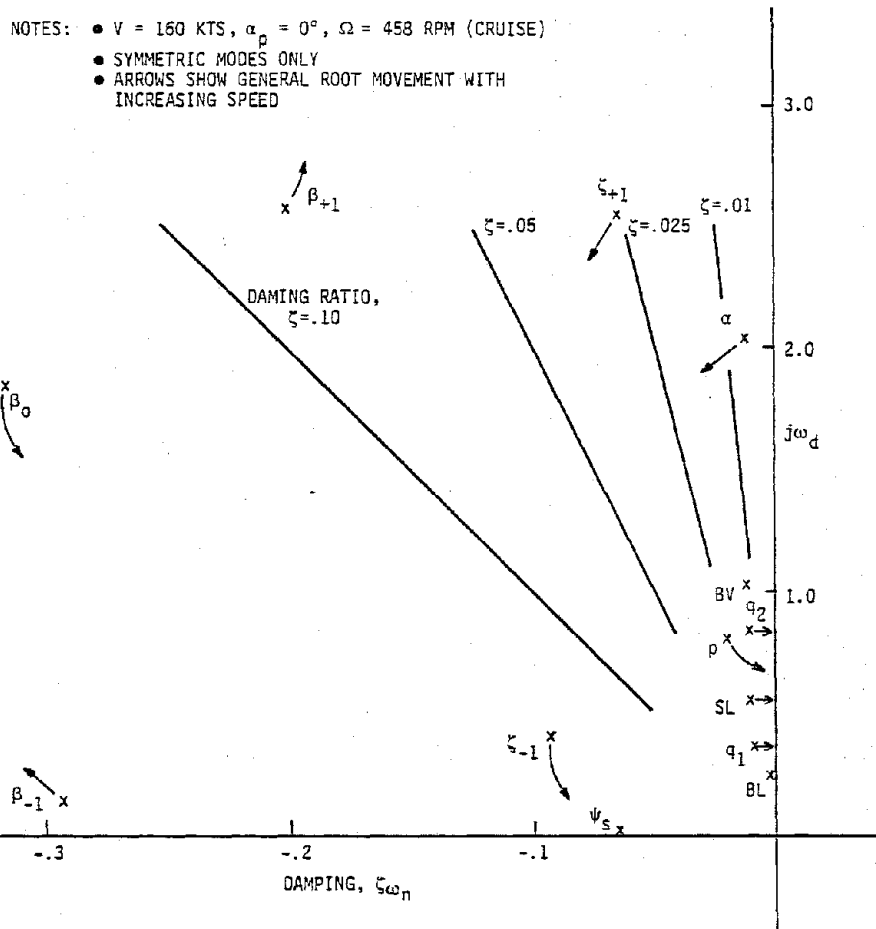


Figure 4.1 Typical Characteristic Root Locations, 13 Degree-of-Freedom Model; XV-15 Plus Wind Tunnel Supports

$$\dot{\underline{x}} = \underline{F}\underline{x} + \underline{G}\underline{u} + \underline{\Gamma}g \tag{4.2}$$

$$y = \underline{H}\underline{x}$$

where \underline{x} , y , \underline{u} , and g are defined in Table C.2 (Appendix C), and \underline{F} , \underline{G} , $\underline{\Gamma}$, and \underline{H} are the system, control, gust disturbance, and observation matrices, respectively. From this analytic formulation are computed the system eigenvalues,

transfer functions, and time histories used in this study. The analytic results are, of course, identical to those from the NASA equation formulation.

4.3 APPLICATION TO XV-15 SIMULATION MODEL: SYMMETRIC MODES

Six flight conditions representative of XV-15 free-air or wind tunnel testing are selected as test points at which the XV-15's dynamic characteristics would be computed and the algorithm's effectiveness in identifying roots investigated. The six flight conditions are shown in Table 4.1. This exercise applies the algorithm to time history data containing thirteen dynamic modes and is representative of the application for which the algorithm was developed.

The approach taken here in generating and identifying XV-15 dynamic characteristics is illustrated in Figure 4.2, indicating that simulation time histories are computed as a substitute for experimental data. The objective of this exercise is twofold: (1) to investigate the basic characteristics of the algorithm per se and the effects of algorithm

Table 4.1
Selected XV-15 Flight Conditions

| CONDITION | V _{KTS} | α_p (°) | Ω , RPM |
|-----------|------------------|----------------|----------------|
| 1 | 0 | 90 | 565 |
| 2 | 80 | 82.3 | 565 |
| 3 | 100 | 60 | 565 |
| 4 | 120 | 30 | 565 |
| 5 | 160 | 0 | 458 |
| 6 | 200 | 0 | 458 |

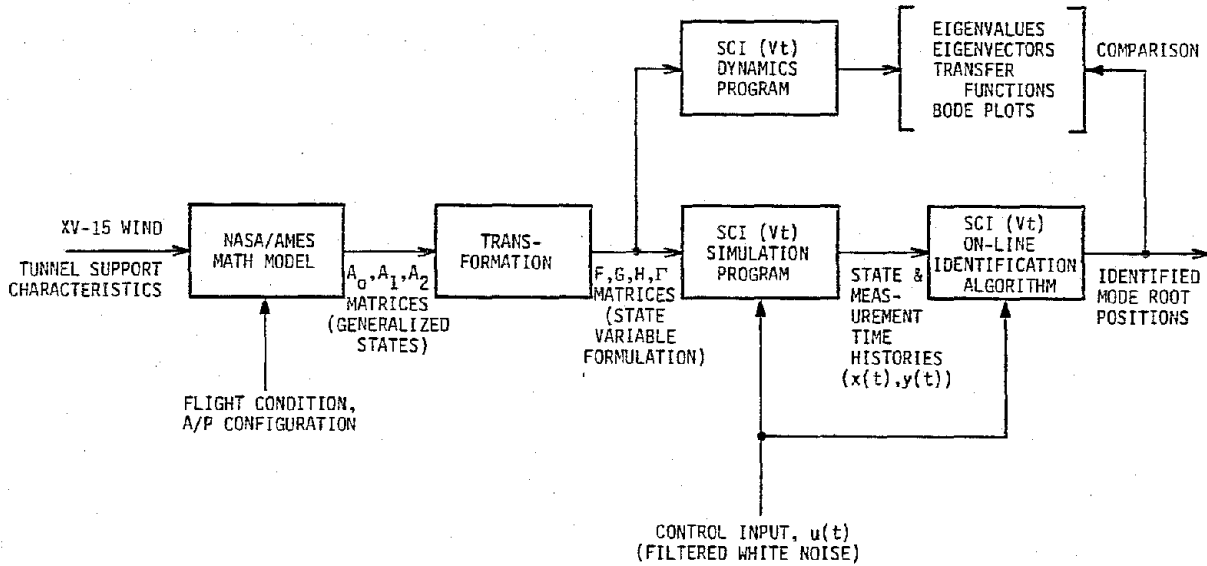


Figure 4.2 XV-15 Simulation Mode Identification Procedure

modifications on mode identifications, when applied to high-order data; and (2) to investigate the algorithm's ability to identify specific XV-15 modes that would be of interest in a test situation. In each case, the results of interest are the accuracy of identification of frequency and damping of critical modes and the overall placement of transfer function poles and zeros, judged by comparison to the analytical roots determined from the state equations. In the first part, measurements of airplane states are used directly for identification; in the second, the time histories of horizontal and vertical wingtip deflections are computed and used as measurements, more realistically simulating experimentally available data.

To evaluate basic algorithm characteristics, the simulation model at flight condition 3 is excited by a random collective pitch input and the resulting time histories of wing vertical and chordwise bending motions (q_1 and q_2 , respectively) are used as measurements. The random control

input is white noise, filtered with a low pass Martin-Graham filter having a constant response up to 0.94 rad/sec and 1.57 rad/sec cutoff frequency. The measured input frequency spectrum is shown in Figure 4.3; the corresponding autocorrelation characteristics of the input time history are shown in Figure 4.4; and an example of this time history is shown in Figure 4.5.

It should be noted that all frequencies in this study are non-dimensionalized with respect to rotor RPM; thus, a frequency of 1 rad/sec actually represents a frequency of

$$\frac{\Omega \text{ (RPM)}}{60} \text{ Hz or } \frac{2\pi\Omega}{60} \text{ rad/sec, true scale.}$$

The effects of the following algorithm parameters are investigated: (1) assumed model order; (2) time delay parameter, τ ; (3) specified number of zeros; (4) the use of two measurements; (5) the effect of specified frequency range; and (6) the effect of various forms of scaling within the algorithm. The results obtained are as follows:

- (1) Model Order. Altering the number of poles and zeros specified for the algorithm (i.e., altering the number of degrees-of-freedom) changes the locations of all the roots. Figure 4.6 shows the effect of assumed model order on the damping of modes identified from q_1 and q_2 measurement time histories. Best identification of this system was obtained with modal orders of 8 to 12.
- (2) Time delay parameter. The recommended value of τ depends on model order and sampling interval, as

$$\tau = 2*n*\Delta t.$$

Figure 4.7 shows that using values smaller than recommended may lead to large errors in damping.

- (3) Number of zeros. The number of zeros specified is generally equal to, or one less than, the number of poles. The damping values are sensitive to this parameter, as seen in Figure 4.8, and different modes may be affected in different ways.

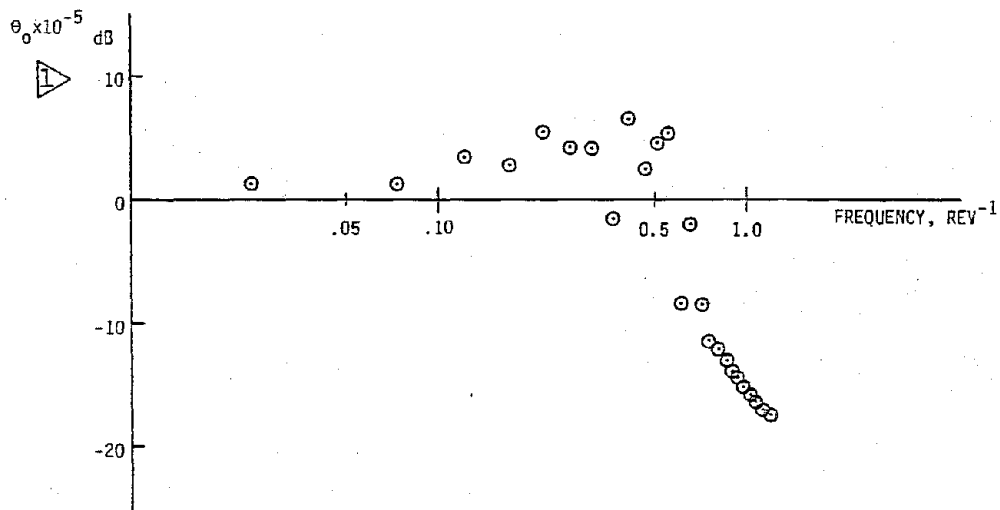


Figure 4.3 Measured Input Spectrum

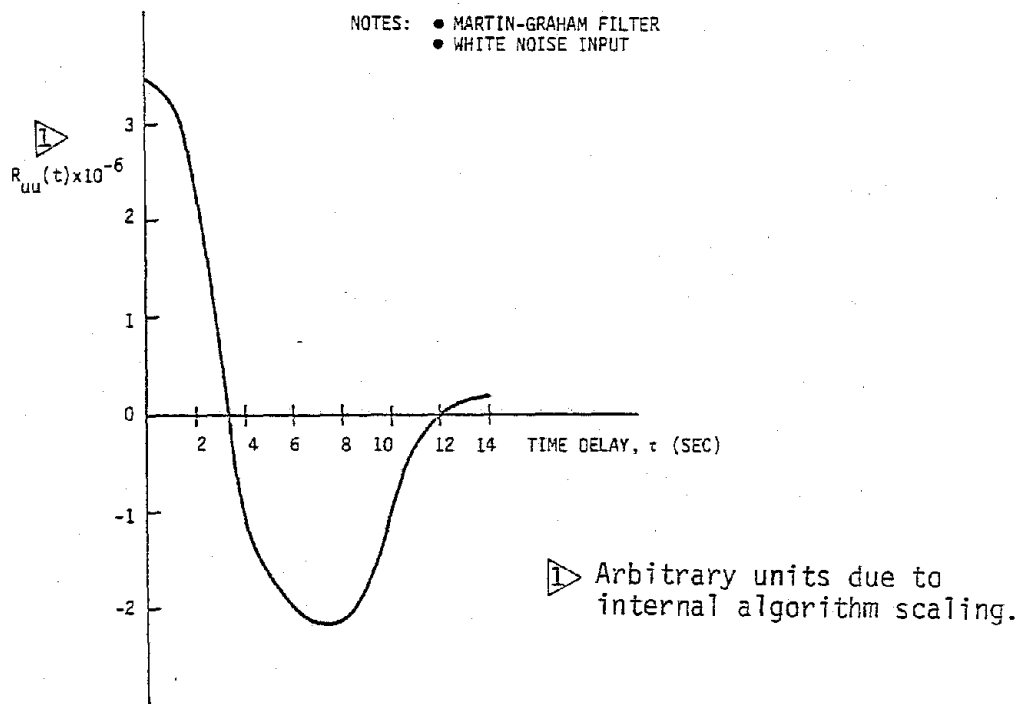


Figure 4.4 Measured Input Autocorrelation Function

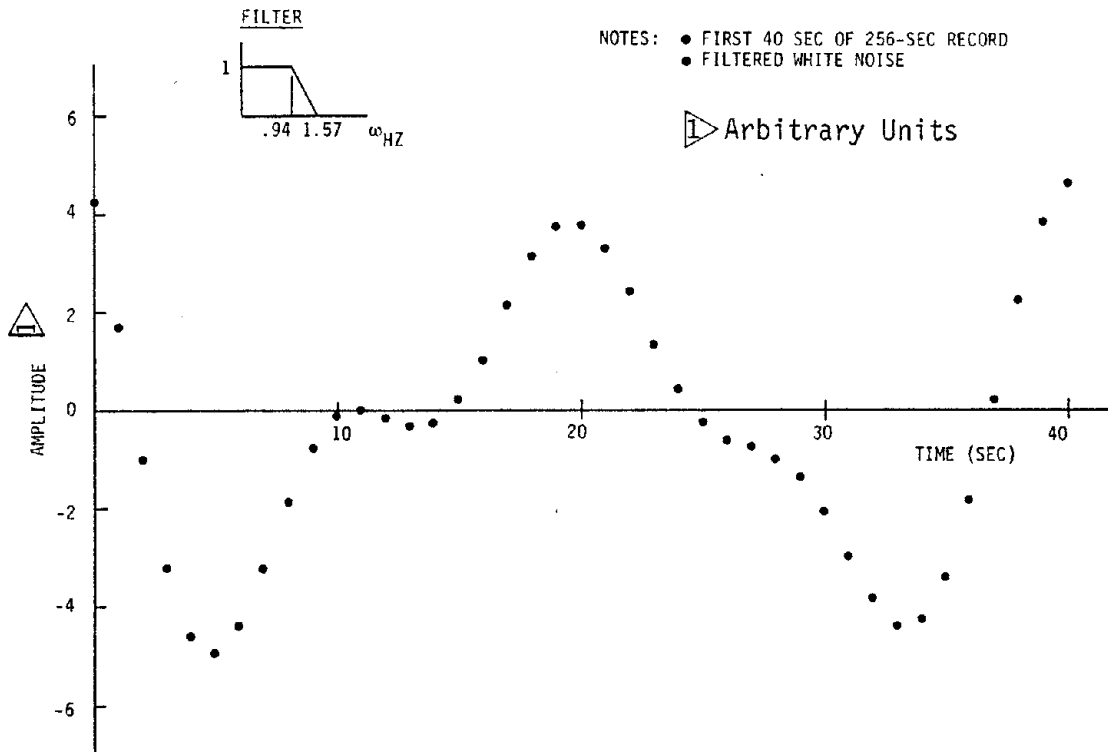


Figure 4.5 Example of Random Control Input Time History

- (4) Frequency range. Restricting the frequency range over which the algorithm identifies a model may improve the identification by eliminating extraneous frequencies, but it also reduces the amount of information available. The specified range is thus a compromise; in general, a wide range (e.g., $0.1 \leq \omega < 0.9$) is desirable, and frequency scaling in some instances yields improved results. This is discussed next.
- (5) Scaling. Because of several numerical operations performed in the algorithm, the magnitudes of the quantities considered can affect identification accuracy due to computer roundoff and program truncations. Specific conclusions are:
 - (a) Scaling FFT output within the algorithm by a large multiplicative constant may be required to ensure convergence of external equation-solving and rooting routines used by the algorithms implying the need to "tailor" the algorithm to

SYMBOLS:
 ○ q_2 MEASURED
 □ q_1 MEASURED

NOTES:
 ● NO. OF POLES = n
 ● NO. OF ZEROS = n
 ● $\tau = n$
 ● $\Delta t = 0.5$
 ● INPUT $\theta_0(t)$
 ● FREQUENCY RANGE $.2 \leq \omega \leq .65$

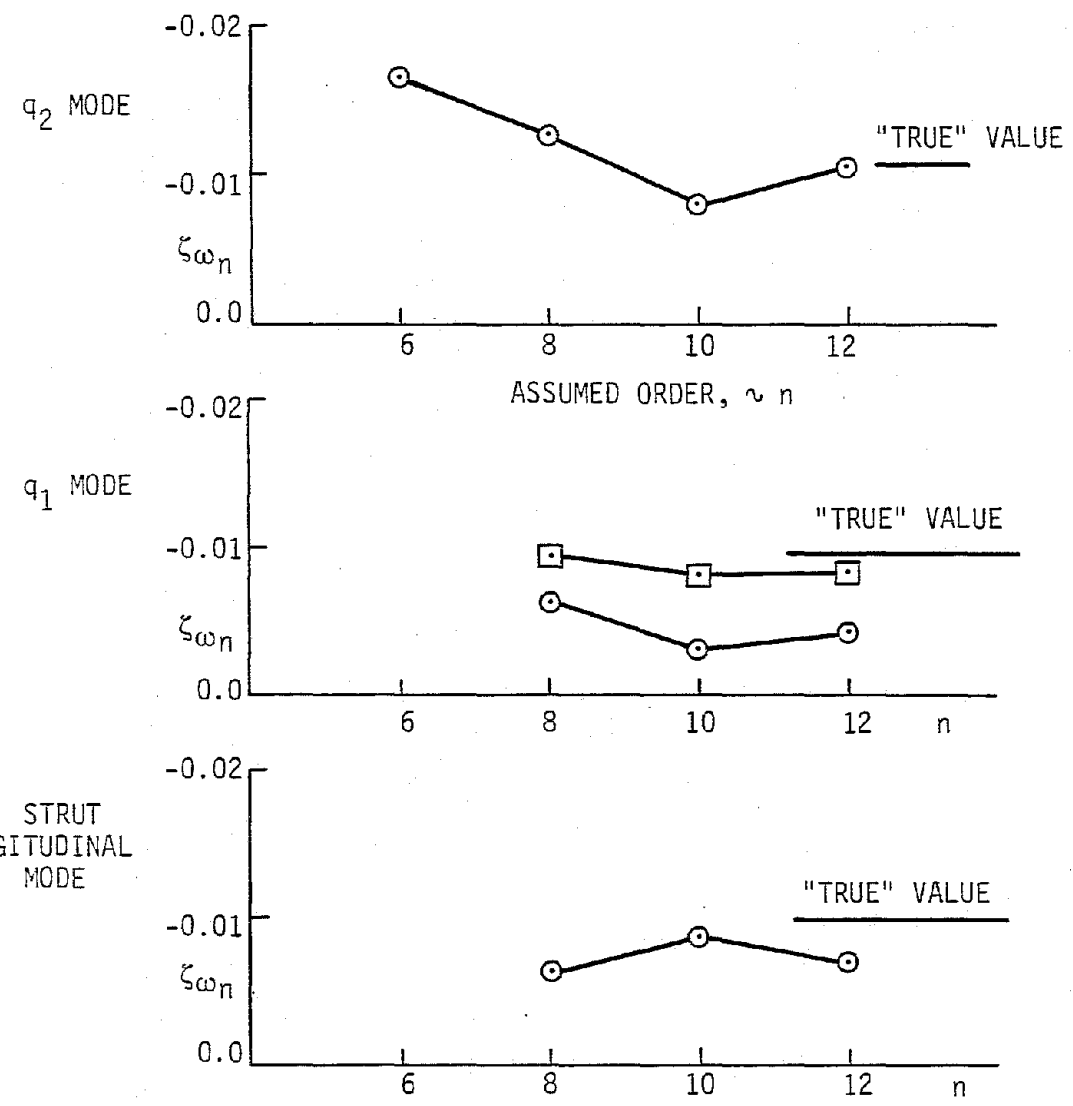


Figure 4.6 Effect of Assumed Model Order on Predicted Damping; 13 DOF Model

- NOTES:
- NO. OF POLES = 12
 - NO. OF ZEROS = 12
 - $\tau = 12$
 - INPUT $\theta_0(t)$
 - FREQUENCY RANGE $.2 \leq \omega \leq .65$

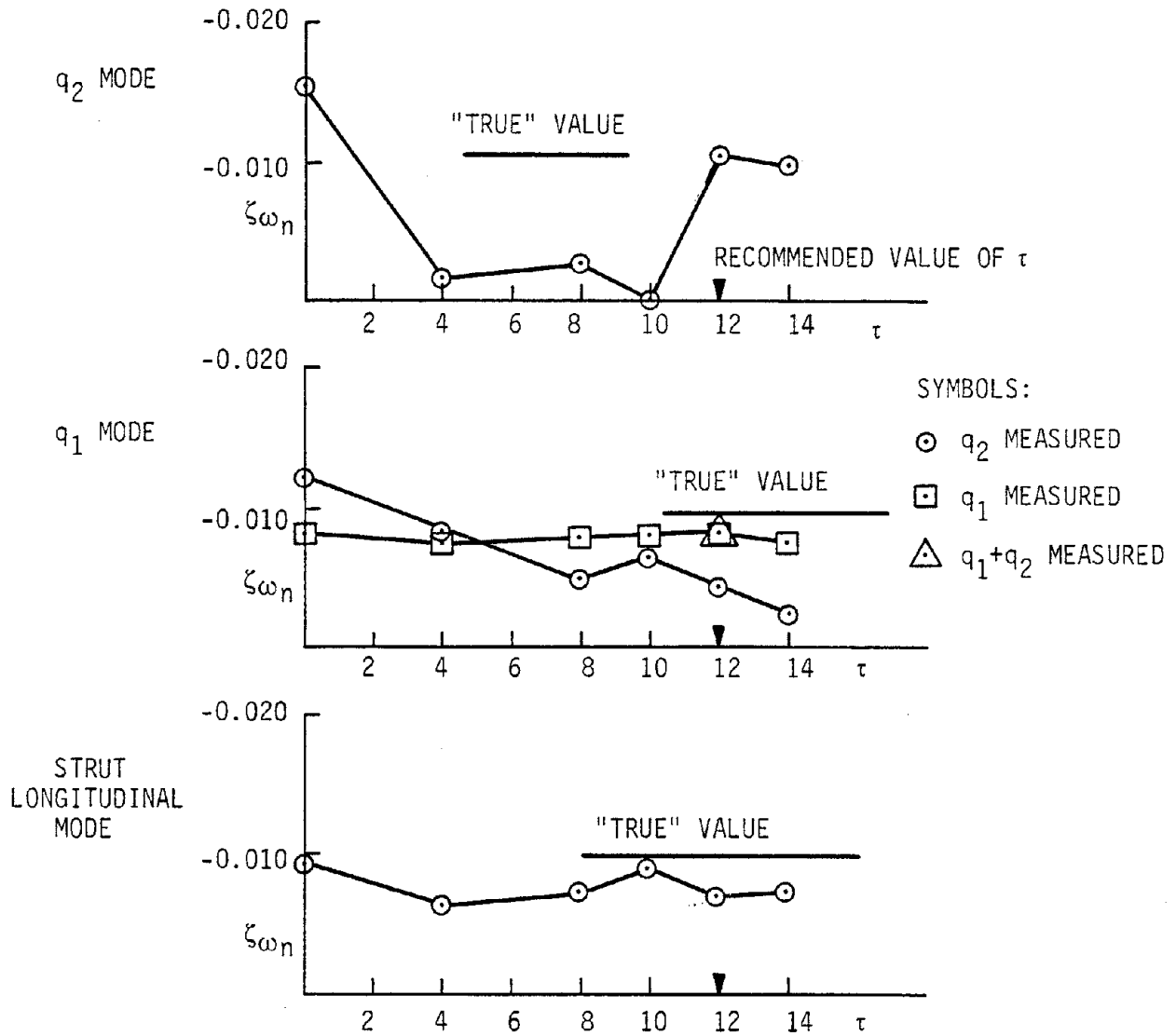


Figure 4.7 Effect of Specified Time Delay on Predicted Damping; 13 DOF Model

- NOTES:
- NO. OF POLES = 10
 - $\tau = 10$
 - $\Delta t = 0.5$
 - INPUT $\theta_0(t)$
 - FREQUENCY RANGE $.2 \leq \omega \leq .65$

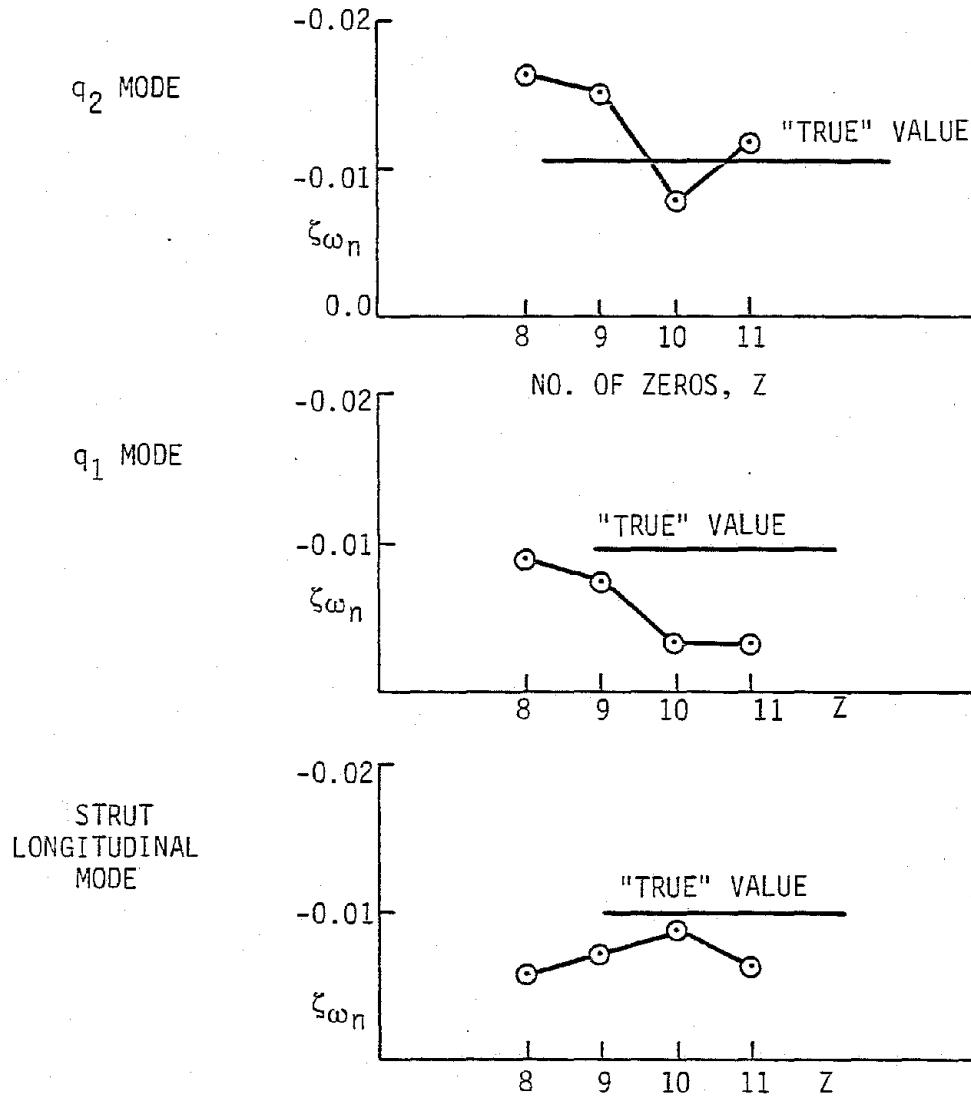


Figure 4.8 Effect of Specified Number of Zeros on Predicted Damping; 13 DOF Model.

the computer system it is run on. Further, scaling the measurement and control input FFT's by their respective RMS values was found to lead to a substantial increase in accuracy in the two-measurement case, as seen in Table 4.2.

- (b) Scaling the frequency range such that the maximum value is unity leads to better mode identification in some cases through computational improvement.
- (c) Scaling FFT output to give a higher weighting to data near the natural frequency of modes improves identification accuracy. This is illustrated by comparing the root predictions of Figure 4.9, without scaling, to those of Figure 4.23 (which will be discussed below) with such scaling.

Figures 4.10 through 4.17 show a series of trial identification runs using the q_2 measurement and varying the parameters discussed in items (1), (2), and (4) above, illustrate that, in this case (where the poles are well separated from other poles or zeros): (a) decreasing the frequency range improves the pole identifications, and (b) successive reductions in assumed model order yield nearly equivalent pole position estimates until the sixth-order model (three degrees-of-freedom) is reached, at which point the roots become poorly identified.

Table 4.2
Effect of Measurement Scaling

| MEASUREMENT | ORDER | q_1 | q_2 | SL |
|----------------------|-------|--------------|--------------|--------------|
| q_2 UNSCALED | 10 | -.0033+.295j | -.0080+.551j | -.0088+.392j |
| q_2 SCALED | | -.0035+.295j | -.0092+.591j | -.0092+.392j |
| $q_1 + q_2$ UNSCALED | 12 | -.0085+.291j | --- | --- |
| $q_1 + q_2$ SCALED | | -.0095+.294j | -.0031+.549j | -.0069+.396j |
| ANALYTIC VALUE | | -.0097+.292j | -.0106+.573j | -.0098+.397j |

NOTES:

- Z_{TIP}/δ_F TRANSFER FUNCTION
- FLT. CONDITION #3: TRANSITION
- $\alpha_p = 60^\circ$, $V = 100$ KTS, $\Omega = 565$ RPM
- $[\omega] =$ PER REV

SYMBOLS:

- ● ANALYTIC POLES, ZEROS
- x ○ IDENTIFIED POLES, ZEROS

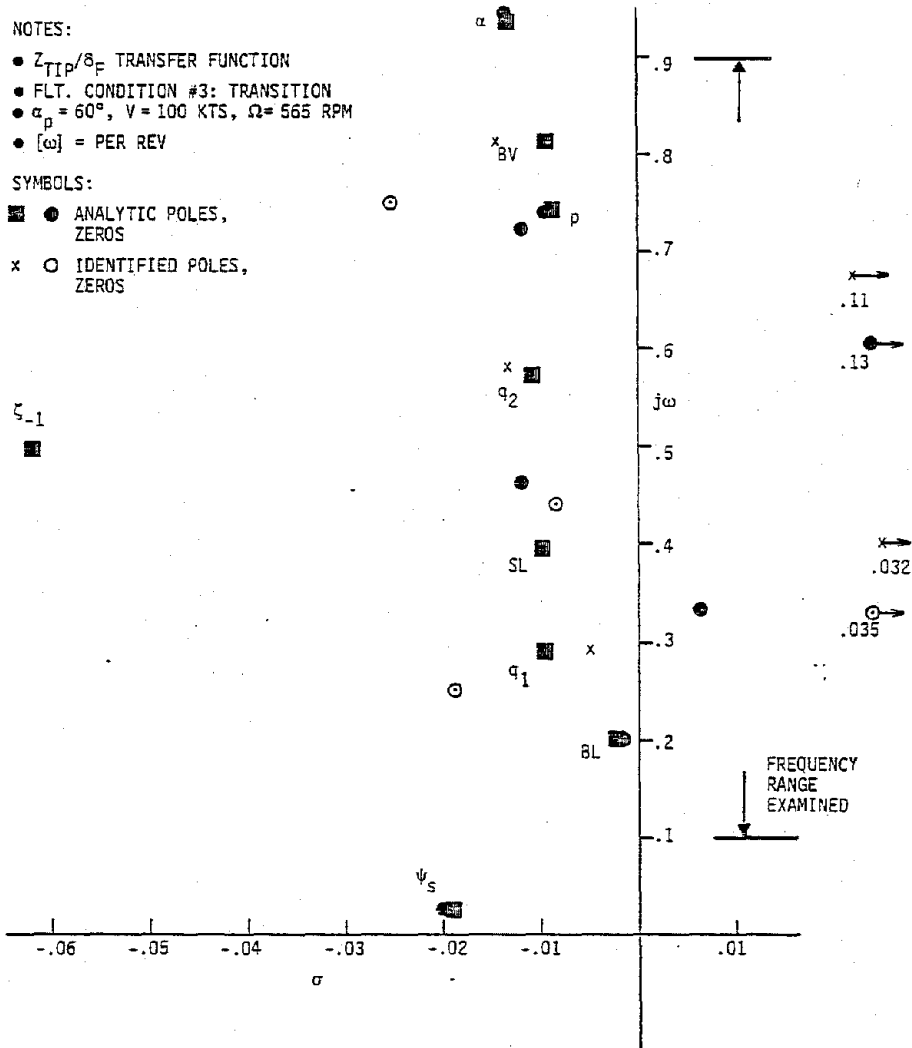


Figure 4.9 XV-15 Simulation Symmetric Mode Identification Without Magnitude Scaling (Compare to Fig. 4.22)

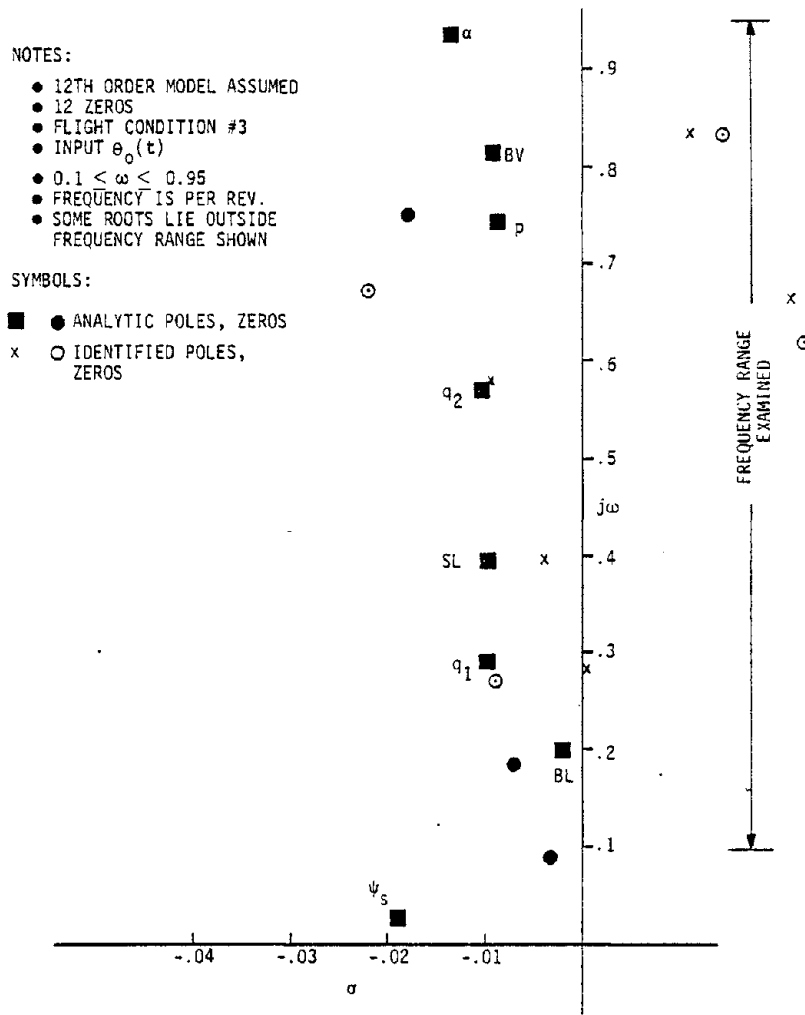


Figure 4.10 XV-15 Simulation Symmetric Mode Identification Based on q_2 Measurement

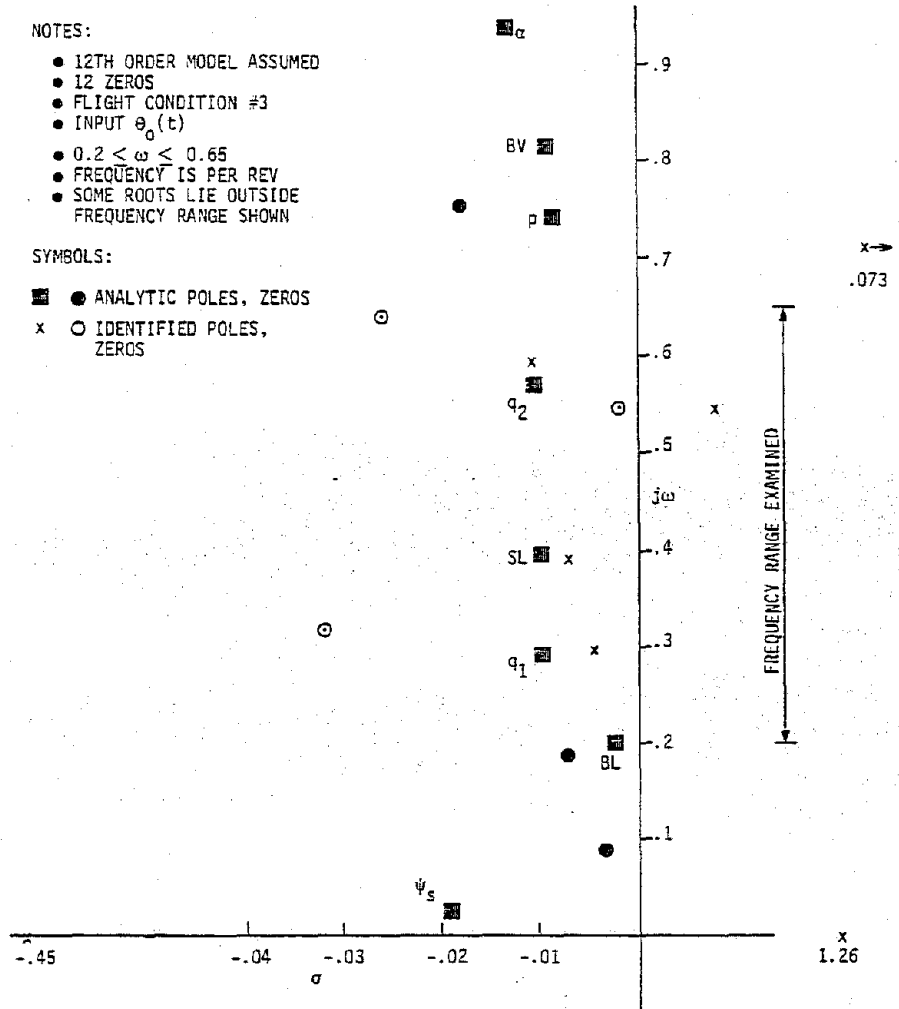


Figure 4.11 XV-15 Simulation Symmetric Mode Identification Based on q_2 Measurement: Effect of Reduced Frequency Range

NOTES:

- 12TH ORDER MODEL ASSUMED
- 11 ZEROS
- FLIGHT CONDITION #3
- INPUT $\theta_0(t)$
- $0.2 \leq \omega \leq 0.65$
- FREQUENCY IS PER REV.
- SOME ROOTS LIE OUTSIDE FREQUENCY RANGE SHOWN

SYMBOLS:

- ● ANALYTIC POLES, ZEROS
- x ○ IDENTIFIED POLES, ZEROS

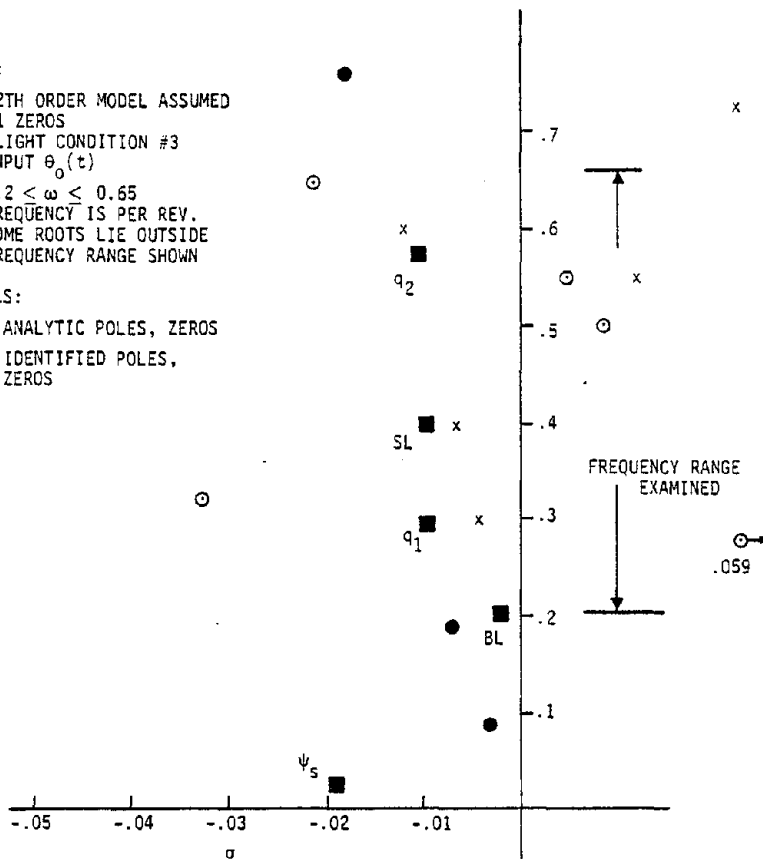


Figure 4.12 XV-15 Simulation Symmetric Mode Identification Based on q_2 Measurement: Varying Model Order

NOTES:

- 10TH ORDER MODEL ASSUMED
- 10 ZEROS
- FLIGHT CONDITION #3
- INPUT $\theta_0(t)$
- FREQUENCY IS PER REV.
- SOME ROOTS LIE OUTSIDE FREQUENCY RANGE SHOWN

SYMBOLS:

- ● ANALYTIC POLES, ZEROS
- x ○ IDENTIFIED POLES, ZEROS

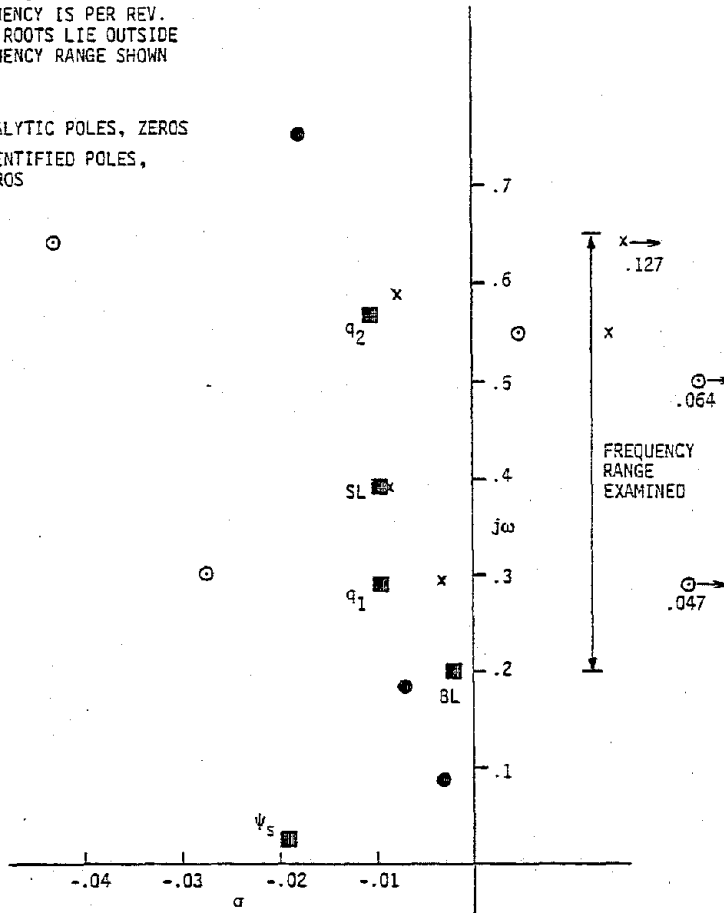


Figure 4.13 XV-15 Simulation Symmetric Mode Identification Based on q_2 Measurement: Varying Model Order

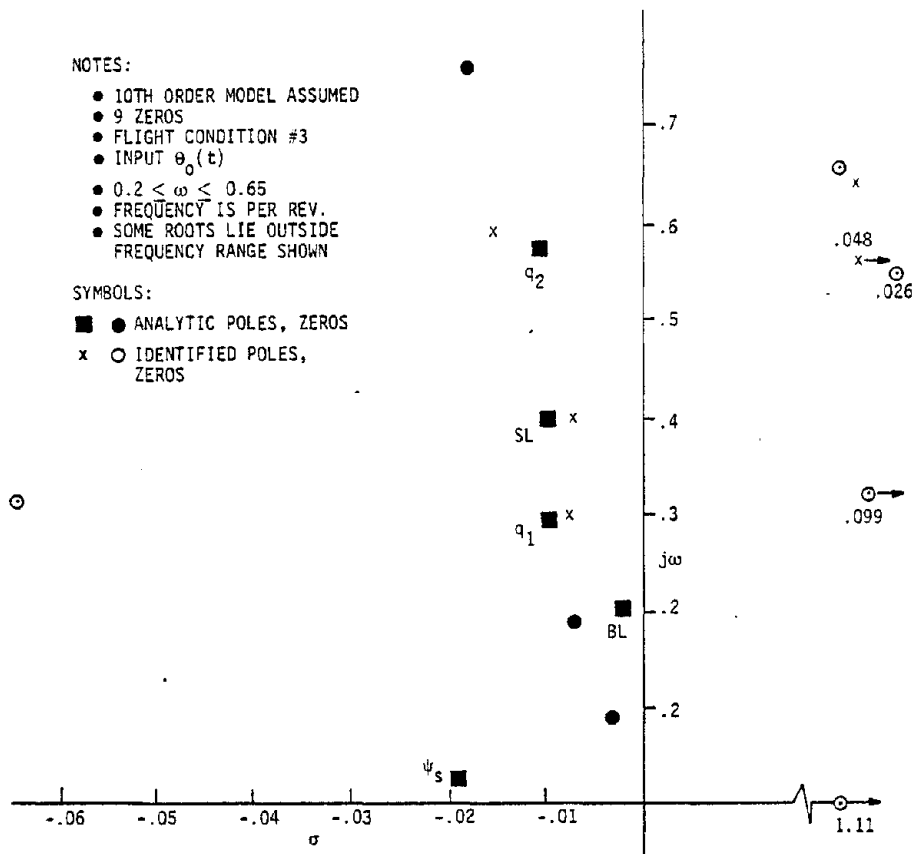


Figure 4.14 XV-15 Simulation Symmetric Mode Identification Based on q_2 Measurement: Varying Model Order

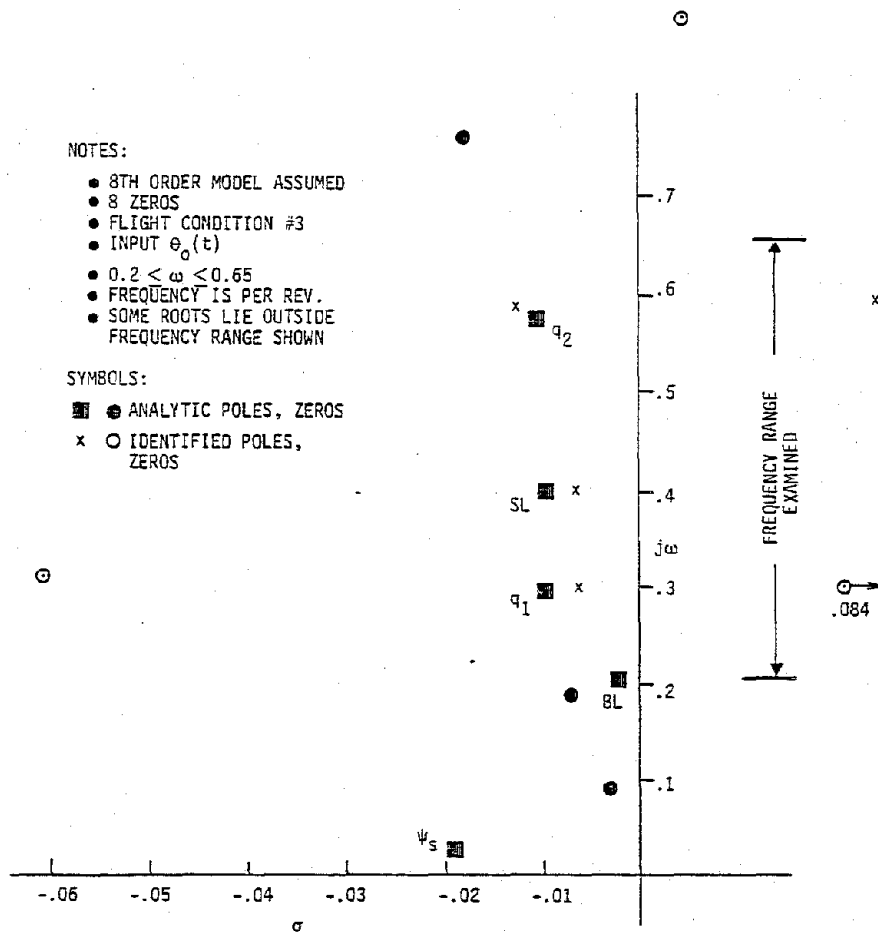


Figure 4.15 XV-15 Simulation Symmetric Mode Identification Based on q_2 Measurement: Varying Model Order

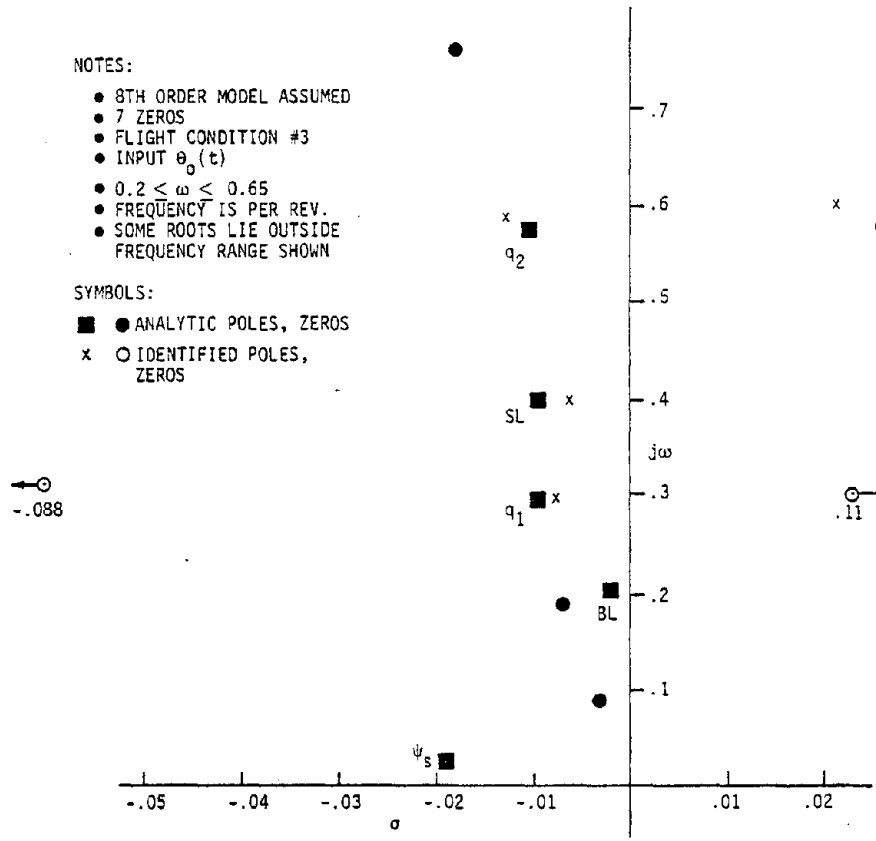


Figure 4.16 XV-15 Simulation Symmetric Mode Identification Based on q_2 Measurement: Varying Model Order

NOTES:

- 6TH ORDER MODEL ASSUMED
- 6 ZEROS
- FLIGHT CONDITION #3
- INPUT $\theta_0(t)$
- $0.2 < \omega < 0.65$
- FREQUENCY IS PER REV.
- SOME ROOTS LIE OUTSIDE FREQUENCY RANGE SHOWN

SYMBOLS:

- ● ANALYTIC POLES, ZEROS
- x ○ IDENTIFIED POLES, ZEROS

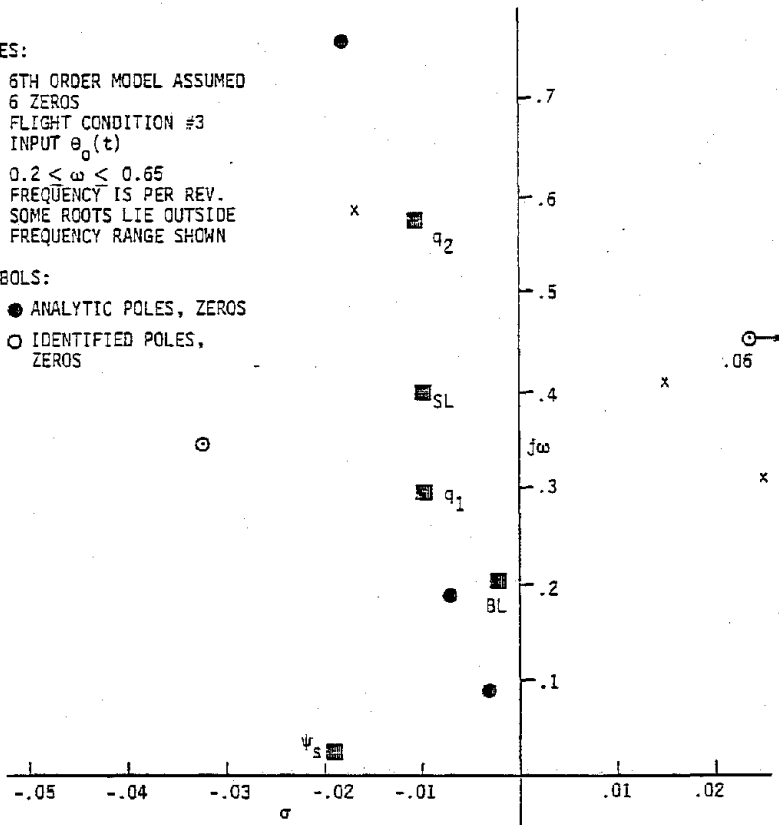


Figure 4.17 XV-15 Simulation Symmetric Mode Identification Based on q_2 Measurement: Varying Model Order

From these and a large number of additional trial identification runs, it is concluded that the assumption of a large model order, e.g., 10 or 12, represents a good starting point for identifying modes of this system. Reductions in model order and selection of frequency range are somewhat dependent on the particular root locations of a given flight condition, and different simplifications may be obtained in different flight conditions. The application of the algorithm for greatest accuracy is thus empirical to the extent of requiring engineering judgment in the selection of these algorithm parameters. Additional development effort is being directed toward removing the need for this operator interaction.

The algorithm was next applied to simulated time histories of symmetric wingtip deflection, of which horizontal and vertical components were computed from the values of state variables using the equations and constants described in Table C.3, Appendix C. The actual states, as defined in this study, cannot be measured directly in an experimental situation, whereas wingtip deflections may be calculated using accelerometers or strain gage instrumentation on the wing. The model was excited by random inputs to either collective pitch or flaperon deflection, using the same random noise and filter as above. This is, again, representative of an experimental condition. Mode identifications were performed in each of the six flight conditions identified in Table 4.1.

The symmetric XV-15 modes of most interest during wind tunnel testing are the wing vertical and chordwise bending, wing torsion and longitudinal support strut modes. The root locations of these and other modes are plotted in Figures 4.18 to 4.28, with system zeros shown for each of the collective pitch and flaperon input cases. The movements of poles and zeros due to changing flight conditions and configurations

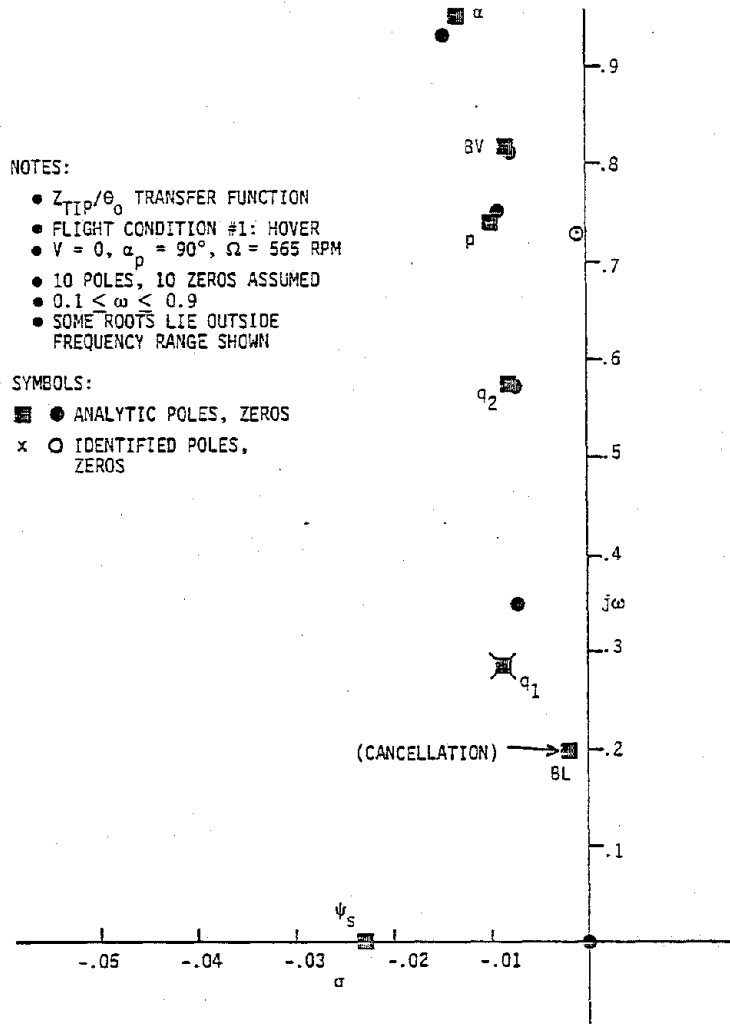


Figure 4.18 XV-15 Simulation Symmetric Mode Identification
Based on Z_{TIP} Measurement, θ_0 Input. Hover.

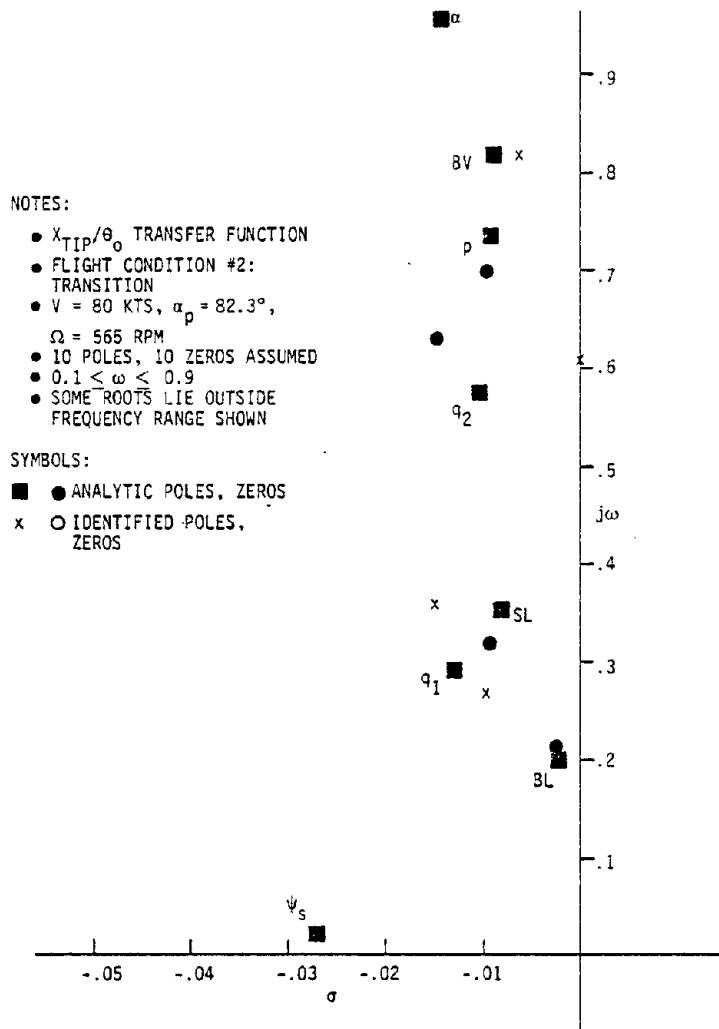


Figure 4.19 XV-15 Simulation Symmetric Mode Identification Based on X_{TIP} Measurement, θ_0 Input. Transition.

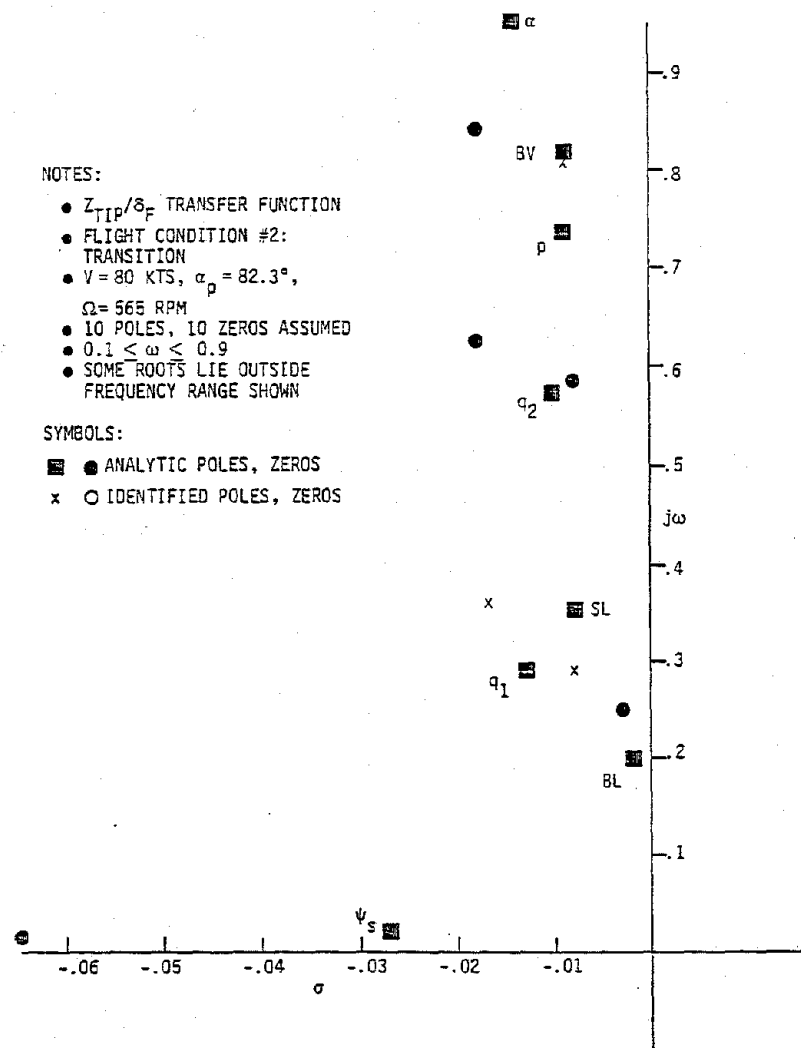


Figure 4.20 XV-15 Simulation Symmetric Mode Identification Based on Z_{TIP} Measurement, δ_F Input. Transition.

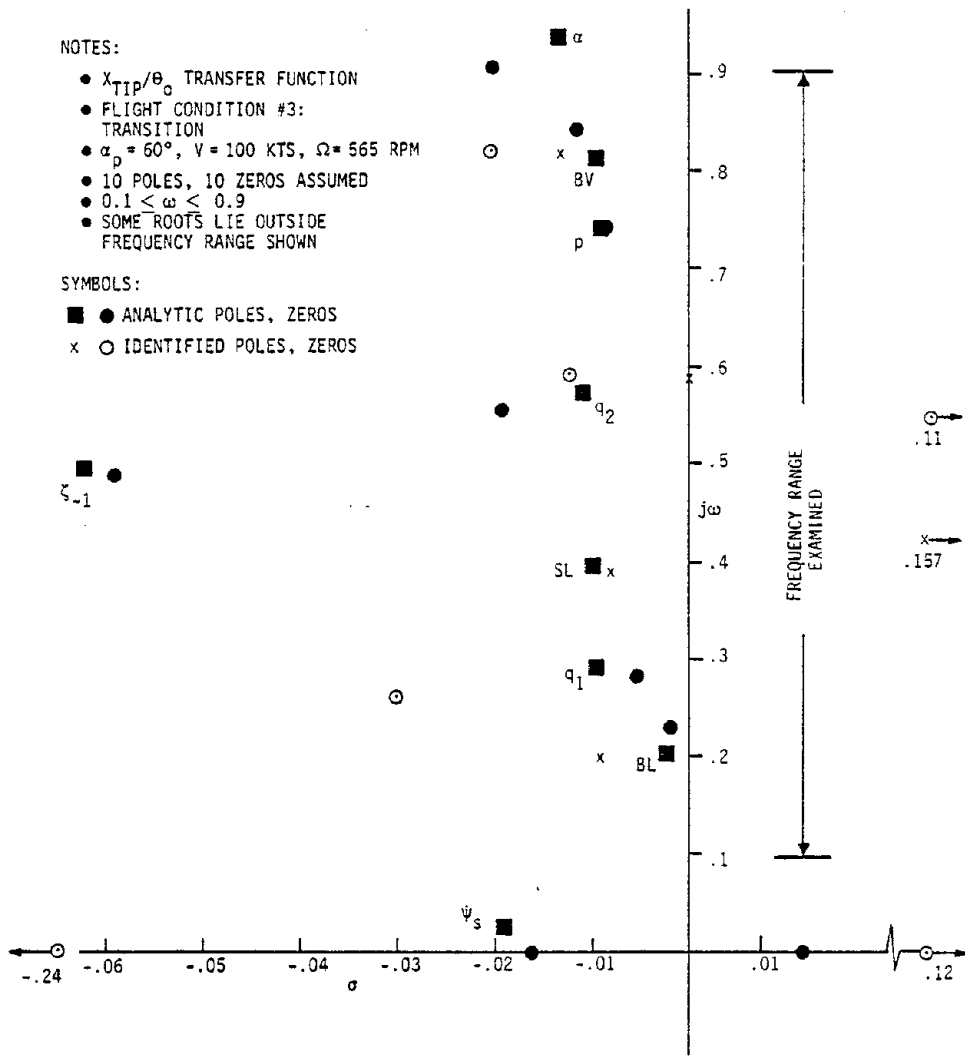


Figure 4.21 XV-15 Simulation Symmetric Mode Identification Based on X_{TIP} Measurement, θ_0 Input. Transition.

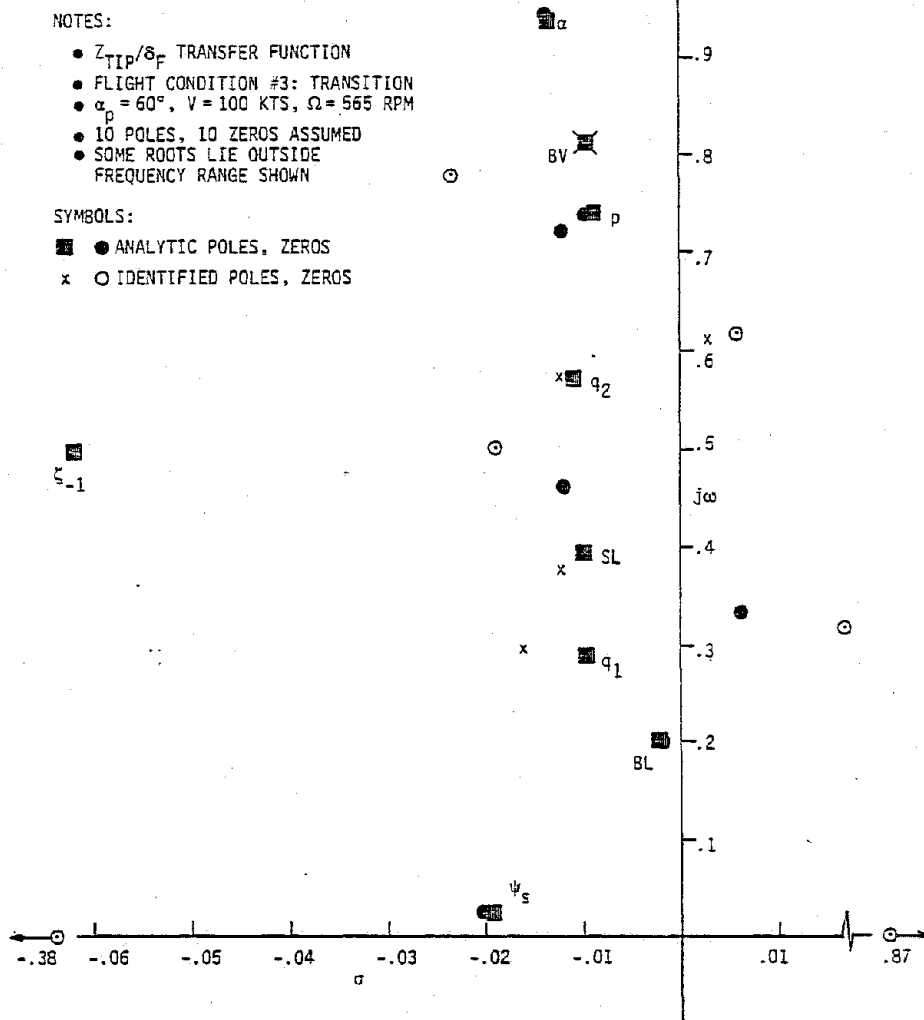


Figure 4.22 XV-15 Simulation Symmetric Mode Identification Based on Z_{TIP} Measurement, δ_F Input. Transition.

NOTES:

- X_{TIP}/θ_0 TRANSFER FUNCTION
- FLIGHT CONDITION #4: TRANSITION
- $V = 120$ KTS, $\alpha_p = 30^\circ$, $\Omega = 565$ RPM
- 10 POLES, 10 ZEROS ASSUMED
- $0.1 < \omega < 0.9$
- SOME ROOTS LIE OUTSIDE FREQUENCY RANGE SHOWN

SYMBOLS:

- ● ANALYTIC POLES, ZEROS
- x ○ IDENTIFIED POLES, ZEROS

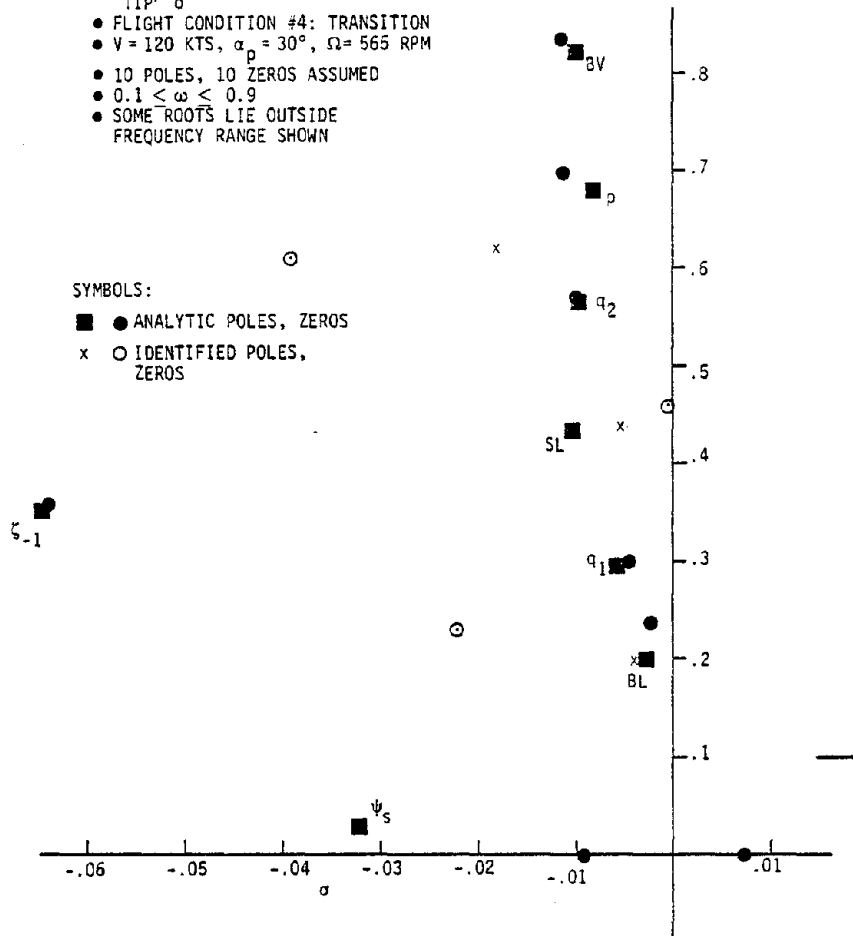


Figure 4.23 XV-15 Simulation Symmetric Mode Identification Based on X_{TIP} Measurement, θ_0 Input. Transition.

NOTES:

- Z_{TIP}/δ_F TRANSFER FUNCTION
- FLIGHT CONDITION #4: TRANSITION
- $V = 120$ KTS, $\alpha_p = 30^\circ$, $\Omega = 565$ RPM
- 10 POLES, 10 ZEROS ASSUMED
- $0.1 < \omega < 0.9$
- SOME ROOTS LIE OUTSIDE FREQUENCY RANGE SHOWN

SYMBOLS:

- ● ANALYTIC POLES, ZEROS
- x ○ IDENTIFIED POLES, ZEROS

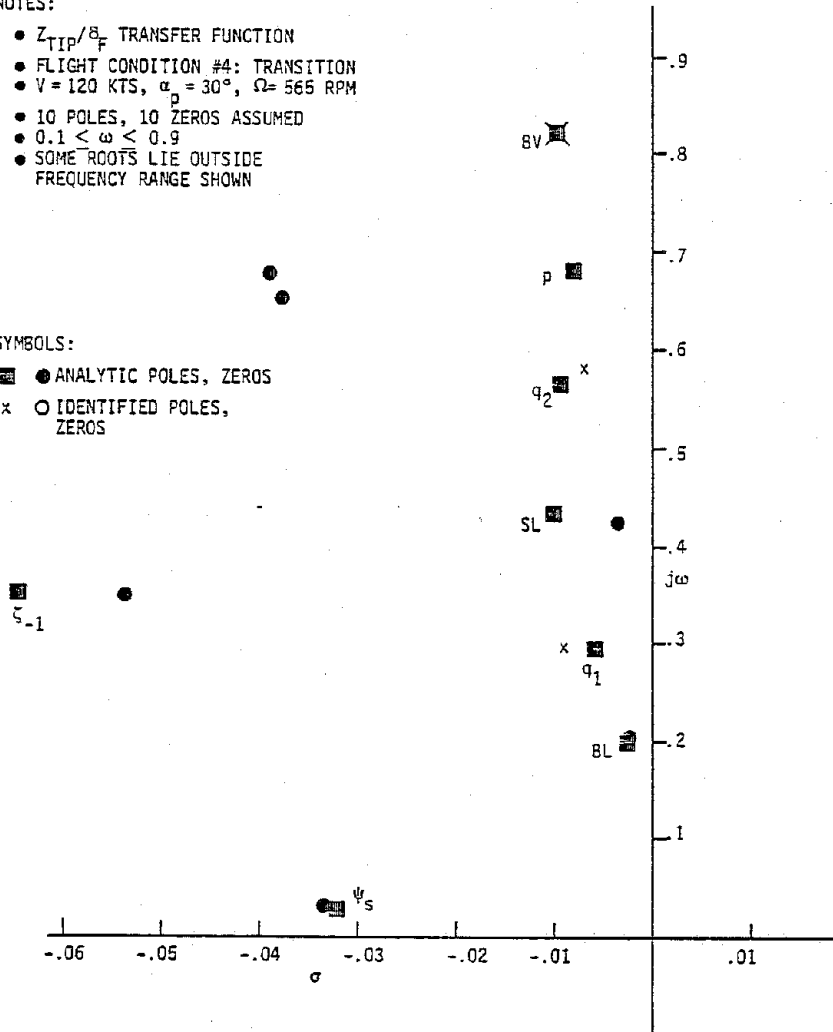


Figure 4.24 XV-15 Simulation Symmetric Mode Identification Based on Z_{TIP} Measurement, δ_F Input. Transition.

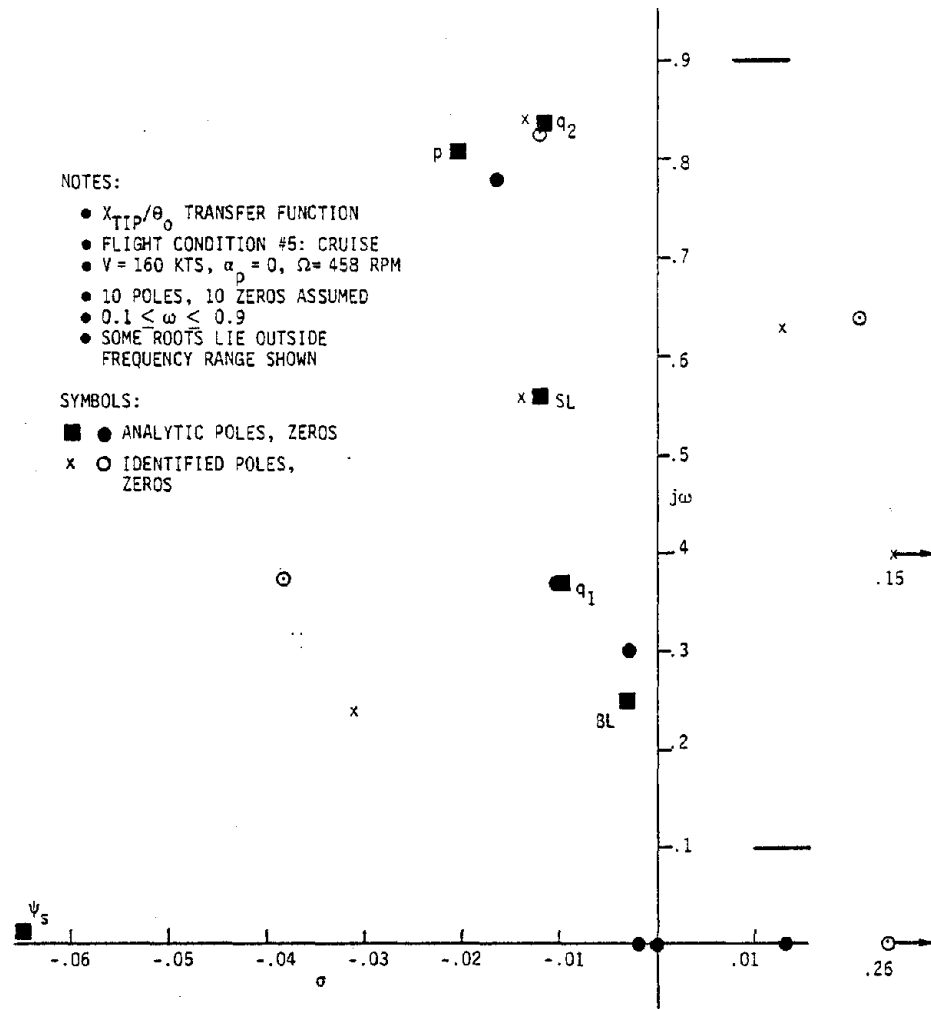


Figure 4.25 XV-15 Simulation Symmetric Mode Identification Based on X_{TIP} Measurement, θ_0 Input. Cruise.

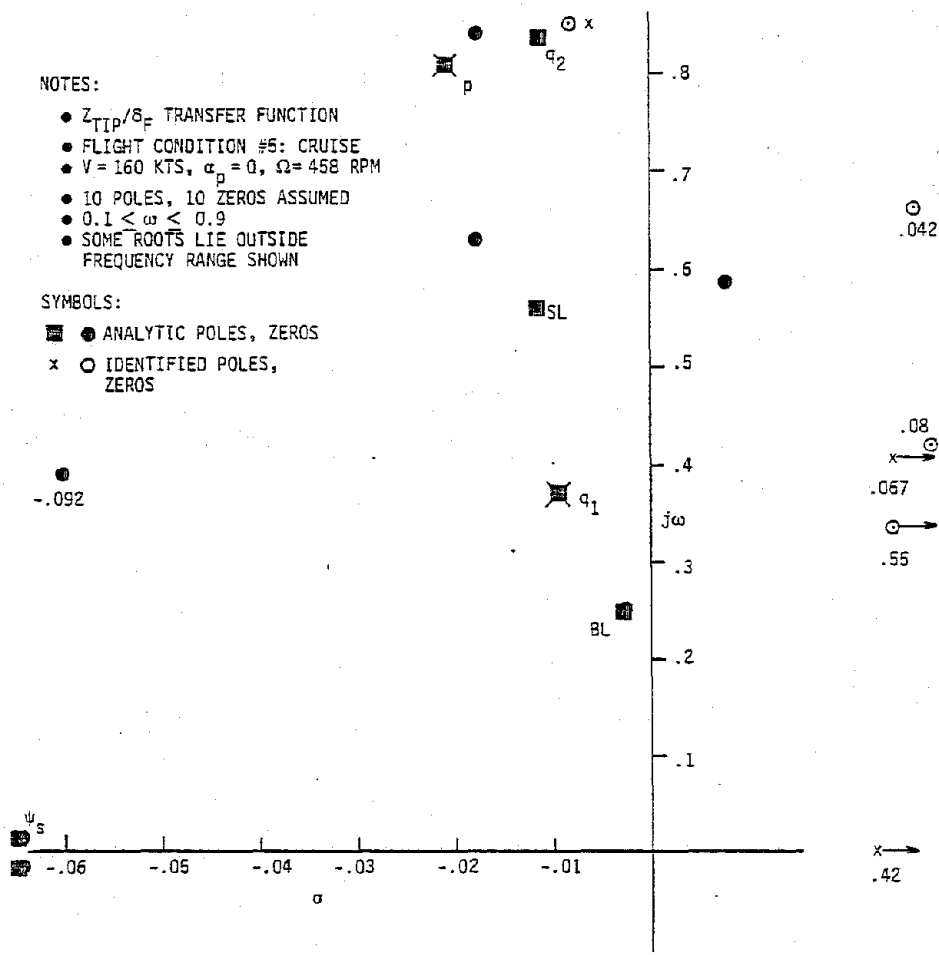


Figure 4.26 XV-15 Simulation Symmetric Mode Identification Based on Z_{TIP} Measurement, δ_F Input. Cruise.

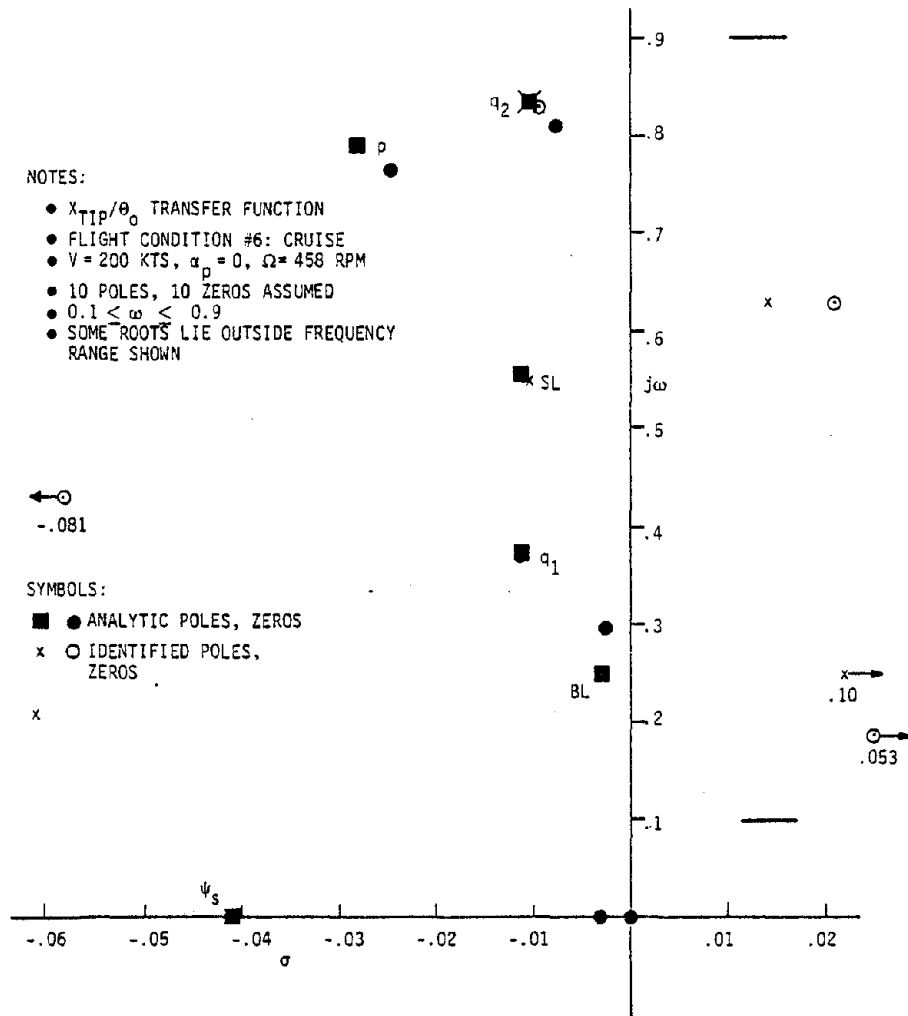


Figure 4.27 XV-15 Simulation Symmetric Mode Identification Based on X_{TIP} Measurement, θ_0 Input. Cruise.

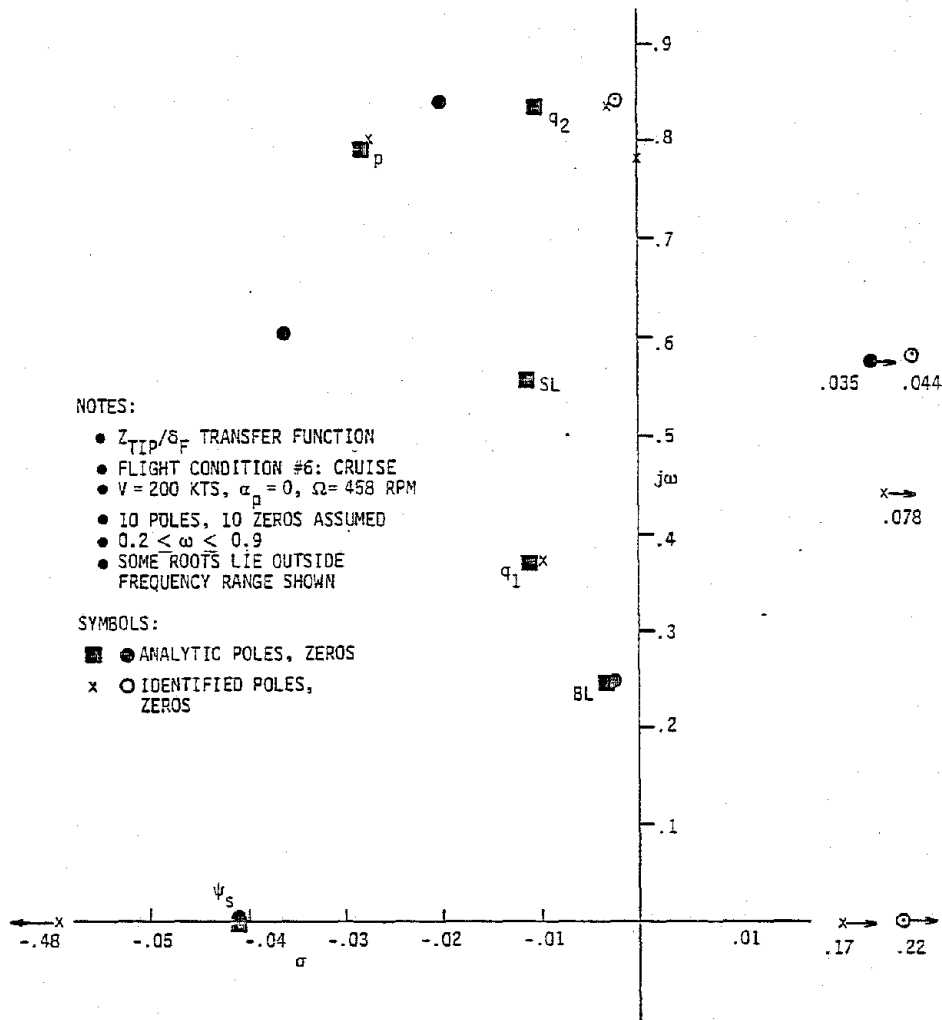


Figure 4.28 XV-15 Simulation Symmetric Mode Identification Based on Z_{TIP} Measurement, δ_F Input. Cruise.

may be noted. Complete tabulations of the transfer function poles and zeros are shown in Appendix C, Tables C.4 to C.9.

The roots identified by the algorithm from the X_{TIP} and Z_{TIP} time histories are shown superimposed on the analytical roots in Figures 4.18 to 4.28. Again, only roots in the low frequency range of interest are shown. The algorithm contains a wide frequency range specification ($0.1 \leq \omega \leq 0.9$) and utilizes scaling as discussed in items 5(a) and 5(c) above. In nearly all cases, good accuracy is seen in the pole locations for the modes of greatest interest, while somewhat more scatter is seen in the zeros.

4.4 XV-15 MODEL IDENTIFICATION: ANTISYMMETRIC MODES

The roots of the antisymmetric modes at each of the six selected flight conditions are shown plotted in Figures 4.29 to 4.39, for the frequency range of interest. Complete tabulations of transfer function poles and zeros are given in Appendix C, Tables C.10 to C.15.

The antisymmetric roots of most interest are the wing vertical and chordwise bending, wing torsion, and strut lateral (side) deflection. As in the symmetric case, these roots tend to become less stable as airspeed increases.

Figures 4.29 to 4.39 show the identification of these roots by the algorithm, superimposed as before on the analytical roots.

4.5 SUMMARY

This chapter considers the ability of the algorithm discussed in Chapter III to identify specific modes from time history data containing many degrees of freedom (in this case, 13). An analytical model of the XV-15 aircraft mounted in the

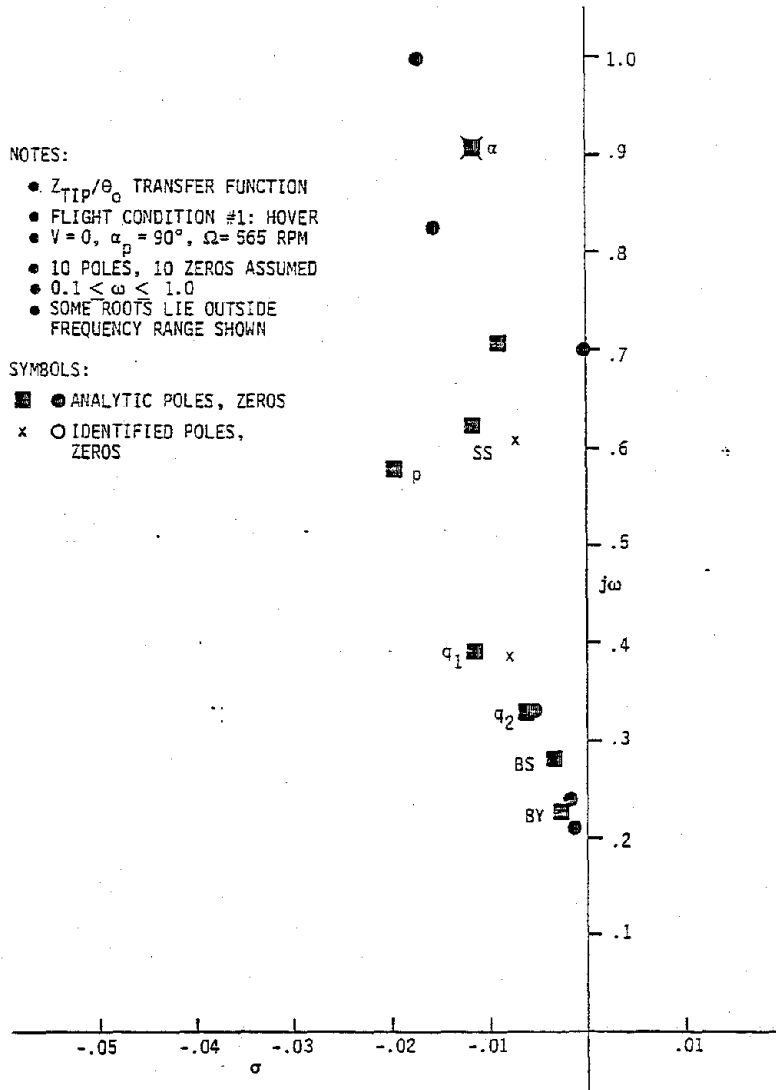


Figure 4.29 XV-15 Simulation Antisymmetric Mode Identification Based on Z_{TIP} Measurement, θ_0 Input. Hover.

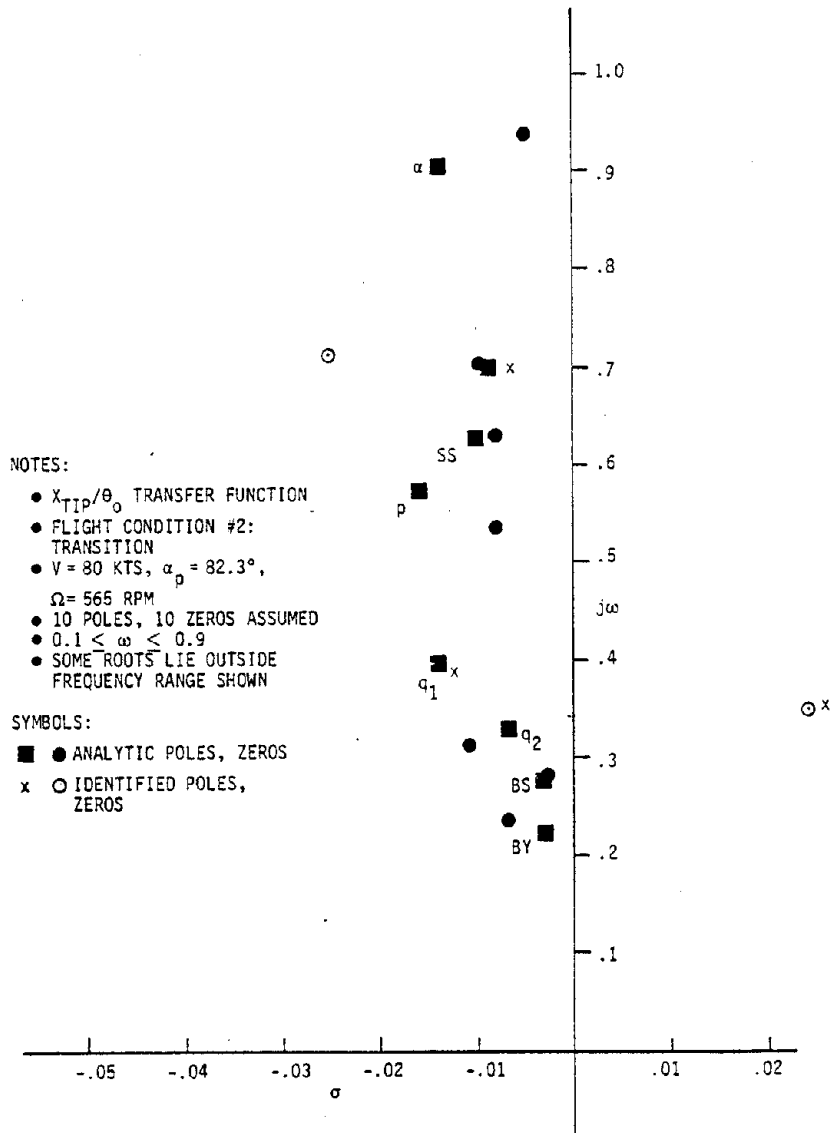


Figure 4.30 XV-15 Simulation Antisymmetric Mode Identification Based on X_{TIP} Measurement, θ_0 Input. Transition.

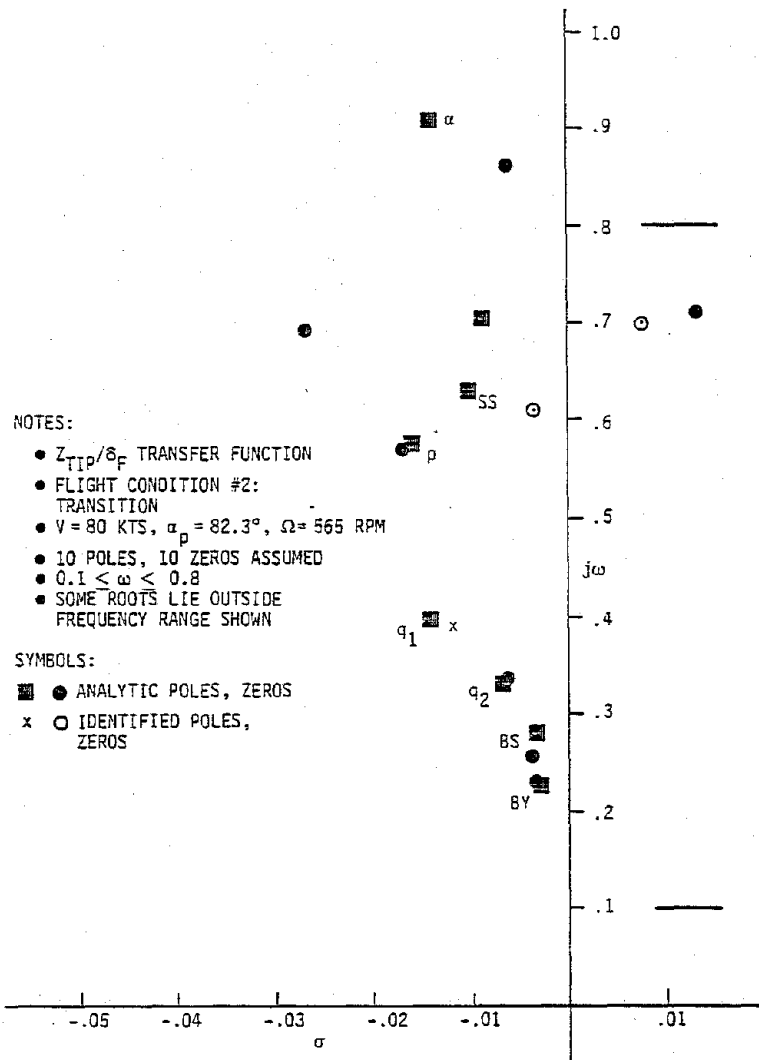


Figure 4.31 XV-15 Simulation Antisymmetric Mode Identification Based on Z_{TIP} Measurement, δ_F Input. Transition.

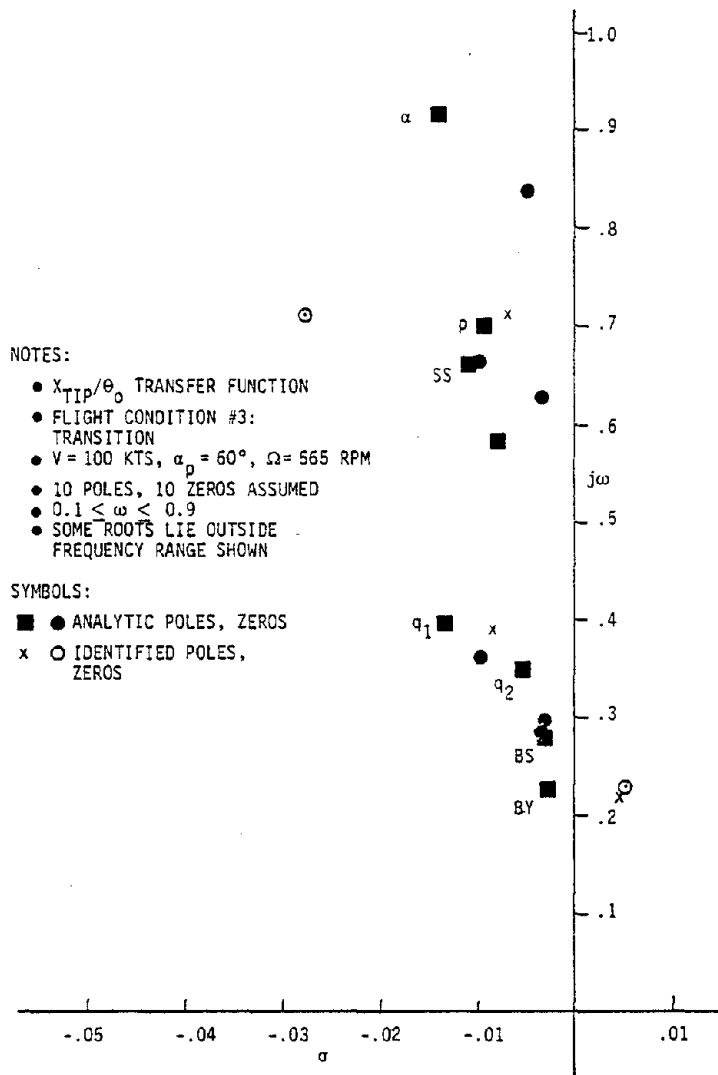


Figure 4.32 XV-15 Simulation Antisymmetric Mode Identification
Based on X_{TIP} Measurement, θ_0 Input. Transition.

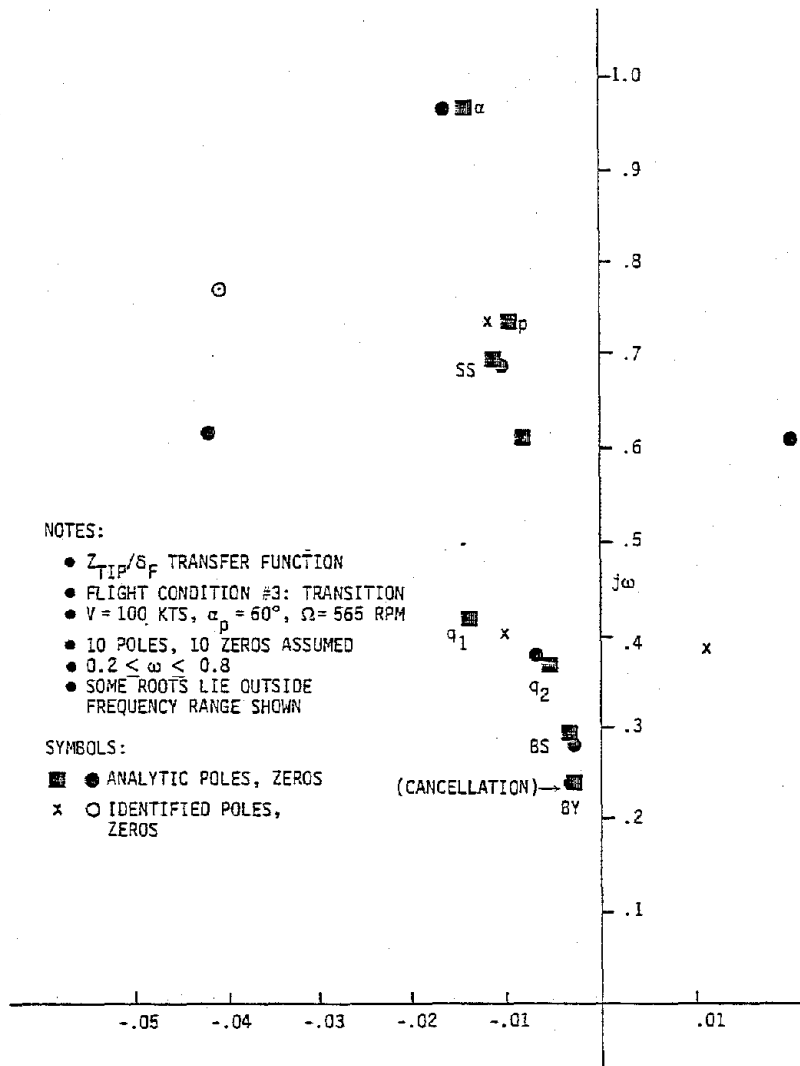


Figure 4.33 XV-15 Simulation Antisymmetric Mode Identification Based on Z_{TIP} Measurement, δ_F Input. Transition.

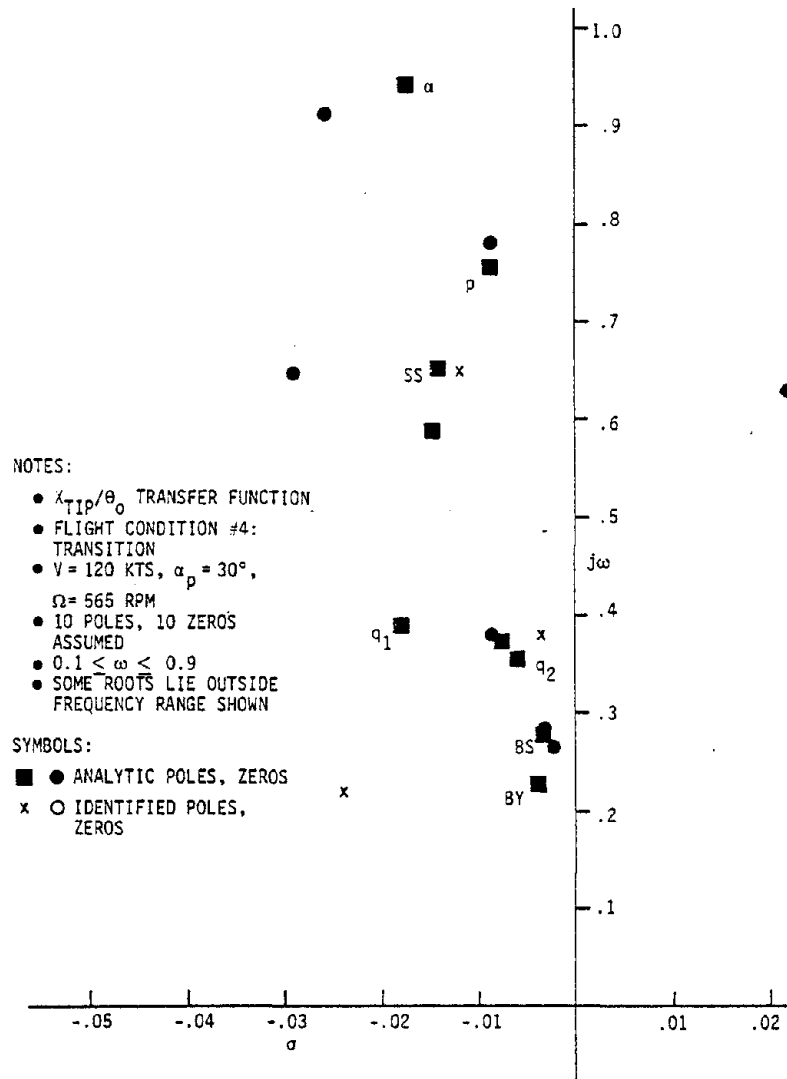


Figure 4.34 XV-15 Simulation Antisymmetric Mode Identification Based on X_{TIP} Measurement, θ_0 Input. Transition.

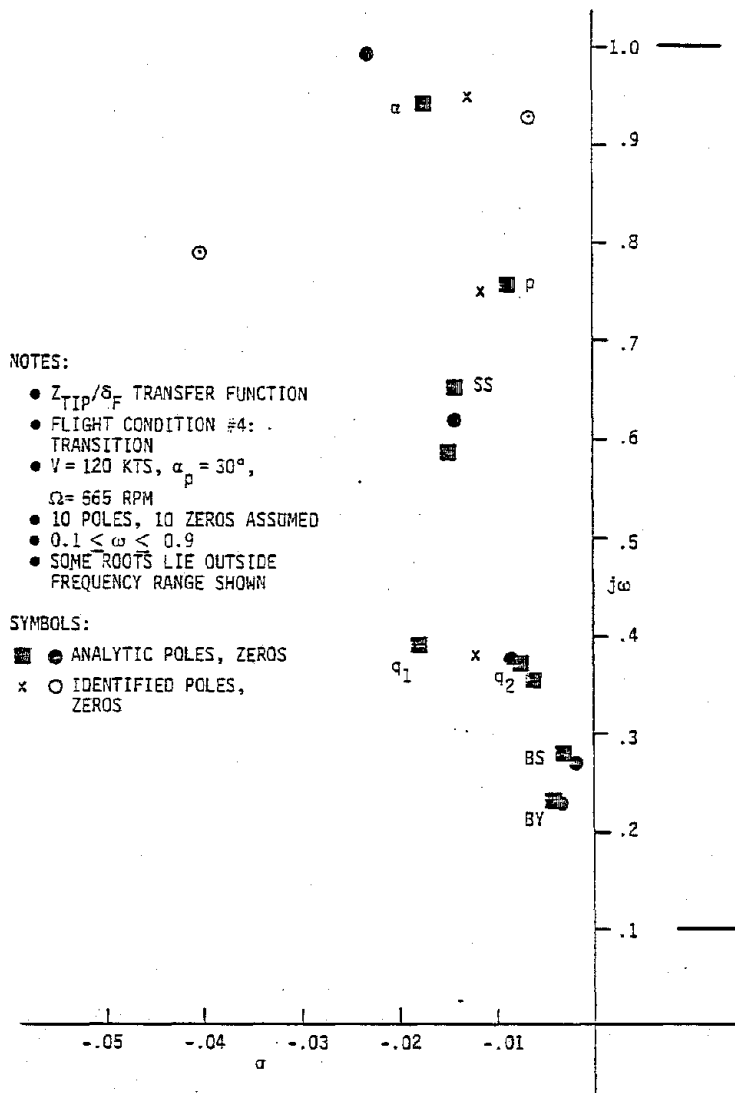


Figure 4.35 XV-15 Simulation Antisymmetric Mode Identification Based on Z_{TIP} Measurement, δ_F Input. Transition.

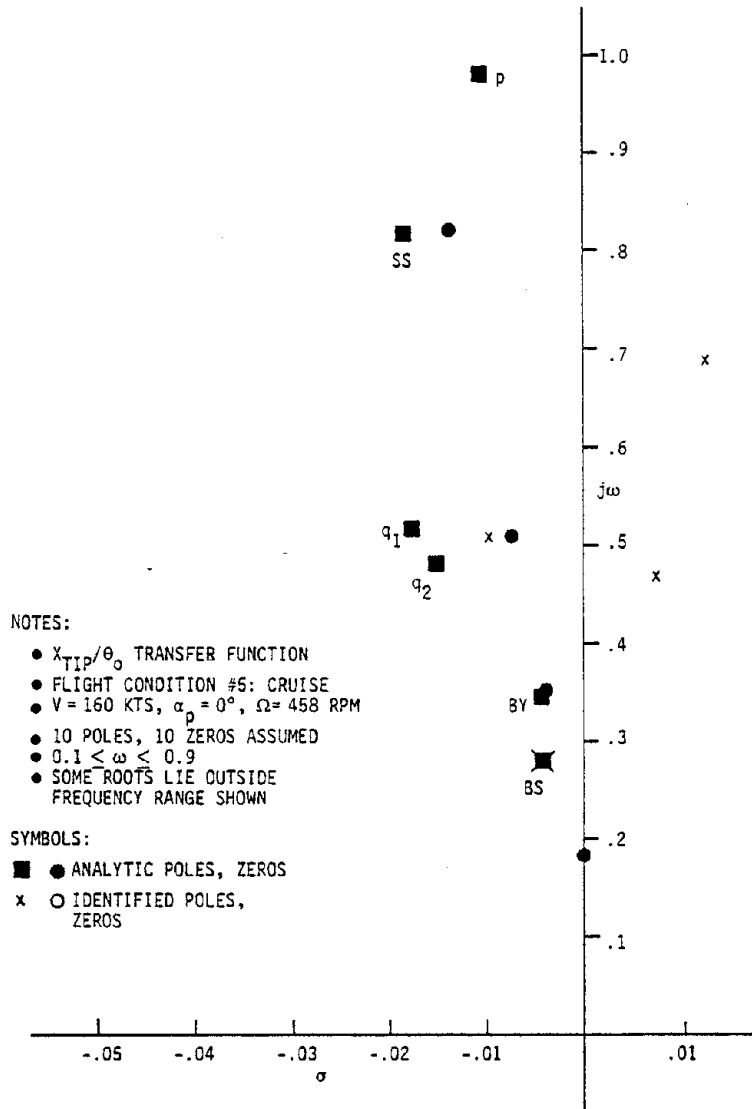


Figure 4.36 XV-15 Simulation Antisymmetric Mode Identification Based on X_{TIP} Measurement, θ_0 Input. Cruise.

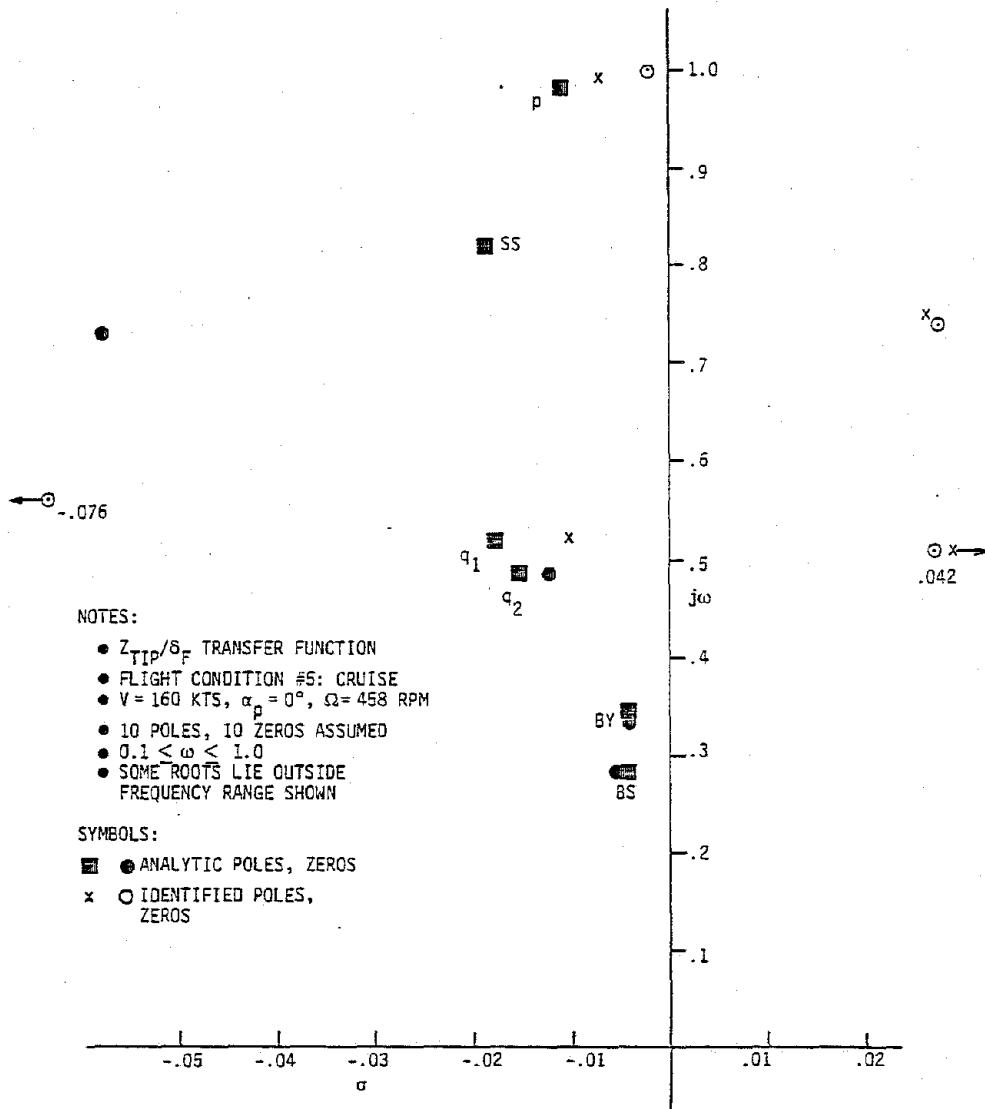


Figure 4.37 XV-15 Simulation Antisymmetric Mode Identification Based on Z_{TIP} Measurement, δ_F Input. Cruise.

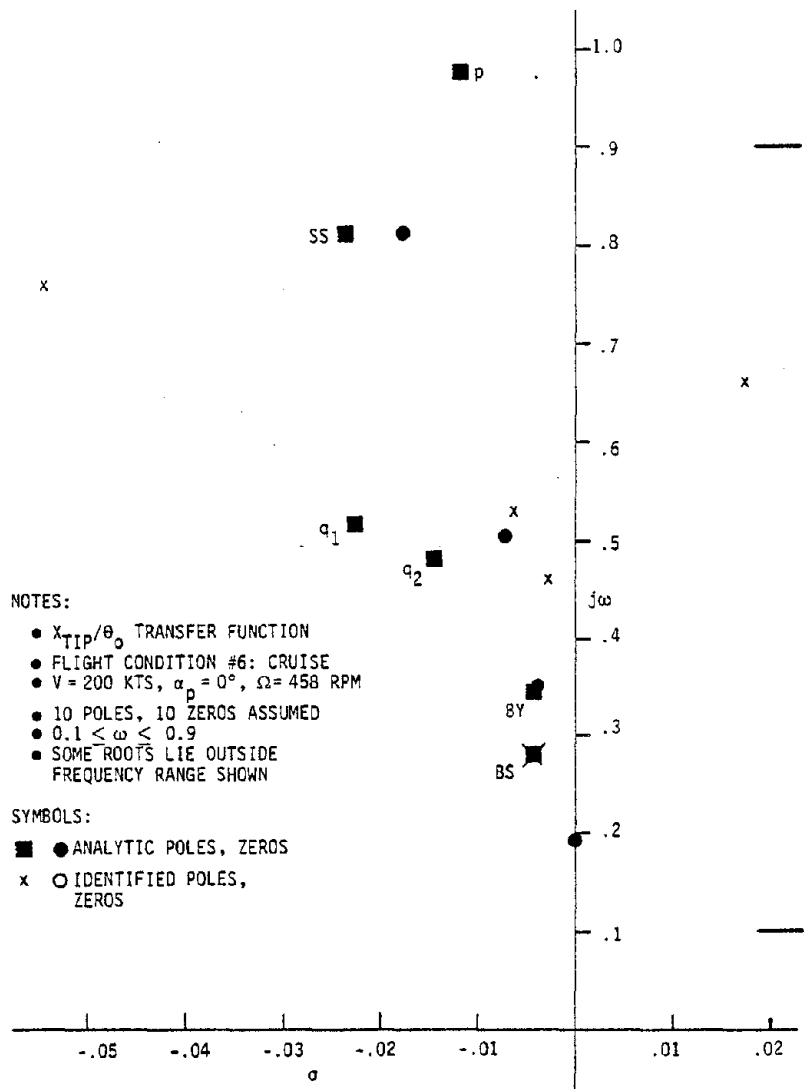


Figure 4.38 XV-15 Simulation Antisymmetric Mode Identification Based on X_{TIP} Measurement, θ_0 Input. Cruise.

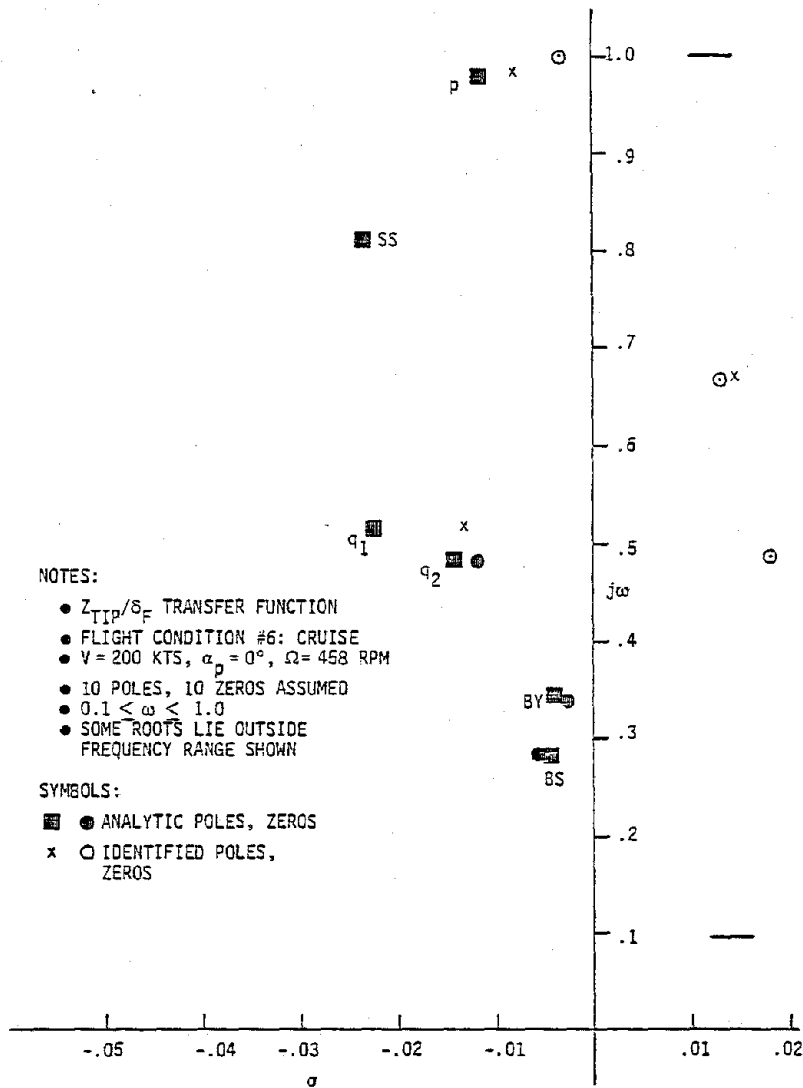


Figure 4.39 XV-15 Simulation Antisymmetric Mode Identification Based on Z_{TIP} Measurement, δ_F Input. Cruise.

40- by 80-foot wind tunnel is used to provide representative simulated time history data. The conclusions from the work of this chapter are:

- (1) In most of the flight conditions examined, important aeroelastic modes are identified with good accuracy from time history measurements of wingtip deflection.
- (2) The algorithm can accurately identify modes in widely differing flight conditions without modification of algorithm parameters.
- (3) Certain pole-zero characteristics of the system are poorly identified and require interaction by the analyst to modify controlling parameters of the algorithm, such as assumed model order or frequency range.
- (4) In general, the number of modes assumed in the model should be equal to or exceed the number of modes actually present, for greatest accuracy.
- (5) The general "rules" described in Chapter III for selecting algorithm parameters give generally the best results with XV-15 data.

CHAPTER V APPLICATION TO CANTILEVER WING WIND TUNNEL DATA

5.1 INTRODUCTION

Tests were conducted by the government on a scaled cantilever wing model in the M.I.T. wind tunnel for the purpose of measuring dynamic stability. Runs were made at four tunnel speeds and four inputs (δ_F , flap deflection; θ_{1s} , longitudinal cyclic; θ_o , collective and θ_{1c} , lateral cyclic) were applied successively (see Table 5.1). At each speed and for each applied input, the output measurements are chordwise bending, q_1 , vertical bending, q_2 , and the first two rotor flapping modes, β_{1c} and β_{1s} . In addition, runs were made without any applied input, where the model was excited by random tunnel turbulence. The sampling interval was 0.02 sec. The data was Fourier transformed and averaged on the basis of about 20 runs. The averaged autospectrum and cross spectrum of the inputs and outputs were supplied by the government for evaluation of the algorithm developed in Chapter III. A typical transfer function obtained by dividing the autospectrum of the input into the cross spectrum of the input and output are shown in Figure 5.1. In spite of the averaging, the transfer functions are quite noisy. The following sections describe the results.

5.2 SINGLE INPUT, SINGLE OUTPUT

The collective pitch input, θ_o , excites primarily the wing chordwise motion, q_2 , and the flaperon input, δ_F , excites primarily the wing vertical motion, q_1 , at all speeds. Therefore, these input-output pairs are used to evaluate the algorithm.

Table 5.1
Summary of Wind Tunnel Test Points

| POINT NUMBER | V/ Ω R | INPUT |
|--------------|---------------|---------------|
| 5 | 0.34 | None |
| 6 | | δ_f |
| 7 | | θ_s |
| 8 | | θ_o |
| 9 | | θ_{1c} |
| 14 | 0.47 | None |
| 16 | | δ_f |
| 16 | | θ_{1s} |
| 17 | | θ_o |
| 18 | | θ_{1c} |
| 23 | 0.58 | None |
| 24 | | δ_f |
| 25 | | θ_{1s} |
| 26 | | θ_o |
| 27 | | θ_{1c} |
| 32 | 0.69 | None |
| 33 | | δ_f |
| 34 | | θ_{1s} |
| 35 | | θ_o |
| 36 | | θ_{1c} |

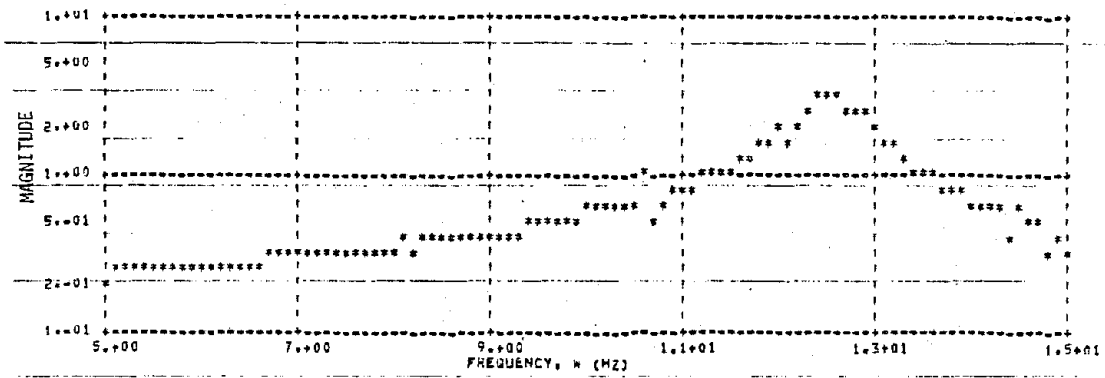


Figure 5.1a Magnitude of Measured Transfer Function
Between q_2 and θ_0

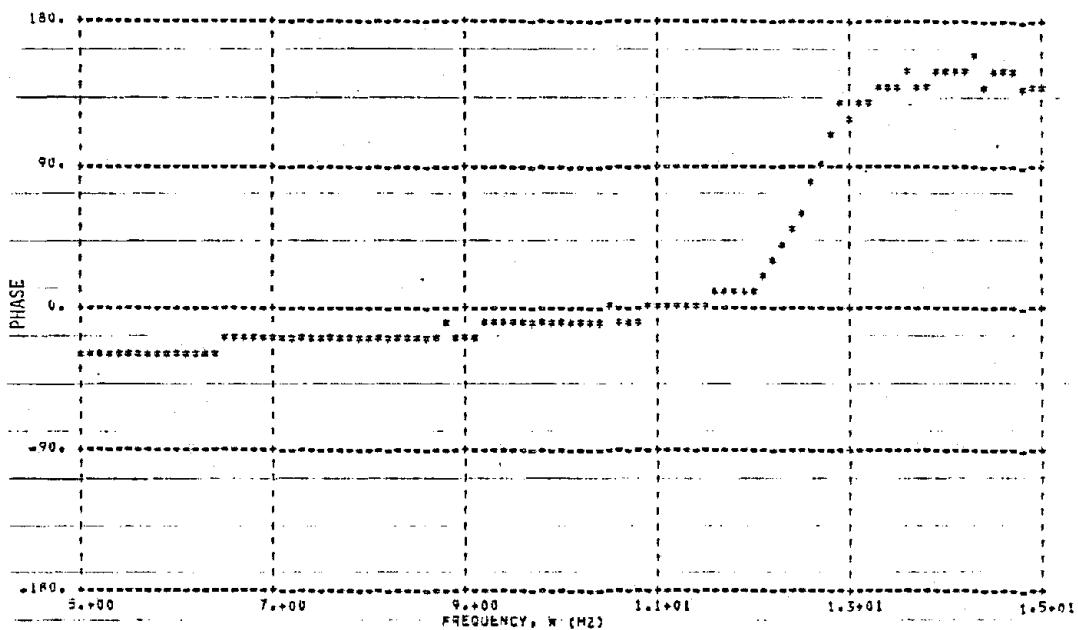


Figure 5.1b Phase Angle of Measured Transfer Function
Between q_2 and θ_0

Several runs are made using input δ_F and output q_1 to study the effect of various algorithm parameters on estimation accuracy. The highest frequency used for this input output pair is 10 Hz, and the model order is set to two (one DOF). The minimum acceptable value of the delay parameter τ is therefore $(2 \times 2)/(10 \times 2) = 0.2$ sec. With a τ of 0.3 and $7 < \omega < 10$, a two-pole, one-zero model gave the results shown in Table 5.2. Except when going from a nondimensional speed of 0.47 to 0.58, the damping ratio increases with speed. If the same model is used except without any zeros, the estimates obtained are again shown in Table 5.2. The estimates when the delay parameter, τ , is set equal to zero with and

Table 5.2
 Estimate of the q_1 Mode from Input δ_F and Output q_1
 (Two Pole Model Assumed)

| | $\frac{V}{\Omega R}$ | NATURAL FREQUENCY | DAMPING RATIO | ZERO | GAIN |
|----------------------|----------------------|-------------------|---------------|------|--------|
| a. $\tau = 0.3$ | 0.34 | 8.29 | 0.0167 | 13.1 | -0.123 |
| $7 < \omega < 10$ | 0.47 | 8.23 | 0.0212 | 11.0 | -0.269 |
| | 0.58 | 8.20 | 0.0198 | 9.54 | -0.446 |
| ONE ZERO | 0.69 | 8.16 | 0.0250 | 12.2 | -0.579 |
| b. $\tau = 0.3$ | 0.34 | 8.29 | 0.0157 | --- | 1.61 |
| $7 < \omega < 10$ | 0.47 | 8.23 | 0.0192 | --- | 2.90 |
| | 0.58 | 8.21 | 0.0182 | --- | 4.21 |
| NO ZEROS | 0.69 | 8.16 | 0.0226 | --- | 7.03 |
| c. $7 < \omega < 10$ | 0.34 | 8.30 | 0.0108 | 13.2 | -0.121 |
| $\tau = 0.0$ | 0.47 | 8.24 | 0.0151 | 11.0 | -0.268 |
| | 0.58 | 8.21 | 0.0148 | 9.67 | -0.440 |
| ONE ZERO | 0.69 | 8.16 | 0.0195 | 12.6 | -0.561 |
| d. $7 < \omega < 10$ | 0.34 | 8.27 | 0.00656 | --- | 1.53 |
| $\tau = 0.0$ | 0.47 | 8.19 | 0.00723 | --- | 2.78 |
| | 0.58 | 8.16 | 0.00642 | --- | 4.08 |
| NO ZEROS | 0.69 | 8.11 | 0.0103 | --- | 6.78 |

without a zero in the transfer function are also given in Table 5.2. A comparison of these results shows that the estimates of natural frequencies, zero locations and gains do not depend upon the value of τ or the absence of zero from the transfer function. The estimate of the damping ratio, however, depends strongly on the correct choice of τ and the number of zeros in the transfer function (see Fig. 5.2).

The response of the output q_2 to input θ_0 is used to estimate the q_2 mode. A two-pole, one-zero model is used and τ is set to 0.3. Two cases are tried with $5 < \omega < 15$ and $11 < \omega < 15$. The results are shown in Table 5.3 and Figure 5.3. In all but one case, the algorithm indicates the presence of a zero in the transfer function.

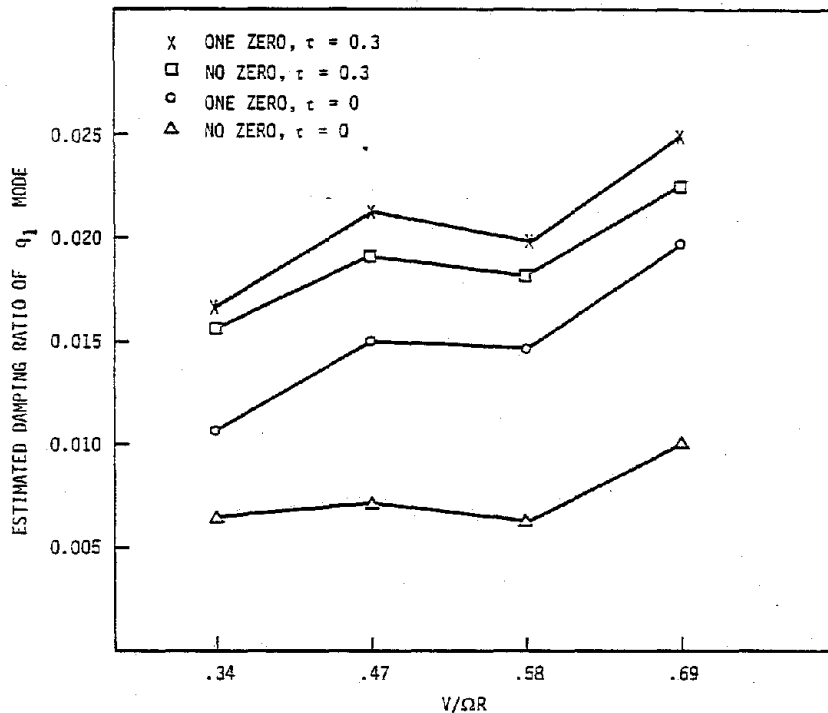


Figure 5.2 Estimate of the Damping Ratio of the q_1 Mode Obtained from the Output q_1 and Input δ_f

Table 5.3

Estimate of the q_2 Mode from Input θ_0 and Output q_2

| | $\frac{V}{\Omega R}$ | NATURAL FREQUENCY | DAMPING RATIO | ZERO | GAIN |
|---|----------------------|-------------------|---------------|-------|--------|
| a. TWO POLE ONE ZERO $7 < \omega < 15$ $\tau = 0.3$ | 0.34 | 12.9 | 0.0396 | -137 | 0.201 |
| | 0.47 | 12.5 | 0.0327 | -18.3 | 1.61 |
| | 0.58 | 12.4 | 0.0250 | -17.5 | 1.90 |
| | 0.69 | 12.4 | 0.0238 | -9.84 | 1.09 |
| b. TWO POLE ONE ZERO $11 < \omega < 15$ $\tau = 0.3$ | 0.34 | 12.9 | 0.0347 | 148 | -0.154 |
| | 0.47 | 12.6 | 0.0308 | -45.6 | 0.594 |
| | 0.58 | 12.5 | 0.0269 | -43.9 | 0.319 |
| | 0.69 | 12.4 | 0.0257 | -23.3 | 0.555 |

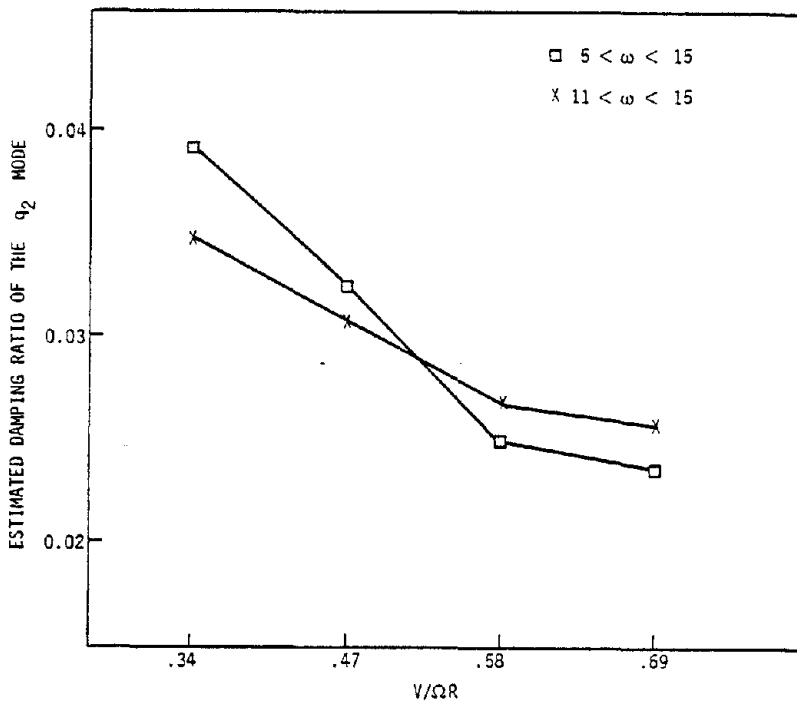


Figure 5.3 Estimate of the Damping of the q_2 Mode Using Output q_2 and Input θ_0

5.3 SINGLE OUTPUT, MULTI-INPUT

The algorithm is applied to measurements of q_1 resulting from inputs δ_F and θ_{1s} . Figure 5.4 shows the estimate of the damping ratio of the q_1 mode based on the selection of different model orders, for $\frac{V}{\Omega R} = 0.47$. The value of the time delay parameter is set to the minimum value corresponding to the model order selected in the estimation. It is clear from Figure 5.4 that the estimate of the damping is relatively independent of the model order. When the degrees of freedom are set to two or three, all but a pair of complex poles cancel out complex zero pairs.

The effect of τ on the estimate of the damping ratio is shown in Fig. 5.5. Note that the estimate is essentially constant for $\tau > 0.6$ (the minimum acceptable value). Figure 5.6 shows the estimate of q_1 damping ratio at various speeds and compares the results with single input, single output cases presented in the previous section.

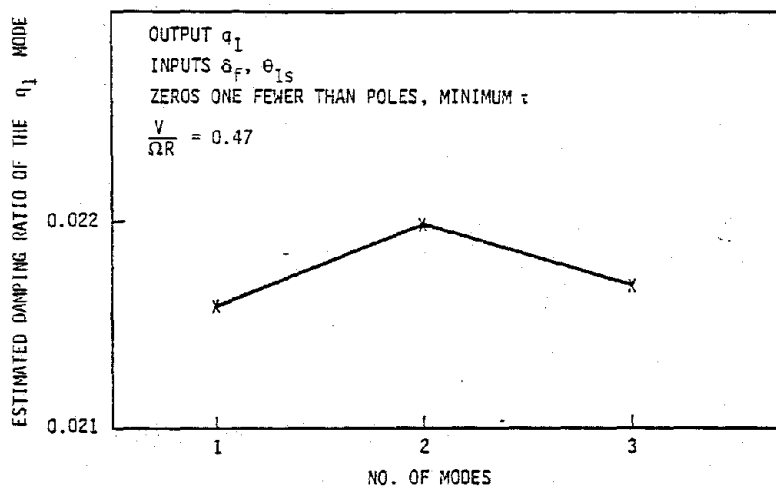


Figure 5.4 Effect of Model Order on the Estimate of q_1 Damping

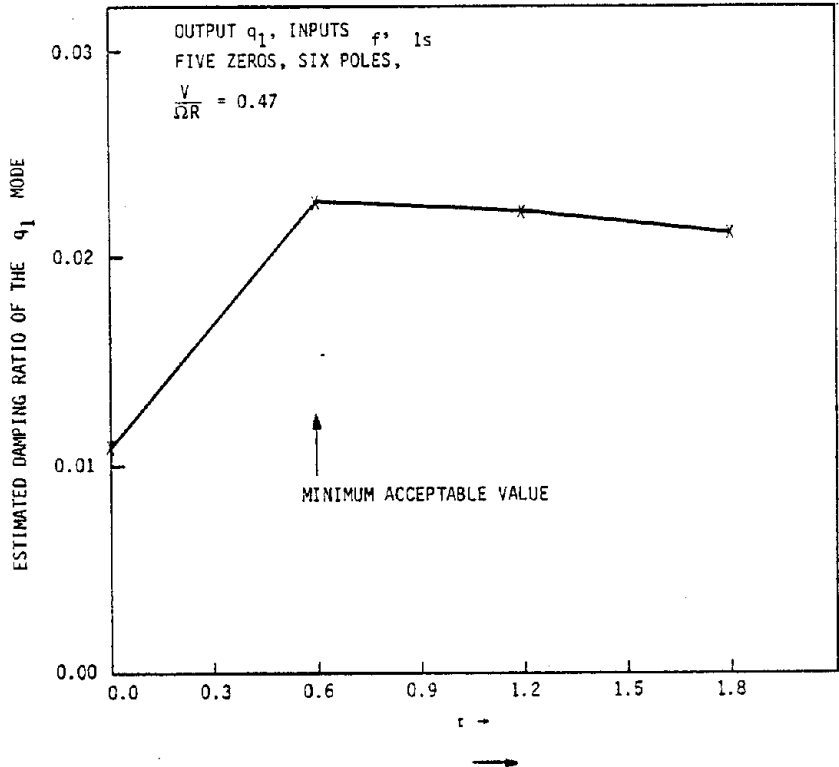


Figure 5.5 Effect of τ on Estimate of q_1 Damping Ratio

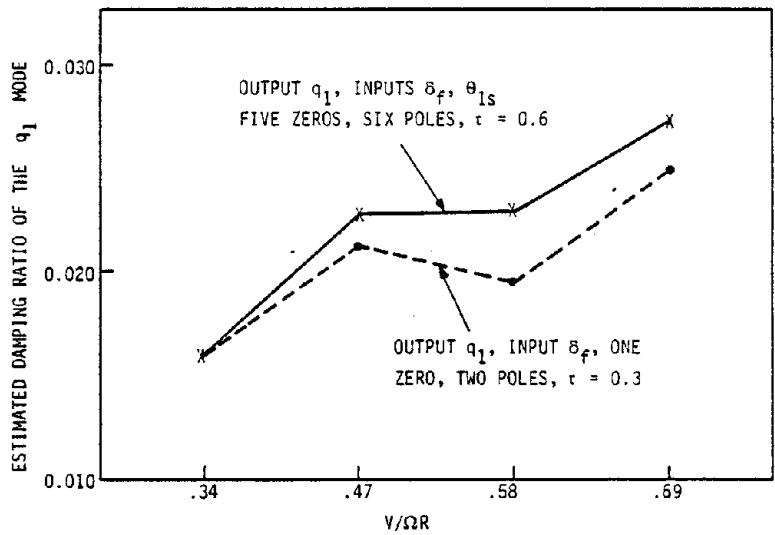


Figure 5.6 Estimate of the q_1 Damping

C-2

5.4 MULTI-INPUT, MULTI-OUTPUT

The responses of the measurements q_1 , β_{1c} and β_{1s} to inputs δ_F and θ_{1c} are used to estimate the modes of the cantilever wing. A six-pole, five-zero model is used and τ is set at 0.6. The estimate of the damping ratio of the q_1 mode is shown in Figure 5.7 for various speeds. These results agree quite closely with the case when only output q_1 is used. This indicates that β_{1c} and β_{1s} are not useful in estimating the q_1 mode. They may, however, be able to estimate other rotor modes.

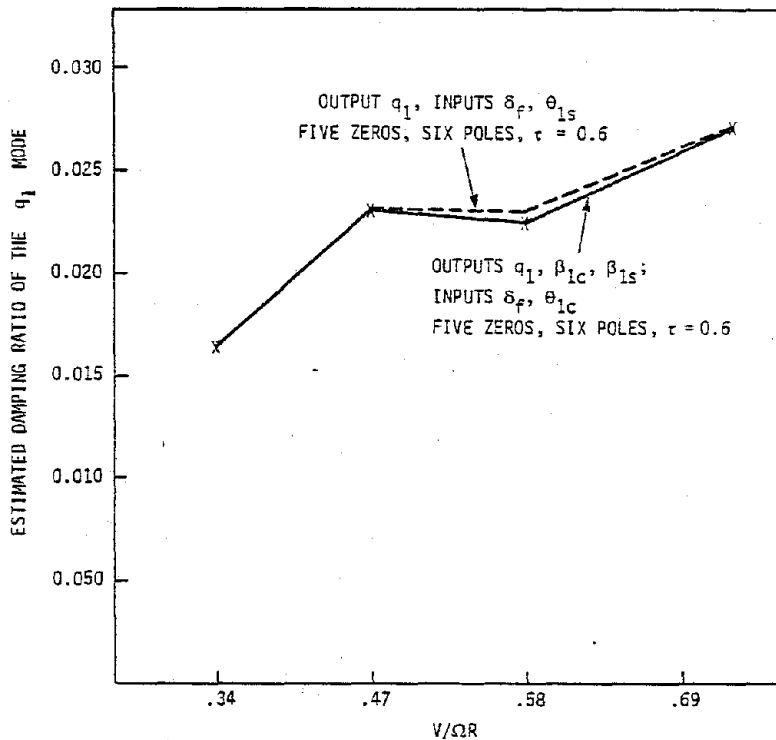


Figure 5.7 Estimate of q_1 Damping from Multi-input, Multi-output Data

5.5 SUMMARY

The estimates of the various modes, obtained from the wind tunnel data through the application of the algorithm developed in Chapter III, are quite reasonable. The basic trends of actual frequencies and damping ratios agree with analytical results and results based on other techniques. Further processing of more wind tunnel data is required to establish the best procedure for using the algorithm.

CHAPTER VI CONCLUSIONS

6.1 ALGORITHM DEVELOPMENT

This study develops an on-line algorithm based on advanced system identification technology for real time measurement of dynamic stability in the Ames 40- by 80-foot Wind Tunnel. The algorithm is a four-step procedure requiring: (1) Fourier transforming the time history data, (2) setting up a set of linear equations, (3) solving these equations, and (4) computing roots of characteristic polynomials to find poles and zeros. The entire procedure is computationally efficient and appears to meet the requirements of the wind tunnel test. In addition, the algorithm can handle multi-input, multi-output data in a statistically optimal manner and minimizes the effects of process and measurement noise sources. Application of the algorithm to ground resonance simulation data indicated the following important features of the algorithm:

- (1) The algorithm provides good estimates of natural frequencies of all modes under every condition used in the simulation. The damping ratio estimates are excellent up to 20% random noise in the output, when a theoretically derived value of the time delay parameter τ is used in the algorithm. The estimates of the damping ratio degrade with increasing output noise and with nonoptimal τ .
- (2) The accuracy of the estimates improves when more outputs are used in identification. In fact, with the measurement of the lateral deflection alone, the rotor modes cannot be estimated.
- (3) The sampling interval and the data length are important variables in determining estimation accuracy. The data record should be long enough to provide good frequency resolution in the region of the modes of interest.

- (4) Discrete frequency noise (e.g., 1/rev noise) could degrade estimation accuracy significantly if it is not properly accounted for. However, the algorithm can be modified such that discrete frequency noise does not affect parameter estimates significantly.

The application of the algorithm to the cantilever wing model indicated, in addition to the above, that:

- (1) If a high order model is specified in the estimation algorithm, several estimated poles are very close to estimated zeros. If pole-zero cancellation is performed, the correct number of poles and zeros are identified.
- (2) The computation time increases with the model order specified in identification, the number of outputs and the number of inputs. The dependence on the model order is the strongest.
- (3) Scaling of inputs and outputs may be required for improved numerical conditioning.

6.2 XV-15 MODE IDENTIFICATION

Applying the new algorithm to 13 DOF simulated XV-15 time history data leads to the following conclusions:

- (1) The algorithm achieves excellent results identifying the frequencies of significant aeroelastic XV-15 modes, and generally very good results in the identification of damping ratios. Cases of reduced accuracy in the estimated damping ratio are generally those in which multiple roots--poles and zeros--occur at the same damped natural frequency in the basic system, a situation which changes with flight condition.
- (2) Good mode identifications are achieved over a wide range of flight conditions with no changes in the algorithm. Improvements can, in some cases, be obtained through specific changes made by the analyst in certain model parameters, such as assumed model order and frequency range, and in some cases, scaling.

- (3) In general, assuming a model with a greater number of modes than actually anticipated gives much-improved accuracy in the identification of the most important modes, with "excess" roots being placed by the algorithm either well outside the frequency-damping range of interest or in self-cancelling pole-zero pairs. Attempting to use too low a model order generally gives poor damping predictions.
- (4) The benefits obtained from using multiple measurements appear to depend on the degree to which the measurements are related. With essentially independent measurements, no improvement in identification was found using two measurements instead of one.
- (5) The basic "rules" on algorithm parameter specification developed on smaller models are valid for high-order models. Particularly careful attention must be paid to the effects of scaling.

6.3 APPLICATION TO WIND TUNNEL DATA

The algorithm of this study is successfully applied to data from the wind tunnel test of a cantilever wing model (Chapter V). The identification is performed off-line through on-line conditions are simulated as much as possible. The following conclusions may be drawn from this limited processing:

- (1) Zeros play an important role in accurate estimation of damping ratios. Neglecting a neighboring zero could significantly alter the identified value of the damping ratio. In addition, a proper selection of the time delay parameter τ is important.
- (2) Estimates of damping ratios, from different sets of inputs and outputs, are close to each other. This verifies the results of the algorithm.

6.4 RECOMMENDATIONS

Based on the studies completed thus far, the following recommendations are made regarding the direction of future development work:

- (1) Additional independence from judgments on the part of the analyst should be sought; e.g., selection of model order, scaling, etc.
- (2) Improved resolution of close pole-zero groupings should be sought.
- (3) Direct measurements of rotor degrees-of-freedom are important in many cases. Methods to extract these time histories from single blade measurements is required.
- (4) The algorithm must be further tested to derive operational procedures for effective use of the algorithm.
- (5) The approach should be thoroughly tested on real wind tunnel data before it can be finally accepted as a method for flutter analysis.

APPENDIX A
STATE, GENERALIZED STATE, AND ARMA MODELS

This appendix discusses briefly the relationships between the generalized state and state variable formulation of the equations of motion, and shows that the state variable formulation is equivalent to the autoregressive moving average (ARMA) formulation used in the parameter identification method of this study.

The generalized state equations are written in the form,

$$A_2 \ddot{x} + A_1 \dot{x} + A_0 x = Bu$$

where A_0 , A_1 , A_2 and B are coefficient matrices and x is a vector whose n elements are the degrees of freedom of the physical system. This set of equations may be transformed uniquely to state variable form by solving for \ddot{x} and defining

$$\underline{x} \equiv \begin{bmatrix} x \\ \dot{x} \end{bmatrix};$$

hence,

$$\dot{\underline{x}} = \begin{bmatrix} 0 & I \\ -A_2^{-1}A_0 & -A_2^{-1}A_1 \end{bmatrix} \underline{x} + \begin{bmatrix} 0 \\ A_2^{-1}B \end{bmatrix} u$$

(2n x 2n) (2nxq)

$$\equiv \underline{F}\underline{x} + \underline{G}u$$

The inverse transformation is, however, not unique. From the state variable form we obtain,

$$C\ddot{x} + CA_2^{-1}A_1\dot{x} + CA_2^{-1}A_0x = CA_2^{-1}Bu,$$

where C is any nonsingular matrix. If it is known that $C = A_2$, the original generalized state equation is obtained.

The ARMA form describes the output, y , where

$$y = H\underline{x} + Du \quad .$$

Taking successive time derivatives of this expression yields

$$\dot{y} = H\dot{\underline{x}} + D\dot{u} = HF\underline{x} + HGu + D\dot{u}$$

$$\ddot{y} = HF\dot{\underline{x}} + H\dot{G}u + D\ddot{u}$$

$$= HF^2\underline{x} + HFGu + H\dot{G}u + D\ddot{u}$$

$$\vdots$$

$$y^{(n)} = HF^n\underline{x} + HF^{n-1}Gu + HF^{n-2}\dot{G}u + \dots + Du^{(n)}$$

The characteristic polynomial of F is

$$N(\lambda) = \lambda^n + \alpha_{n-1}\lambda^{n-1} + \dots + \alpha_0 = 0 ,$$

hence, by the Cayley-Hamilton theorem, we may write

$$F^n = -\alpha_{n-1}F^{n-1} - \alpha_{n-2}F^{n-2} - \dots - \alpha_1F - \alpha_0 \quad .$$

Therefore,

$$\begin{aligned} y^{(n)} &= -\sum_{i=0}^{n-1} \alpha_i HF^i \underline{x} + HF^{n-1}Gu + HF^{n-2}\dot{G}u + \dots + Du^{(n)} \\ &= \sum_{i=0}^{n-1} \alpha_i (y^{(i)} - HF^{i-1}Gu - \dots - Du^{(i)}) + HF^{n-1}Gu + \dots + Du^{(n)} \end{aligned}$$

or

$$\begin{aligned} y^{(n)} + \sum_{i=0}^{n-1} \alpha_i y^{(i)} &= \sum_{i=0}^{n-1} \alpha_i (HF^{i-1}Gu + HF^{i-2}Gu + \dots + Du^{(i)}) \\ &\quad + HF^{n-1}Gu + \dots + Du^{(n)} \\ &\equiv B_n u^{(n)} + B_{n-1} u^{(n-1)} + \dots + B_0 u, \end{aligned}$$

which is the ARMA model upon which the new algorithm was based.

APPENDIX B
ON-LINE PARAMETER ESTIMATION USING THE
INSTRUMENTAL VARIABLES APPROACH

This appendix describes an algorithm for estimating the parameters of the autoregressive moving average model (Eq. (3.1)) using the instrumental variables approach. Equation (3.1) may be written as

$$y^{(n)}(t) + \sum_{i=1}^n a_i I y^{(n-i)}(t) = \sum_{i=0}^n (B_i u^{(n-i)}(t) + C_i v^{(n-i)}(t)) \quad (B.1)$$

Define

$$\begin{aligned} U(t) &= \{u^{(n)T}(t), u^{(n-1)T}(t), \dots, u^T(t)\} \\ Y_i(t) &= \{y_i^{(n-1)}(t), y_i^{(n-2)}(t), \dots, y_i(t)\} \\ a^T &= -(a_1, a_2, \dots, a_n) \\ B_i^T &= ((B_0)_i^T, (B_1)_i^T, \dots, (B_n)_i^T) \end{aligned} \quad (B.2)$$

where $y_i(t)$ is the i th element of vector $y(t)$ and $(B_j)_i$ is the i th column of B_j . Let

$$Q(t) = \begin{bmatrix} Y_1(t) & U(t) & 0 & \dots & 0 \\ Y_2(t) & 0 & U(t) & \dots & 0 \\ \vdots & \vdots & \vdots & \ddots & \vdots \\ Y_p(t) & 0 & 0 & \dots & U(t) \end{bmatrix} \quad (B.3)$$

Then Eq. (B.1) may be written as

$$y^{(n)}(t) = Q(t) \begin{pmatrix} a \\ B_1 \\ B_2 \\ \vdots \\ B_p \end{pmatrix} + \sum_{i=0}^n C_i v^{(n-i)}(t) \quad (B.4)$$

Premultiply both sides of the above equation by $P(t, \tau)$ given by

$$P(t, \tau) = \begin{bmatrix} Y_1^T(t-\tau) & Y_2^T(t-\tau) & \dots & Y_p^T(t-\tau) \\ U^T(t) & 0 & 0 & \dots & 0 \\ 0 & U^T(t) & 0 & \dots & 0 \\ \vdots & \vdots & & & \\ 0 & 0 & & & U^T(t) \end{bmatrix} \quad (B.5)$$

and take the expected value. For $\tau > 0$, the expected value of

$$P(t, \tau) \sum_{i=0}^n C_i v^{(n-i)}(t)$$

is zero. Therefore,

$$E(P(t, \tau) y^{(n)}(t)) = E(P(t, \tau) Q(t)) \begin{pmatrix} a \\ B_1 \\ B_2 \\ \vdots \\ B_p \end{pmatrix} \quad (B.6)$$

where E is the expected value operator. Let

$$R_{ab}(\tau) = E(u(t+\tau)y^T(t)) \quad (B.7)$$

$$R_{a^T a}(\tau) = \text{tr}(R_{aa}(\tau))$$

and use the following identities

$$(a) E(a^{(i)}(t+\tau)b^{(j)}(t)) = (-1)^j R_{ab}^{(i+j)}(\tau), \tau \geq 0 \quad (B.8)$$

$$(b) R_{ab}(\tau) = R_{ba}^T(-\tau)$$

The indicial superscript on $R_{ab}(\tau)$ implies differentiation with respect to τ . Then

$$E(P(t,\tau)\nabla^n y(t)) \triangleq \begin{bmatrix} b_0 \\ b_1 \\ b_2 \\ \vdots \\ b_p \end{bmatrix} \quad (B.9)$$

$$b_0 = \left. \begin{bmatrix} (-1)^{n-1} R^{(2n-1)}(\tau) \\ y^T y \\ (-1)^{n-2} R^{(2n-2)}(\tau) \\ y^T y \\ \vdots \\ (-1)^0 R^{(n)}(\tau) \\ y^T y \end{bmatrix} \right\} n \text{ elements}$$

$$b_i = (-1)^n \begin{bmatrix} R_{uy_i}^{(2n)}(0) \\ R_{uy_i}^{(2n-1)}(0) \\ \vdots \\ R_{uy_i}^{(n)}(0) \end{bmatrix} \left. \begin{array}{l} i=1,2,\dots,p \\ (n+1) \text{ elements} \end{array} \right\} \quad (\text{B.10})$$

and

$$E(P(t,\tau)Q(t)) \triangleq \begin{bmatrix} A_{11} & | & A_{12} \\ \hline A_{21} & | & A_{22} \end{bmatrix} \begin{array}{l} \} n \\ \} (n+1)pq \end{array} \quad (\text{B.11})$$

n (n+1)pq

$$A_{11} = \begin{bmatrix} (-1)^{n-1} R_{y^T y}^{(2n-2)}(\tau) & (-1)^{n-1} R_{y^T y}^{(2n-3)}(\tau) & \dots & (-1)^{n-1} R_{y^T y}^{(n-1)}(\tau) \\ (-1)^{n-2} R_{y^T y}^{(2n-3)}(\tau) & (-1)^{n-2} R_{y^T y}^{(2n-4)}(\tau) & \dots & (-1)^{n-2} R_{y^T y}^{(n-2)}(\tau) \\ \vdots & & & \vdots \\ (-1)^0 R_{y^T y}^{(n-1)}(\tau) & (-1)^0 R_{y^T y}^{(n-2)}(\tau) & \dots & (-1)^0 R_{y^T y}(\tau) \end{bmatrix} \quad (\text{B.12})$$

$$A_{12} = \{ (A_{12})_1, (A_{12})_2, \dots, (A_{12})_p \} \quad (\text{B.13})$$

$$(A_{12})_i = \begin{bmatrix} (-1)^{n-1} R_{uy_i}^{(2n-1)T}(\tau) & \dots & (-1)^{n-1} R_{uy_i}^{(n-1)}(\tau) \\ \vdots & & \vdots \\ (-1)^0 R_{uy_i}^{(n)T}(\tau) & \dots & (-1)^0 R_{uy_i}^T(\tau) \end{bmatrix} \quad (\text{B.14})$$

$$A_{21} = \begin{bmatrix} (A_{21})_1 \\ \vdots \\ (A_{21})_i \\ \vdots \\ (A_{21})_p \end{bmatrix} \quad (B.15)$$

$$(A_{21})_i = \begin{bmatrix} (-1)^{n-1} R_{uy_i}^{(2n-1)}(0) & \dots & (-1)^0 R_{uy_i}^{(n)}(0) \\ \vdots & & \vdots \\ (-1)^{n-1} R_{uy_i}^{(n-1)}(0) & \dots & (-1)^0 R_{uy_i}(0) \end{bmatrix} \quad (B.16)$$

$$A_{22} = \begin{bmatrix} \bar{A}_{22} & 0 & \dots & 0 \\ 0 & \bar{A}_{22} & & 0 \\ \vdots & & \ddots & \\ 0 & 0 & & \bar{A}_{22} \end{bmatrix} \quad (B.17)$$

$$\bar{A}_{22} = \begin{bmatrix} (-1)^n R_{uu}^{(2n)}(0) & \dots & (-1)^0 R_{uu}^{(n)}(0) \\ \vdots & & \vdots \\ (-1)^n R_{uu}^{(n)}(0) & \dots & (-1)^0 R_{uu}(0) \end{bmatrix} \quad (B.18)$$

In the light of Eqs. (B.9) - (B.18), Eq. (B.6) may be written as

$$b_0 = A_{11} a + \sum_{i=1}^p (A_{12})_i \beta_i \quad (B.19)$$

$$b_i = (A_{21})_i a + \bar{A}_{22} \beta_i, \quad i=1,2,\dots,p \quad (B.20)$$

Equation (B.20) may be solved for β_i

$$\beta_i = \bar{A}_{22}^{-1} (b_i - (A_{21})_i a) \quad (\text{B.21})$$

Therefore, the equation for determining a is

$$b_0 - \sum_{i=1}^p (A_{12})_i \bar{A}_{22}^{-1} b_i = \{A_{11} - \sum_{i=1}^p (A_{12})_i \bar{A}_{22}^{-1} (A_{21})_i\} a \quad (\text{B.22})$$

This is a set of n linear equations in n unknowns a . If the zeroes of the transfer function are desired they may be obtained by substituting a in Eq. (B.22).

Estimation of Differentials of Correlation Functions:

Matrices A 's and vectors B 's in Eq. (B.22) are functions of differentials and auto- and cross-correlations of input u and output y . These differentials must be estimated from data, which would typically be discrete input and output time histories (or equivalently the corresponding Fourier transforms). There are two approaches which may be used to estimate differentials of the correlation functions. Let the inputs and outputs be $u(i)$ and $y(i)$, $i=1,2,\dots,N$, respectively.

In the direct approach the auto- and cross-correlations of the inputs and the outputs are computed.

$$\begin{aligned} R_{yy}(r\Delta) &= \frac{1}{N} \sum_{i=1}^{N-r} y(i+r)y^T(i) \\ R_{uy}(r\Delta) &= \frac{1}{N} \sum_{i=0}^{N-r} u(i+r)y^T(i) \\ R_{uu}(r\Delta) &= \frac{1}{N} \sum_{i=0}^{N-r} u(i+r)u^T(i) \end{aligned} \quad (\text{B.23})$$

where Δ is the sampling interval. τ is chosen to be a multiple of Δ . The derivatives of the correlation functions are determined by numerical differentiation, e.g.

$$\begin{aligned} R_{yy}^{(1)}(\tau) &= \frac{1}{2\Delta} (R_{yy}(\tau+\Delta) - R_{yy}(\tau-\Delta)) \\ R_{yy}^{(2)}(\tau) &= \frac{1}{\Delta^2} (R_{yy}(\tau+\Delta) + R_{yy}(\tau-\Delta) - 2R_{yy}(\tau)) \end{aligned} \quad (\text{B.24})$$

etc.

In the second approach, the differentials of correlation functions are estimated from the Fourier transforms of the inputs and the outputs given by

$$Y(k) = \sum_{i=1}^N y(i) e^{-j2\pi(i-1)k/N} \quad (\text{B.25})$$

$$U(k) = \sum_{i=1}^N u(i) e^{-j2\pi(i-1)k/N}$$

$$k = 0, 1, 2, \dots, N-1$$

The autospectrum of y and the cross-spectrum of y and u are given by (for N even)

$$S_{yy}(k) = \frac{1}{N} Y(k) Y^*(k) \quad (\text{B.26})$$

$$S_{yu}(k) = \frac{1}{N} Y(k) U^*(k)$$

$$k = -\frac{N}{2} + 1, -\frac{N}{2} + 2, \dots, 0, 1, \frac{N}{2} - 1$$

The autocorrelation of y is given by

$$R_{yy}(\tau) = \sum_{k = -\frac{N}{2} + 1}^{N/2 - 1} S_{yy}(k) e^{\frac{j2\pi\tau k}{N\Delta}} \quad (\text{B.27})$$

Therefore,

$$R_{yy}^{(n)}(\tau) = \sum_{k = -\frac{N}{2} + 1}^{N/2 - 1} S_{yy}(k) \left(\frac{j2\pi k}{N\Delta} \right)^n e^{\frac{j2\pi\tau k}{N\Delta}} \quad (\text{B.28})$$

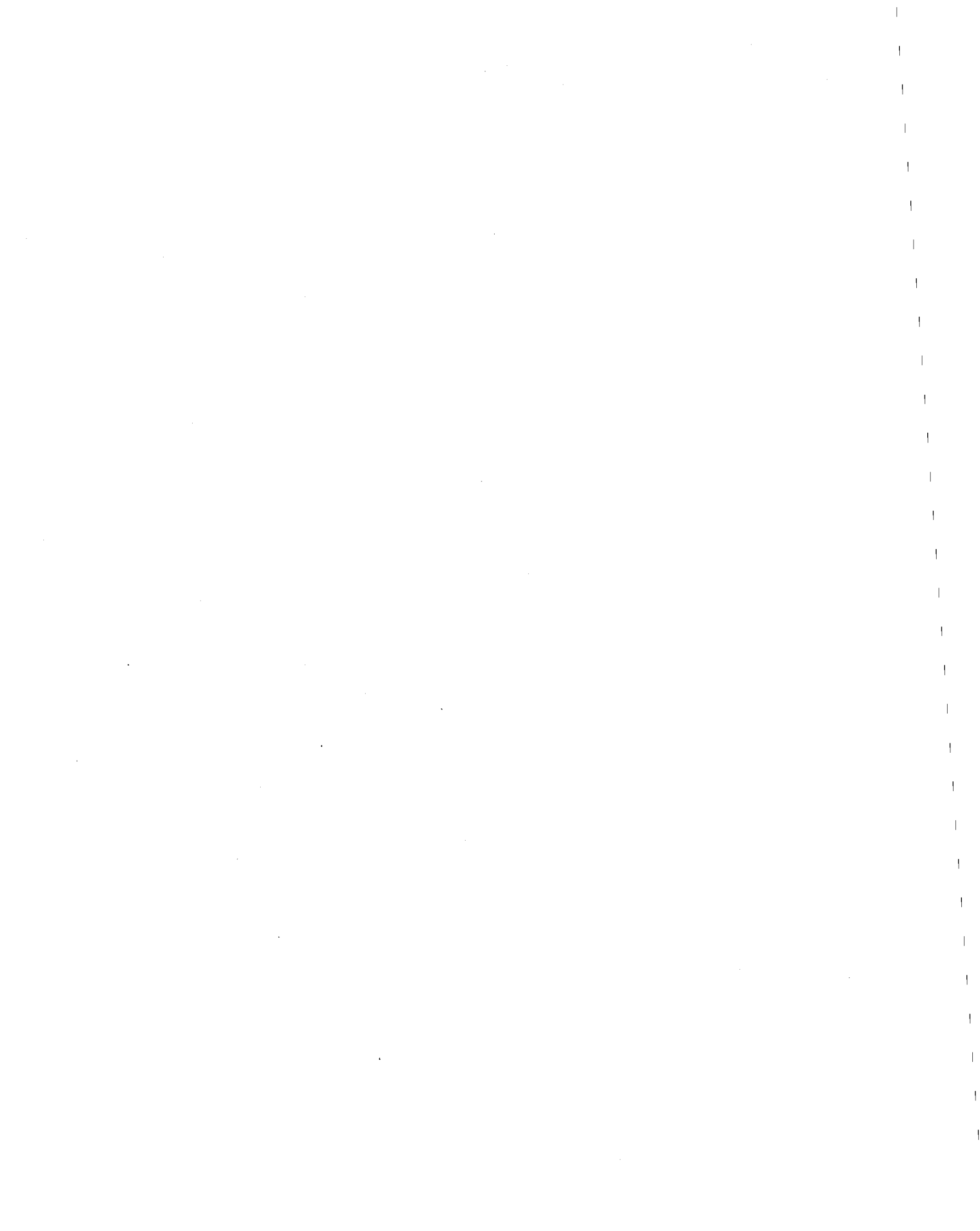
Similarly,

$$R_{uy}^{(n)}(\tau) = \sum_{k = -\frac{N}{2} + 1}^{N/2 - 1} S_{uy}(k) \left(\frac{j2\pi k}{N\Delta} \right)^n e^{\frac{j2\pi\tau k}{N\Delta}} \quad (\text{B.29})$$

and

$$R_{uu}^{(n)}(\tau) = \sum_{k = -\frac{N}{2} + 1}^{N/2 - 1} S_{uu}(k) \left(\frac{j2\pi k}{N\Delta} \right)^n e^{\left(\frac{j2\pi\tau k}{N\Delta} \right)} \quad (\text{B.30})$$

Equations (B.28) - (B.30) are very flexible. Since the system is linear, $S_{yy}(k)$, $S_{uy}(k)$, and $S_{uu}(k)$ may be passed through the same filter and then used in Eqs. (B.28) - (B.30). This is equivalent to passing the input and output data through the same filter before identification. It is useful when there is discrete frequency noise or a certain frequency range does not contain much information about the system modes. A band pass filter can then be applied to reject these frequencies.



APPENDIX C

XV-15 MODEL AND DYNAMIC CHARACTERISTICS

This appendix presents additional information on the XV-15 model and on its predicted aeroelastic characteristics at the six flight conditions studied in this report (Chapter IV). These data comprise the analytical solutions to which the results of algorithm application were compared. The contents of this appendix are:

Table C.1: Analytical model degrees of freedom and modes.

Table C.2: State, control, gust, and observation vectors.

Table C.3: Wingtip deflection constants.

Tables C.4 to C.9: Roots of symmetric wingtip deflection/
control input transfer functions.

Tables C.10 to C.15: Roots of antisymmetric wingtip
deflection/control input transfer functions

PRECEDING PAGE BLANK NOT FILMED

Table C.1
Analytic Model Degrees of Freedom and Modes

| DEGREES OF FREEDOM | | MODES | |
|--------------------|---------------|--------------|---------------|
| SYMMETRIC | ANTISYMMETRIC | SYMMETRIC | ANTISYMMETRIC |
| β_0 | β_0 | β_0 | β_0 |
| β_{1c} | β_{1c} | β_{+1} | β_{+1} |
| β_{1s} | β_{1s} | β_{-1} | β_{-1} |
| ζ_{1c} | ζ_{1c} | ζ_{+1} | ζ_{+1} |
| ζ_{1s} | ζ_{1s} | ζ_{-1} | ζ_{-1} |
| ψ_s | ψ_s | ψ_s | ψ_s |
| α | α | α | α |
| q_1 | q_1 | q_1 | q_1 |
| q_2 | q_2 | q_2 | q_2 |
| p | p | p | p |
| BV | BV | BY | BY |
| SL | SS | SL | SS |
| BL | BS | BL | BS |

Table C.2

State, Control, Gust, and Observation Vectors

$$\underline{x}_{\text{SYMMETRIC}}^T = [\zeta_{1c} \ \zeta_{1s} \ \beta_0 \ \beta_{1c} \ \beta_{1s} \ \psi_s \ \text{BL} \ q_1 \ \text{SL} \ q_2 \ p \ \text{BV} \ \alpha]$$

$$\underline{x}_{\text{ANTI-SYMMETRIC}}^T = [\zeta_{1c} \ \zeta_{1s} \ \beta_0 \ \beta_{1c} \ \beta_{1s} \ \psi_s \ \text{BY} \ \text{BS} \ q_2 \ q_1 \ \text{SS} \ p \ \alpha]$$

$$\underline{\dot{x}}^T = [\underline{x}^T \ ; \ \dot{\underline{x}}^T] \quad (\text{SYMMETRIC AND ANTISYMMETRIC})$$

$$\underline{y}^T = [X_{\text{TIP}} \ \ Z_{\text{TIP}}]$$

$$\underline{u}^T = [\theta_0 \ \theta_{1c} \ \theta_{1s} \ \delta_F]$$

$$\underline{g}^T = [u_g \ \ v_g \ \ w_g]$$

$$\underline{u}^T = [\underline{u}^T \ ; \ \underline{g}^T]$$

NOTE: Vector elements are defined in "Nomenclature", pp.vi-x.

Table C.3
Wingtip Deflection Constants

EQUATIONS:

$$X_{TIP} = \sum_{i=1}^7 \epsilon_{x_i} x_i, \text{ ft}; \quad Z_{TIP} = \sum_{i=1}^7 \epsilon_{z_i} x_i, \text{ ft.}$$

CONSTANTS:

| SYMMETRIC DEGREES OF FREEDOM | | | |
|------------------------------|----------|------------------|------------------|
| i | x_i | ϵ_{x_i} | ϵ_{z_i} |
| 1 | BL | 12.48 | 0.64 |
| 2 | q_1 | -0.16 | -11.78 |
| 3 | SL | 11.92 | 0.58 |
| 4 | q_2 | -6.54 | -3.58 |
| 5 | p | 3.18 | -1.36 |
| 6 | BV | 6.23 | -6.15 |
| 7 | α | -2.46 | -0.71 |

| ANTISYMMETRIC DEGREES OF FREEDOM | | | |
|----------------------------------|----------|------------------|------------------|
| i | x_i | ϵ_{x_i} | ϵ_{z_i} |
| 1 | BY | -10.15 | 0.42 |
| 2 | BS | 0.49 | -2.74 |
| 3 | q_2 | 10.80 | -1.04 |
| 4 | q_1 | 10.36 | 9.52 |
| 5 | SS | 1.88 | -3.10 |
| 6 | p | -4.29 | -6.36 |
| 7 | α | 1.29 | -4.78 |

Table C.4
Symmetric Transfer Function Roots

Flight Condition #1: Hover

$$\alpha_p = 90^\circ$$

$$V = 0$$

$$\Omega = 565 \text{ RPM}$$

| MODE | POLES | | ZEROS | |
|--------------|---------|---------------|--------------------|---------------|
| | | | Z_{TIP}/θ_o | |
| | REAL | IMAGINARY | REAL | IMAGINARY |
| ψ_s | -0.023 | 0 | 0 | 0 |
| ψ_s | -0.071 | 0 | -0.049 | 0 |
| BL | -0.0021 | <u>+0.202</u> | -0.0021 | <u>+0.202</u> |
| q_1 | -0.0087 | <u>+0.286</u> | -0.0070 | <u>+0.348</u> |
| SL | -0.0067 | <u>+0.348</u> | -0.264 | <u>+0.107</u> |
| β_{-1} | -0.264 | <u>+0.108</u> | -0.089 | <u>+0.465</u> |
| ζ_{-1} | -0.089 | <u>+0.467</u> | -0.0077 | <u>+0.573</u> |
| q_2 | -0.0082 | <u>+0.574</u> | -0.0091 | <u>+0.751</u> |
| p | -0.0100 | <u>+0.738</u> | -0.0080 | <u>+0.817</u> |
| BV | -0.0083 | <u>+0.820</u> | -0.0146 | <u>+0.933</u> |
| α | -0.0132 | <u>+0.952</u> | -0.316 | <u>+1.91</u> |
| β_{+1} | -0.316 | <u>+1.91</u> | -0.0180 | <u>+2.53</u> |
| β_o | -0.225 | <u>+2.21</u> | -0.426 | <u>+16.6</u> |
| ζ_{+1} | -0.0155 | <u>+2.54</u> | | |

Table C.5
Symmetric Transfer Function Roots

Flight Condition #2

$\alpha_p = 82.3^\circ$

$V = 80$ kts

$\Omega = 565$ RPM

| MODE | POLES | | ZEROS | | | |
|--------------|---------|-------------|--------------------|-------------|--------------------|-------------|
| | | | X_{TIP}/θ_o | | Z_{TIP}/δ_F | |
| | REAL | IMAGINARY | REAL | IMAGINARY | REAL | IMAGINARY |
| ψ_s | -0.027 | ± 0.022 | -0.100 | 0 | -0.0282 | ± 0.020 |
| BL | -0.0022 | ± 0.202 | +0.073 | 0 | -0.0019 | ± 0.202 |
| q_1 | -0.0129 | ± 0.291 | -0.192 | ± 0.093 | 0.0002 | ± 0.325 |
| SL | -0.0080 | ± 0.353 | -0.0026 | ± 0.213 | -0.262 | ± 0.116 |
| β_{-1} | -0.2659 | ± 0.106 | -0.0092 | ± 0.319 | -0.0725 | ± 0.542 |
| ζ_{-1} | -0.0751 | ± 0.549 | -0.0746 | ± 0.538 | 0.0472 | ± 0.617 |
| q_2 | -0.0102 | ± 0.575 | -0.0146 | ± 0.631 | -0.0764 | ± 0.650 |
| p | -0.0091 | ± 0.737 | -0.0095 | ± 0.700 | -0.0861 | ± 0.807 |
| BV | -0.0089 | ± 0.820 | +0.0373 | ± 0.844 | 0.0621 | ± 0.819 |
| α | -0.0142 | ± 0.956 | -0.0809 | ± 0.857 | -0.311 | ± 1.909 |
| β_{+1} | -0.307 | ± 1.92 | -0.363 | ± 1.81 | -0.262 | ± 2.235 |
| β_o | -0.260 | ± 2.26 | -0.070 | ± 2.57 | -0.0085 | ± 2.658 |
| ζ_{+1} | -0.008 | ± 2.63 | 2.77 | 0 | --- | --- |
| | | | -3.81 | 0 | | |

Table C.6
Symmetric Transfer Function Roots

Flight Condition #3

$\alpha_p = 60^\circ$

V = 100 kts

$\Omega = 565$ RPM

| MODE | POLES | | ZEROS | | | |
|--------------|---------|-------------|--------------------|-------------|--------------------|-------------|
| | | | X_{TIP}/θ_0 | | Z_{TIP}/δ_F | |
| | REAL | IMAGINARY | REAL | IMAGINARY | REAL | IMAGINARY |
| ψ_s | -0.019 | ± 0.028 | 0.0116 | 0 | -0.020 | ± 0.029 |
| BL | -0.0023 | ± 0.203 | -0.0162 | 0 | -0.0017 | ± 0.201 |
| q_1 | -0.0097 | ± 0.292 | -0.0018 | ± 0.231 | +0.0064 | ± 0.335 |
| SL | -0.0098 | ± 0.397 | -0.0053 | ± 0.284 | -0.310 | ± 0.135 |
| β_{-1} | -0.310 | ± 0.126 | -0.312 | ± 0.121 | -0.0118 | ± 0.464 |
| ζ_{-1} | -0.062 | ± 0.496 | -0.059 | ± 0.488 | -0.072 | ± 0.498 |
| q_2 | -0.0106 | ± 0.573 | -0.0193 | ± 0.556 | -0.0116 | ± 0.723 |
| p | -0.0087 | ± 0.743 | -0.0088 | ± 0.742 | -0.0092 | ± 0.740 |
| BV | -0.0094 | ± 0.814 | -0.0115 | ± 0.843 | -0.0135 | ± 0.947 |
| α | -0.0134 | ± 0.938 | -0.020 | ± 0.907 | -0.296 | ± 1.89 |
| β_{+1} | -0.298 | ± 1.89 | -0.272 | ± 1.87 | -0.276 | ± 2.25 |
| β_0 | -0.274 | ± 2.26 | -0.319 | ± 2.58 | -0.0164 | ± 2.61 |
| ζ_{+1} | -0.0128 | ± 2.58 | 4.55 | 0 | --- | --- |
| | | | -4.77 | 0 | | |

Table C.7
Symmetric Transfer Function Roots

Flight Condition #4

$\alpha_p = 30^\circ$

$V = 120$ kts

$\Omega = 565$ RPM

| MODE | POLES | | ZEROS | | | |
|--------------|---------|-------------|--------------------------|-------------|--------------------|-------------|
| | | | λ_{TIP}/θ_0 | | Z_{TIP}/δ_F | |
| | REAL | IMAGINARY | REAL | IMAGINARY | REAL | IMAGINARY |
| ψ_s | -0.0320 | ± 0.031 | +0.0073 | 0 | -0.0336 | ± 0.032 |
| BL | -0.0026 | ± 0.202 | -0.0091 | 0 | -0.0022 | ± 0.203 |
| q_1 | -0.0056 | ± 0.296 | -0.0021 | ± 0.239 | -0.0535 | ± 0.35 |
| ζ_{-1} | -0.0645 | ± 0.353 | -0.0044 | ± 0.302 | -0.0034 | ± 0.426 |
| SL | -0.0101 | ± 0.435 | -0.0638 | ± 0.345 | -0.325 | ± 0.164 |
| β_{-1} | -0.3157 | ± 0.138 | -0.319 | ± 0.131 | -0.0375 | ± 0.652 |
| q_2 | -0.0095 | ± 0.566 | -0.0096 | ± 0.568 | -0.0387 | ± 0.677 |
| p | -0.0079 | ± 0.680 | -0.0110 | ± 0.699 | 0.364 | ± 1.15 |
| BV | -0.0095 | ± 0.822 | -0.0112 | ± 0.837 | -0.683 | ± 1.09 |
| α | -0.0141 | ± 1.004 | -0.0186 | ± 0.988 | -0.200 | ± 1.81 |
| β_{+1} | -0.320 | ± 1.88 | -0.2847 | ± 1.87 | -0.262 | ± 2.16 |
| β_0 | -0.253 | ± 2.21 | -0.0194 | ± 2.43 | 1.11 | ± 3.07 |
| ζ_{+1} | -0.0216 | ± 2.44 | -0.0809 | ± 8.30 | --- | --- |

Table C.8
Symmetric Transfer Function Roots

Flight Condition #5

$\alpha_p = 0^\circ$

V = 160 kts

$\Omega = 458$ RPM

| MODE | POLES | | ZEROS | | | |
|--------------|---------|-------------|-----------------------|-------------|--------------------|-------------|
| | | | χ_{TIP}/θ_0 | | Z_{TIP}/δ_F | |
| | REAL | IMAGINARY | REAL | IMAGINARY | REAL | IMAGINARY |
| ψ_s | -0.0646 | ± 0.016 | 0 | 0 | -0.0646 | ± 0.016 |
| BL | -0.0031 | ± 0.250 | -0.0016 | 0 | -0.0030 | ± 0.249 |
| q_1 | -0.0096 | ± 0.372 | -0.0027 | ± 0.296 | -0.309 | ± 0.136 |
| ζ_{-1} | -0.0933 | ± 0.405 | -0.0096 | ± 0.371 | -0.092 | ± 0.394 |
| β_{-1} | -0.293 | ± 0.142 | -0.094 | ± 0.406 | +0.0079 | ± 0.587 |
| SL | -0.0117 | ± 0.560 | -0.292 | ± 0.141 | -0.0176 | ± 0.627 |
| p | -0.0205 | ± 0.809 | -0.165 | ± 0.776 | -0.0176 | ± 0.840 |
| q_2 | -0.0111 | ± 0.838 | -0.0103 | ± 0.816 | -0.0021 | ± 1.25 |
| BV | -0.0124 | ± 1.03 | -0.0119 | ± 1.02 | -0.0035 | ± 1.51 |
| β_{+1} | -0.316 | ± 1.84 | -0.306 | ± 1.82 | -0.290 | ± 1.89 |
| α | -0.013 | ± 2.04 | -0.020 | ± 1.96 | -0.094 | ± 2.48 |
| β_0 | -0.066 | ± 2.55 | -0.0607 | ± 2.55 | -0.209 | ± 2.57 |
| ζ_{+1} | -0.201 | ± 2.57 | -0.104 | ± 5.23 | --- | --- |

Table C.9
Symmetric Transfer Function Roots

Flight Condition #6

$\alpha_p = 0^\circ$

V = 200 kts

$\Omega = 458$ RPM

| MODE | POLES | | ZEROS | | | |
|--------------|---------|-------------|--------------------|-------------|--------------------|-------------|
| | | | x_{TIP}/θ_o | | z_{TIP}/δ_F | |
| | REAL | IMAGINARY | REAL | IMAGINARY | REAL | IMAGINARY |
| ψ_s | -0.041 | 0 | 0 | 0 | -0.041 | 0 |
| ψ_s | -0.152 | 0 | -0.0032 | 0 | -0.152 | 0 |
| BL | -0.0030 | ± 0.250 | -0.0026 | ± 0.296 | -0.0028 | ± 0.25 |
| z_{-1} | -0.0897 | ± 0.314 | -0.090 | ± 0.315 | -0.0884 | ± 0.308 |
| q_1 | -0.0111 | ± 0.372 | -0.0118 | ± 0.371 | -0.346 | ± 0.188 |
| β_{-1} | -0.315 | ± 0.196 | -0.315 | ± 0.194 | +0.035 | ± 0.576 |
| SL | -0.0112 | ± 0.558 | -0.0245 | ± 0.764 | -0.036 | ± 0.602 |
| p | -0.0280 | ± 0.791 | -0.0076 | ± 0.809 | -0.020 | ± 0.839 |
| q_2 | -0.0102 | ± 0.835 | -0.0123 | ± 1.02 | +0.0038 | ± 1.25 |
| BV | -0.0130 | ± 1.03 | -0.337 | ± 1.77 | -0.052 | ± 1.50 |
| β_{+1} | -0.351 | ± 1.79 | -0.0211 | ± 1.95 | -0.317 | ± 1.87 |
| α | -0.0118 | ± 2.03 | -0.0768 | ± 2.47 | -0.104 | ± 2.39 |
| β_o | -0.0792 | ± 2.47 | -0.108 | ± 5.15 | -0.206 | ± 2.51 |
| z_{+1} | -0.198 | ± 2.51 | --- | --- | --- | --- |

Table C.10
Antisymmetric Transfer Function Roots

Flight Condition #1

$\alpha_p = 90^\circ$

$V = 0$

$\Omega = 565 \text{ RPM}$

| MODE | POLES | | ZEROS | |
|--------------|---------|-------------|--------------------|-------------|
| | | | Z_{TIP}/θ_0 | |
| | REAL | IMAGINARY | REAL | IMAGINARY |
| BS | -0.0032 | ± 0.281 | -0.0012 | ± 0.211 |
| BY | -0.0027 | ± 0.228 | -0.0018 | ± 0.240 |
| q_2 | -0.0062 | ± 0.330 | -0.0054 | ± 0.332 |
| q_1 | -0.0114 | ± 0.391 | -0.269 | ± 0.113 |
| ζ_{-1} | -0.0877 | ± 0.467 | -0.0964 | ± 0.462 |
| β_{-1} | -0.264 | ± 0.108 | -0.148 | ± 0.686 |
| ψ_s | -0.0196 | ± 0.577 | -0.0004 | ± 0.699 |
| p | -0.0116 | ± 0.621 | +0.150 | ± 0.683 |
| SS | -0.0088 | ± 0.707 | -0.0170 | ± 0.999 |
| α | -0.0113 | ± 0.908 | -0.312 | ± 1.93 |
| β_{+1} | -0.318 | ± 1.914 | -0.075 | ± 2.54 |
| β_0 | -0.211 | ± 2.364 | -2.54 | 0 |
| ζ_{+1} | -0.0152 | ± 2.53 | 2.61 | 0 |

Table C.11
Antisymmetric Transfer Function Roots

Flight Condition #2

$$\alpha_p = 82.3^\circ$$

$$V = 80 \text{ kts}$$

$$\Omega = 565 \text{ RPM}$$

| MODE | POLES | | ZEROS | | | |
|--------------|---------|-------------|--------------------|-------------|--------------------|-------------|
| | | | x_{TIP}/θ_0 | | z_{TIP}/δ_F | |
| | REAL | IMAGINARY | REAL | IMAGINARY | REAL | IMAGINARY |
| BS | -0.0034 | ± 0.281 | -0.0069 | ± 0.237 | -0.0031 | ± 0.229 |
| BY | -0.0030 | ± 0.229 | -0.0030 | ± 0.281 | -0.0037 | ± 0.259 |
| q_2 | -0.0067 | ± 0.333 | -0.0108 | ± 0.312 | -0.0064 | ± 0.335 |
| q_1 | -0.0140 | ± 0.397 | -0.238 | ± 0.088 | -0.272 | ± 0.109 |
| β_{-1} | -0.2670 | ± 0.106 | -0.0081 | ± 0.538 | -0.0794 | ± 0.542 |
| ζ_{-1} | -0.0740 | ± 0.545 | -0.0784 | ± 0.544 | -0.0168 | ± 0.572 |
| ψ_s | -0.0158 | ± 0.578 | -0.0081 | ± 0.631 | -0.0265 | ± 0.690 |
| p | -0.0099 | ± 0.630 | -0.0098 | ± 0.704 | +0.0135 | ± 0.711 |
| SS | -0.0085 | ± 0.704 | -0.0051 | ± 0.939 | -0.0059 | ± 0.861 |
| α | -0.0139 | ± 0.909 | -0.346 | ± 1.89 | -0.3100 | ± 1.92 |
| β_{+1} | -0.307 | ± 1.91 | -0.0047 | ± 2.61 | -0.230 | ± 2.45 |
| β_0 | -0.239 | ± 2.45 | 5.68 | 0 | -0.0773 | ± 2.59 |
| ζ_{+1} | -0.0101 | ± 2.62 | -6.19 | 0 | --- | --- |

Table C.12
Antisymmetric Transfer Function Roots

Flight Condition #3

$\alpha_p = 60^\circ$

V = 100 kts

$\Omega = 565$ RPM

| MODE | POLES | | ZEROS | | | |
|----------------|---------|-------------|--------------------------|-------------|--------------------|-------------|
| | | | λ_{TIP/θ_0} | | Z_{TIP/δ_F} | |
| | REAL | IMAGINARY | REAL | IMAGINARY | REAL | IMAGINARY |
| BS | -0.0032 | ± 0.282 | -0.0032 | ± 0.280 | -0.0030 | ± 0.230 |
| BY | -0.0031 | ± 0.231 | -0.0031 | ± 0.298 | -0.0028 | ± 0.270 |
| q ₂ | -0.0053 | ± 0.352 | -0.0095 | ± 0.363 | -0.0066 | ± 0.361 |
| q ₁ | -0.0134 | ± 0.398 | -0.0616 | ± 0.491 | -0.0611 | ± 0.494 |
| ζ_{-1} | -0.0654 | ± 0.494 | -0.315 | ± 0.093 | -0.313 | ± 0.121 |
| ψ_s | -0.0079 | ± 0.585 | -0.0032 | ± 0.628 | -0.0402 | ± 0.589 |
| β_{-1} | -0.309 | ± 0.126 | -0.0097 | ± 0.665 | 0.0194 | ± 0.583 |
| SS | -0.0110 | ± 0.663 | -0.0046 | ± 0.838 | -0.0103 | ± 0.658 |
| P | -0.0093 | ± 0.702 | -0.261 | ± 1.47 | -0.0161 | ± 0.918 |
| α | -0.0138 | ± 0.918 | 0.798 | ± 1.34 | -0.300 | ± 1.89 |
| β_{+1} | -0.299 | ± 1.89 | -1.57 | ± 1.63 | -0.267 | ± 2.41 |
| β_0 | -0.262 | ± 2.43 | -0.0453 | ± 2.63 | 0.0084 | ± 2.56 |
| ζ_{+1} | -0.0135 | ± 2.58 | --- | --- | --- | --- |

Table C.13
Antisymmetric Transfer Function Roots

Flight Condition #4

$\alpha_p = 30^\circ$

V = 120 kts

$\Omega = 565$ RPM

| MODE | POLES | | ZEROS | | | |
|--------------|---------|-------------|--------------------|-------------|--------------------|-------------|
| | | | X_{TIP}/θ_0 | | Z_{TIP}/δ_F | |
| | REAL | IMAGINARY | REAL | IMAGINARY | REAL | IMAGINARY |
| BY | -0.0038 | ± 0.231 | -0.0024 | ± 0.266 | -0.0036 | ± 0.231 |
| BS | -0.0031 | ± 0.282 | -0.0030 | ± 0.283 | -0.0020 | ± 0.272 |
| q_2 | -0.0073 | ± 0.375 | -0.0613 | ± 0.355 | -0.0627 | ± 0.352 |
| q_1 | -0.0177 | ± 0.392 | -0.0083 | ± 0.378 | -0.0081 | ± 0.376 |
| r_{-1} | -0.0060 | ± 0.357 | -0.3111 | ± 0.129 | -0.316 | ± 0.132 |
| β_{-1} | -0.3148 | ± 0.137 | 0.022 | ± 0.631 | -0.0142 | ± 0.620 |
| ψ_s | -0.0146 | ± 0.588 | -0.0288 | ± 0.648 | -0.0794 | ± 0.634 |
| SS | -0.0140 | ± 0.653 | -0.0085 | ± 0.784 | 0.053 | ± 0.629 |
| p | -0.0086 | ± 0.759 | -0.0254 | ± 0.914 | -0.0228 | ± 0.993 |
| α | -0.0171 | ± 0.944 | -0.293 | ± 1.96 | -0.322 | ± 1.88 |
| β_{+1} | -0.321 | ± 1.88 | -0.0201 | ± 2.44 | -0.272 | ± 2.30 |
| β_0 | -0.267 | ± 2.32 | -11.65 | 0 | -0.0057 | ± 2.44 |
| r_{+1} | -0.0216 | ± 2.44 | 16.1 | 0 | --- | --- |

Table C.14
Antisymmetric Transfer Function Roots

Flight Condition #5

$$\alpha_p = 0$$

V = 160 kts

$\Omega = 458$ RPM

| MODE | POLES | | ZEROS | | | |
|--------------|---------|-------------|--------------------|-------------|--------------------|-------------|
| | | | x_{TIP}/θ_o | | Z_{TIP}/θ_F | |
| | REAL | IMAGINARY | REAL | IMAGINARY | REAL | IMAGINARY |
| q_2 | -0.0152 | ± 0.486 | 0 | ± 0.184 | -0.0053 | ± 0.285 |
| BS | -0.0041 | ± 0.348 | -0.0040 | ± 0.348 | -0.0041 | ± 0.339 |
| q_1 | -0.0177 | ± 0.520 | -0.0938 | ± 0.401 | -0.0931 | ± 0.402 |
| BY | -0.0044 | ± 0.284 | -0.295 | ± 0.139 | -0.0122 | ± 0.486 |
| ζ_{-1} | -0.0929 | ± 0.402 | -0.0074 | ± 0.510 | -0.293 | ± 0.138 |
| β_{-1} | -0.293 | ± 0.140 | -0.0136 | ± 0.820 | -0.0576 | ± 0.729 |
| ψ_s | -0.0624 | ± 0.723 | -0.114 | ± 1.03 | -0.152 | ± 0.773 |
| SS | -0.0183 | ± 0.820 | -0.0934 | ± 1.03 | +0.110 | ± 0.789 |
| p | -0.0105 | ± 0.984 | -0.314 | ± 1.89 | -0.305 | ± 1.87 |
| β_{+1} | -0.320 | ± 1.87 | -0.0781 | ± 2.44 | -0.0236 | ± 2.47 |
| ζ_{+1} | -0.0375 | ± 2.42 | -0.0559 | ± 2.80 | -0.237 | ± 2.64 |
| β_o | -0.240 | ± 2.65 | -8.39 | 0 | -0.117 | ± 3.36 |
| α | -0.0405 | ± 2.87 | 8.26 | 0 | --- | --- |

Table C.15
Antisymmetric Transfer Function Roots

Flight Condition #6

$$\alpha_p = 0$$

V = 200 kts

$\Omega = 458$ RPM

| MODE | POLES | | ZEROS | | | |
|--------------|---------|-------------|--------------------|-------------|--------------------|-------------|
| | | | x_{TIP}/θ_0 | | z_{TIP}/δ_F | |
| | REAL | IMAGINARY | REAL | IMAGINARY | REAL | IMAGINARY |
| q_2 | -0.0142 | ± 0.485 | 0.0002 | ± 0.196 | -0.0057 | ± 0.285 |
| q_1 | -0.0224 | ± 0.517 | -0.0906 | ± 0.314 | -0.0027 | ± 0.341 |
| BS | -0.0042 | ± 0.348 | -0.0041 | ± 0.349 | -0.0904 | ± 0.312 |
| BY | -0.0044 | ± 0.283 | -0.317 | ± 0.194 | -0.0117 | ± 0.484 |
| ζ_{-1} | -0.0908 | ± 0.314 | -0.0072 | ± 0.505 | -0.316 | ± 0.189 |
| β_{-1} | -0.317 | ± 0.192 | -0.0175 | ± 0.813 | -0.0799 | ± 0.726 |
| ψ_s | -0.0950 | ± 0.716 | -0.146 | ± 1.03 | -0.168 | ± 0.759 |
| SS | -0.0234 | ± 0.812 | 0.116 | ± 1.04 | 0.102 | ± 0.784 |
| p | -0.0117 | ± 0.980 | -0.358 | ± 1.87 | -0.339 | ± 1.84 |
| β_{+1} | -0.362 | ± 1.84 | -0.085 | ± 2.34 | -0.034 | ± 2.38 |
| ζ_{+1} | -0.0398 | ± 2.33 | -0.0527 | ± 2.80 | -0.232 | ± 2.56 |
| β_0 | -0.235 | ± 2.56 | -8.22 | 0 | -0.118 | ± 3.35 |
| α | -0.0423 | ± 2.86 | 8.08 | 0 | --- | --- |

REFERENCES

1. Hall, W.E., Jr., Mohr, R., and Walker, R., "Analytical Evaluation of Tilting Proprotor Wind Tunnel Test Requirements," Report on Contract NAS2-8799, Jan. 1976.
2. Hall, W.E., "Proprotor Stability at High Advance Ratios," Journal of the American Helicopter Society, Vol. 11, No. 2., pp. 11-26, 1966.
3. Edenborough, H.K., Gaffey, T.M., Weiberg, J.A., "Analysis and Tests Confirm Design of Proprotor Aircraft," AIAA Paper 72-803.
4. Alexander, H.R., Amos, A.K., Tarzanin, F.J., Taylor, R.B., "V/STOL Dynamics and Aeroelastic Rotor-Airframe Technology," AFFDL-TR-72-40, Vol. 2, Boeing Co., Sept. 1972.
5. Johnson, W., "Dynamics of Tilting Proprotor Aircraft in Cruise Flight," NASA TN D-7677, May 1974.
6. Johnson, W., "Analytical Model for Tilting Proprotor Aircraft Dynamics, Including Blade Torsion and Coupled Bending Modes, and Conversion Mode Operation," NASA TM X-62369, Aug. 1974.
7. Johnson, W., "Analytical Modeling Requirements for Tilting Proprotor Aircraft Dynamics," Draft NASA TN, Aug. 1974.
8. Johnson, W., "Theory and Comparison with Tests of Two Full-Scale Proprotors," presented at the AHS/NASA-Ames Specialist's Meeting on Rotorcraft Dynamics, 13-15 Feb. 1974.
9. Johnson, W., "A Discussion of Dynamic Stability Measurement Techniques," NASA TM X-73081, Nov. 1975.
10. DeRusso, P.M., Roy, R.J. and Close, C.M., State Variables for Engineers, John Wiley and Sons, Inc., New York, 1965.
11. Greenwood, D.T., Principles of Dynamics, Prentice-Hall, Englewood Cliffs, New Jersey, 1965.
12. Hurty, W.C. and Rubinstein, M.F., Dynamics of Structures, Prentice-Hall, Englewood Cliffs, New Jersey, 1964.
13. D'Azzo, J.J. and Houpis, C.H., Feedback Control System Analysis and Synthesis, McGraw-Hill, New York, 1966.

14. Jenkins, G.M. and Watts, D.G., Spectral Analysis and Its Applications, Holden-Day, San Francisco, 1968.
15. Bendat, J.S. and Piersol, A.G., Random Data: Analysis and Measurement Procedures, Wiley-Interscience, New York, 1971.
16. Sanathanan, C.K. and Kocina, J., "Transfer Function Synthesis as a Ratio of Two Complex Polynomials," IEEE Trans. Auto. Control, Jan. 1963.
17. Cole, H.A., Jr., "On-line Failure Detection and Damping Measurement of Aerospace Structures by Random Decrement Signatures," NASA CR-2205, March 1973.
18. Chang, C.S., "Study of Dynamic Characteristics of Aeroelastic Systems Utilizing Randomdec Signatures," NASA CR-132563, 1975.
19. Hall, W.E. and Gupta, N.K., "System Identification for Nonlinear Flight Regimes," AIAA Journal of Spacecraft and Rockets, March 1977.
20. Gupta, N.K. and Mehra, R.K., "Computational Aspects of Maximum Likelihood Estimation and Reduction in Sensitivity Function Computations," IEEE Trans. of Auto. Control, Dec. 1974, pp. 774-783.
21. Saridis, G.N. and Stein, G., "Stochastic Approximation Algorithms for Linear System Identification," IEEE Trans. Auto. Control, AC-13, 515-523, 1968.
22. Chen, R.T.N., et al., "Development of the Advanced Techniques for the Identification of V/STOL Aircraft Stability and Control Parameters," CAL Report No. BM-2820-F-1, Final Report to NAVAIR, August 1971.
23. Wong, K.Y. and Polak, E., "Identification of Linear Discrete Time Systems Using an Instrumental Variable Method," IEEE Trans. Auto. Control, AC-12, 1967.
24. Young, P.C., "An Instrumental Variable Method for Real Time Identification of a Noisy Process," IFAC Automatica, Vol. 6, 1970.
25. Pandaya, R., "Instrumental Variable Technique for System Identification," submitted to IEEE Trans. Auto. Control, Special Issue on Identification and Time Series Analysis, Dec. 1974.

26. Kashyap, R.L., "Maximum Likelihood Identification of Stochastic Linear Systems," IEEE Trans. Auto. Control, AC-15, 25-34, 1970.
27. Gertler, J. and Banyacz, C.S., "A Recursive (On-line) Maximum Likelihood Identification Method," IEEE Trans. Auto. Control, pp. 816-819, Dec. 1974.
28. Gupta, N.K. and Hall, W.E., "Methods for Real Time Identification of Vehicle Parameters," Systems Control, Inc. Report to Office of Naval Research on Contract N00014-72-C-0328, March 1975.
29. Hannan, E.J., Multiple Time Series, Wiley, New York, 1970.
30. Akaike, H., "Stochastic Theory of Minimal Realization," IEEE Trans. Auto. Control, Vol. 19, No. 6, pp. 716-723, Dec. 1974.
31. Tse, E. and Wienert, H., "Structure Determination and Parameter Identification for Multivariable Stochastic Linear Systems," IEEE Trans. Auto. Control, Vol. AC-20, pp. 603-613, 1975.
32. Milliken, W., "Dynamic Stability and Control Research," Proc. of the Anglo-American Aeronautical Conf., Brighton, England, 1951, pp. 447-524, Roy. Aero. Society.

